Final Report

Project Title: Cooperative Small-molecule Activation toward Sustainable Catalysis

By Dr.Pannee Leeladee

January /2018 (finish date)

Contract No. TRG5880235

Final Report

Project Title: Cooperative Small-molecule Activation toward Sustainable Catalysis

Dr.Pannee Leeladee Chulalongkorn University

Professor Dr.Thawatchai Tuntulani Chulalongkorn University

This project granted by the Thailand Research Fund and Chulalongkorn University

Abstract

Project Code: TRG5880235

Project Title: Cooperative Small-molecule Activation toward Sustainable Catalysis

Investigator: Dr.Pannee Leeladee Chulalongkorn University

E-mail Address: pannee.l@chula.ac.th

Project Period: 1st July 2015–30th June 2017 (2 years)

Abstract:

In this research, a series of copper complexes containing polypyridyl ligands were designed to study the influence from ligands, nuclearity, solvents and secondary coordination on reactivity toward small-molecule activation. This structure-reactivity relationship was used in investigation for oxygen reduction reactions (ORR), and applied in detection of ascorbic acid (AsH_2). Firstly, copper(II) complexes containing polypyridyl derivatives ligands (*i.e.,* Cu(**dpa**), Cu(**adpa**) and Cu_2(**addpa**)) were synthesized and fully characterized by elemental analysis, mass spectrometry and X-ray crystallography. Their electrochemical behaviors were studied by cyclic voltammetry. The Cu(I) complexes which are active species for ORR were generated using AsH_2 as a reducing agent. Redox states of the metal were examined by UV-Vis, NMR and EPR. It was found that copper complexes with various ligand topologies exhibited different reactivity toward O_2. Anthracence moiety in Cu(**adpa**) and Cu_2(**addpa**) played a vital role in facilitating reduction of Cu(II) as well as stability enhancement of Cu(I). The dinuclear complex, Cu_2(**addpa**) showed significantly higher ORR activity than that of the mononuclear analogue. The product of ORR was found to be H_2O_2, indicating $2e^-$, $2H^+$ reduction process. Being stable and inactive towards ORR, Cu(**adpa**) was further investigated as a fluorescence sensor for AsH_2. Reaction of $[Cu(\textbf{adpa})]^{2+}$ with AsH_2 in CH_3CN resulted in turn-on fluorescence due to $[Cu(\textbf{adpa})]^+$ formation. However, when the same reaction was carried out in aqueous solution, the Cu(I) species was gradually oxidized to Cu(II) which hampered the accurate measurement. Notably, addition of Zn(II) in combination with acetate anions helped to stabilize the Cu(I) complex and allowed an accurate detection of ascorbic acids in vitamin C tablets. Secondary coordination sphere modulation of the copper center was proposed to account for this stability enhancement. Overall, the findings obtained from this research have been shown to be applicable in various fields. Also, this can be further used in design for efficient catalysts as well as molecular sensors in the future.

Keywords: small-molecule activation, copper complexes, oxygen reduction, ascorbic acid, structure-reactivity relationship

Content

1. Executive Summary

Our research project focuses on synthesis, characterization and reactivity of first-row transition metal complexes bearing polypyridine ligands, in part to gain further mechanistic understanding for related biological processes catalyzed by metalloenzymes and to provide guidelines for the rational design and synthesis of effective metal-based catalysts for future applications. Toward this end, we have carried out experiments to get insight into mechanism of O_2 reduction mediated by our synthetic copper complexes.

To begin with, our copper complexes were designed to study the influence from ligands, nuclearity, solvents and secondary coordination on reactivity toward small-molecule activation. All copper complexes were synthesized and fully characterized to obtain their structural information. Then, the complexes were examined for oxygen reduction reaction (ORR), so that the structure-reactivity relationship was obtained. Such findings can be further used in a variety of applications. For example, a dinuclear copper complex (Cu_2(**addpa**)) was shown to be competent to catalyze ORR *via* 2-electron, 2-proton process giving rise to the production of H_2O_2. This reaction is useful in development of fuel cells. In addition, an ORR-inactive mononuclear complex, Cu(**adpa**), was found to be an effective sensor for ascorbic acid detection under aerobic conditions.

This fundamental research has shown that understanding in our synthetic complexes in molecular level can serve as basic knowledge which can be applied in various fields. Moreover, the achievements of this project are one oral and two poster presentations in international conferences, as well as two publications in an international journal.

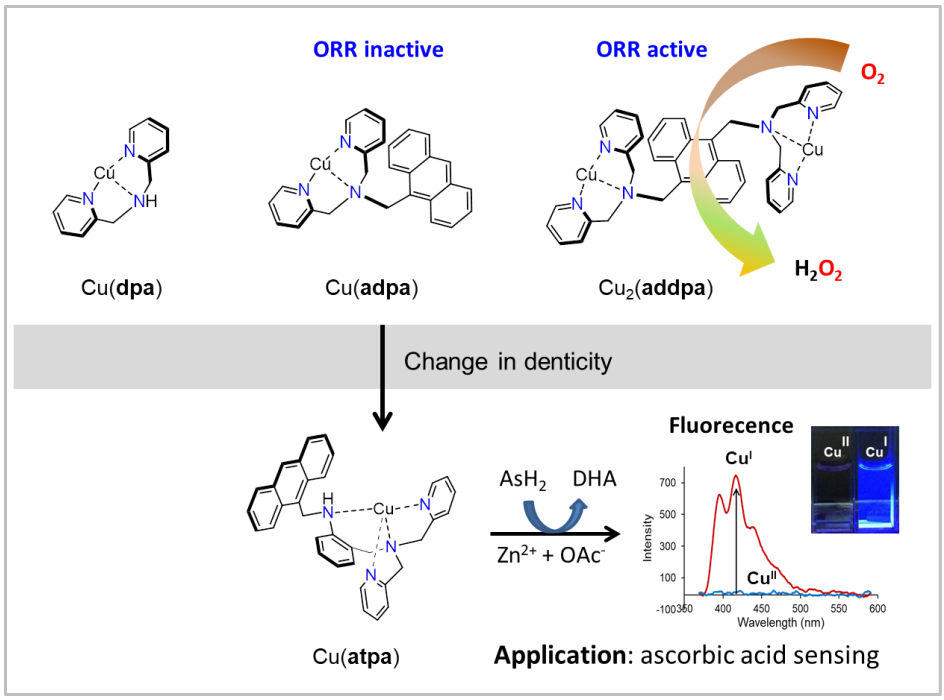

2. Objective

2.1 Synthesis and characterization of mono and dinuclear copper metal complexes with polypyridyl-based ligands

2.2 Electrochemical study and comparison between mono and dinuclear metal complexes as catalysts for small-molecule activation focusing on oxygen reduction reaction (ORR)

2.3 Mechanistic investigation towards small-molecule activation by the metal complexes.

3. Research Methodology

3.1 Synthesis and characterization of copper(II) complexes

3.1.1 Ligand synthesis

2,2'-dipicolylamine (**dpa**)

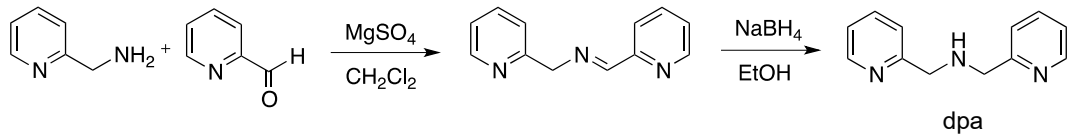

dpa

The **dpa** ligand was prepared according to a published procedure. To the suspension of anhydrous $MgSO_4$ (2.78 g, 23.1 mmol) in CH_2Cl_2 (3.80 mL) was added 2-pyridinecarboxaldehyde (0.50 g, 4.60 mmol) and 2-(aminomethyl)pyridine (0.50 g, 4.60 mmol). The mixture was stirred for 3 h at room temperature under N_2. After that, the suspension was filtered, and solvent in the filtrate was removed under vacuum to obtain a yellow-oil product. The product was redissolved in CH_3CN (12.00 mL) and cooled to -5°C for 15 min. The $NaBH_4$ was slowly added in the solution and stirred for 18 h at room temperature. The reaction was quenched with conc. HCl (7.70 mL) and heated at 60°C for 2h to give the white precipitates in yellow solution. The white solid was filtered out, and solvent in the filtrate was removed under vacuum. The crude product was redissoved in H_2O. To the aqueous solution was added NaOH pellets (3.30 g, 82.5 mmol) and the mixture was stirred for 15 min. The solution was extracted with diethyl ether (3 x 200 mL) and dried under vacuum to obtain the yellow oil product. Yield: 80 %. ^{1}H-NMR (400 MHz, $CDCl_3$, ppm): δ 8.49 (m, 2H, Ar*H*), 7.50 (m, 2H, Ar*H*), 7.23 (d, 2H, *J* = 8.0 Hz, Ar*H*), 7.01 (m, 2H, Ar*H*), 3.84 (s, 4H, -CH_2-).

9-[(2,2'-dipicolylamino)methyl]anthracene (**adpa**)

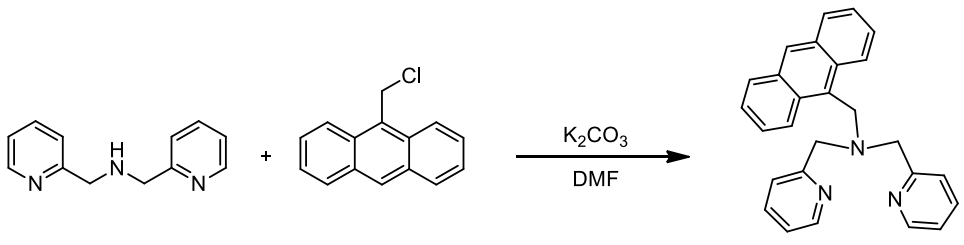

adpa

The stirred solution of 9-bis(chloromethyl)anthracene (1.00 g, 4.40 mmol), 2,2'-dipicolylamine (1.05 g, 5.20 mmol) and K_2CO_3 (2.43 g, 1.70 mmol) in anhydrous DMF (6.8 mL) was slowly added a solution of KI (0.73 g, 4.40 mmol) in DMF (3.6 mL). The reaction was stirred at room temperature over 1 h. To the reaction was added 1M HCl, and the solution was washed with EtOAc. Then, the aqueous solution was alkalized

with 4 M NaOH and extracted by EtOAc : THF (1 : 1). The organic layer was washed with H_2O and brine solution. The solution was dried over anhydrous $MgSO_4$, and the solvent was removed under reduced pressure. The product was obtain after crystallization in MeOH : Et_2O. Yield: 27%, a pale yellow solid. ^{1}H-NMR (400 MHz, $CDCl_3$, ppm): δ 8.49 (d, 2H, *J* = 4.0 Hz, Ar*H*), 8.39 (s, 1H, Ar*H*), 8.37 (d, 2H, *J* = 4.8 Hz, Ar*H*), 7.95 (m, 2H, Ar*H*), 7.57 (ddd, 2H, *J* = 1.6, 7.6, 7.6 Hz, Ar*H*), 7.41-7.47 (m, 4H, Ar*H*), 7.31 (d, 2H, *J* = 7.6 Hz, Ar*H*), 7.11 (dd, 2H, *J* = 4.8, 6.0 Hz, Ar*H*), 4.67 (s, 2H, -CH_2-), 3.88 (s, 4H, -CH_2-).

9,10-Bis[(2,2'-dipicolylamino)methyl]anthracene (**addpa**)

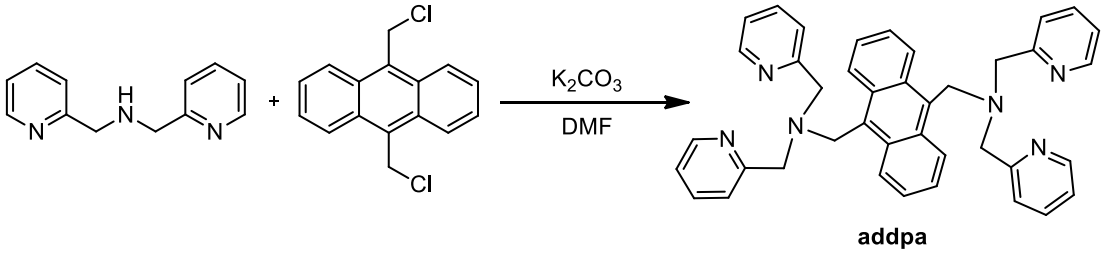

addpa

To a stirred mixture of **dpa** (6.90 g, 34.7 mmol), 9,10-dimethylchloroanthracene (4.30 g, 15.6 mmol) and K_2CO_3 (8.71 g, 63 mmol) in DMF, the solution of KI (2.62 g, 15.8 mmol) in DMF was added dropwise. The mixture was stirred over 1 h, and 1 M HCl was added into this solution. After that, the solution was washed with EtOAc and the aqueous phase was alkalized with 4M NaOH. The aqueous solution was extracted with 1:1 EtOAc and THF. Then, the organic layer was washed with water and followed by brine solution. The solution was dried by $MgSO_4$ and the solvent was removed by rotary evaporation. The yellow solid of **addpa** was obtained from recrystallization with CH_3OH and Et_2O. ^{1}H-NMR (400 MHz, $CDCl_3$, ppm): δ 8.43 (d, 4H, J=4.9 Hz, Ar*H*), 8.40 (dd, 4H, J=3.3, 6.9 Hz, Ar*H*), 7.50-7.54 (m, 4H, Ar*H*), 7.43 (dd, 4H, J=3.2, 7.4 Hz, Ar*H*), 7.28 (d, 4H, J=8 Hz, Ar*H*), 7.03 (dd, 4H, J=5.2, 6.0 Hz, Ar*H*), 4.64 (s, 4H, -CH_2-), 3.87 (s, 8H, -CH_2-).

2-[bis(2-pyridylmethyl)aminomethyl]nitrobenzene

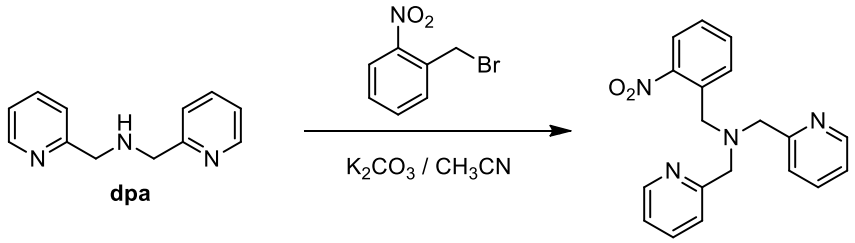

dpa

This ligand was prepared by following a published procedure. The mixture solution of **dpa** (3.86 g, 19.37 mmol), 2-nitrobenzylbromide (4.19 g, 19.40 mmol) and molecular sieve (5 g) was prepared in CH_3CN (80 mL). The reaction was stirred at room temperature under N_2 for 16 h. The suspension was filtered, and the organic solvent was evaporated. Then, the crude product was redissolved in CH_2Cl_2 and washed with H_2O (3 x 300 ml). The organic layer was dried with anhydrous $NaSO_4$, and the solvent was removed to obtain a dark-brown oil. Yield: 80 %. ^{1}H-

NMR (400 MHz, $CDCl_3$, ppm): δ 8.49 (d, 2H, *J* = 4.4 Hz, Ar*H*), 7.75 (m, 1H, Ar*H*), 7.70 (d, 2H, *J* = 15.6 Hz, Ar*H*), 7.64 (t of d, 1H, *J* = 6 Hz ,Ar*H*), 7.49 (t, 1H, *J* = 7.2 Hz, Ar*H*), 7.39 (d, 1H, *J* = 7.6 Hz, Ar*H*), 7.33 (t, 2H, *J* = 7.6 Hz, Ar*H*), 7.13 (m, 2H, Ar*H*), 4.07 (s, 2H, -CH_2-), 3.79 (s, 4H,-CH_2-).

2-[bis(2-pyridylmethyl)aminomethyl]aniline (**tpa**)

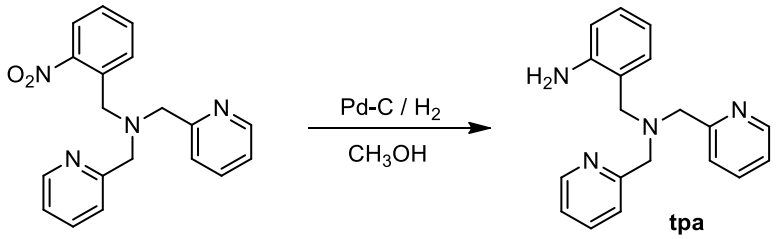

tpa

The **tpa** ligand was prepared following a published procedure. Into a 2-[bis(2-pyridylmethyl)aminomethyl]nitrobenzene (3 g, 8.97 mmol) in two-neck round bottom flask, Pd-C (0.3 g) and MeOH (150 ml) were added and stirred under H_2 for 24 hr. The mixture was filtered through celite and the solvent was removed under reduced pressure. Yield: 98%, red brown oil. ^{1}H-NMR (400 MHz, $CDCl_3$, ppm): δ 8.56 (m, 2H, Ar*H*), 7.62 (m, 2H, Ar*H*), 7.36 (d, 2H, *J* = 7.2 Hz, Ar*H*), 7.16 (m, 2H, Ar*H*), 7.07 (m, 2H, Ar*H*), 6.63 (t, 2H, *J* = 6.0 Hz, Ar*H*), 3.82 (s, 4H, -CH_2-), 3.71 (s, 2H, -CH_2-).

9-[(2,2'-dipicolylamino)methyl]anthracene (**atpa**)

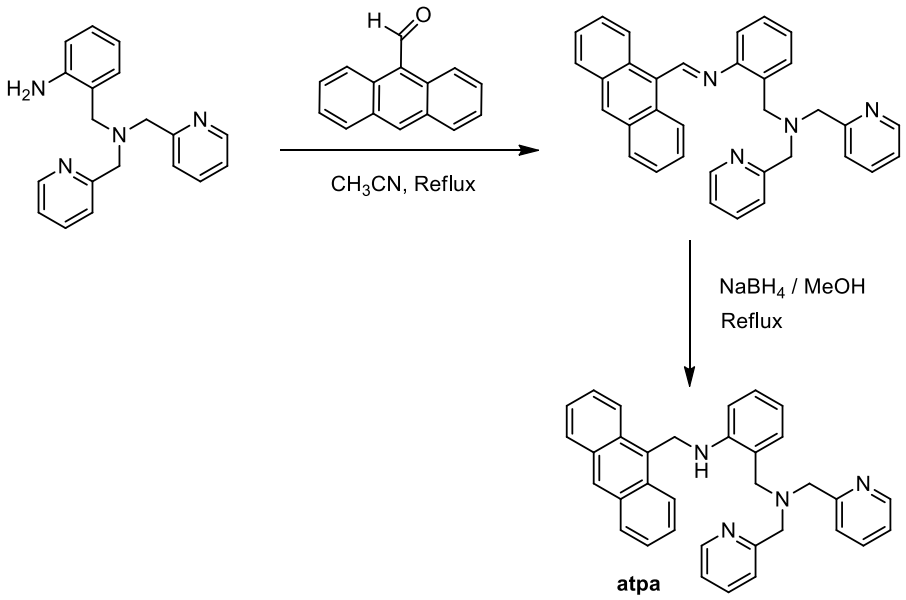

atpa

The **atpa** ligand was synthesized according to a published method. The stirred solution of 9-bis(chloromethyl)anthracene (1.00 g, 4.40 mmol), 2,2`-dipicolylamine (1.05 g, 5.20 mmol) and K_2CO_3 (2.43 g, 1.70 mmol) in anhydrous DMF (6.8 mL) was slowly added a solution of KI (0.73 g, 4.40 mmol) in DMF (3.6 mL). The reaction was stirred at room temperature over 1 h. The solution was add 1M HCl and wa shed with EtOAc (3X). Then, the aqueous solution was alkalized with 4 M NaOH and extracted by EtOAc : THF (1 : 1).

The organic layer was washed with H_2O and brine solution. The solution was dried over anhydrous $MgSO_4$ and the solvent was removed under reduced pressure. The product was obtain after crystallization in MeOH : ether. Yield: 27%, a pale yellow solid. ^{1}H-NMR (400 MHz, $CDCl_3$, ppm): δ 8.49 (d, 2H, *J* = 4.0 Hz, Ar*H*), 8.39 (s, 1H, Ar*H*), 8.37 (d, 2H, *J* = 4.8 Hz, Ar*H*), 7.95 (m, 2H, Ar*H*), 7.57 (ddd, 2H, *J* = 1.6, 7.6, 7.6 Hz, Ar*H*), 7.41-7.47 (m, 4H, Ar*H*), 7.31 (d, 2H, *J* = 7.6 Hz, Ar*H*), 7.11 (dd, 2H, *J* = 4.8, 6.0 Hz, Ar*H*), 4.67 (s, 2H, -CH_2-), 3.88 (s, 4H, -CH_2-).

3.1.2 Synthesis and characterization of copper(II) complexes

Cu(**dpa**)

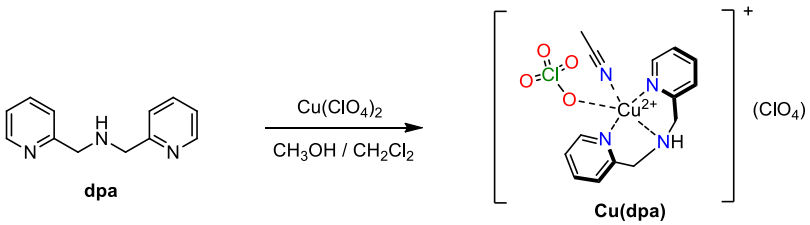

[Cu(**dpa**)(ClO_4)](ClO_4) was prepared from the reaction of **dpa** (0.20 g, 1.00 mmol) and $Cu(ClO_4)_2$ (0.56 g, 1.51 mmol) in CH_2Cl_2/CH_3OH (1:1 v:v). Yield: 0.28 g (60%). Blue single crystals suitable for X-ray structure determination were obtained by recrystallization of the complex *via* layer diffusion in CH_2Cl_2/CH_3CN for 7 days. Anal. Calcd (found) of $C_{12}H_{15}Cl_2CuN_3O_9$: %C = 30.04 (30.34), %H = 3.15 (3.05), %N = 8.76 (8.72). MALDI-TOF MS (m/z) of [Cu(**dpa**)-H]$^+$ for calculated: 261.03; found: 261.23. λ_{max}/nm (ε/$M^{-1}cm^{-1}$) in CH_3CN: 606 (117.2).

Cu(**adpa**)

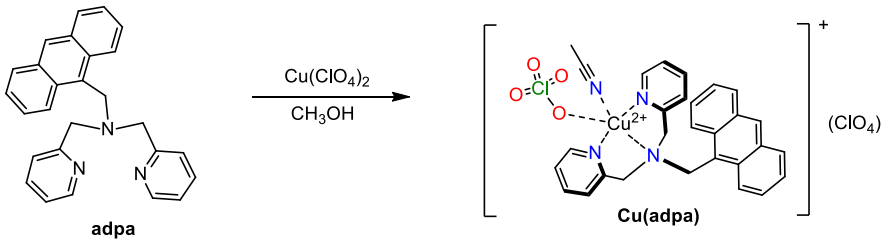

[Cu(**adpa**)(ClO_4)](ClO_4) was prepared according to a modified published method.[1] Reaction of **adpa** (0.15 g, 0.39 mmol) and $Cu(ClO_4)_2$ (0.16 g, 0.43 mmol) in CH_3OH resulted in dark green products. Yield: 0.15 g (61%). The single crystals suitable for X-ray crytallography were recrystallized by vapor diffusion of Et_2O into the solution in CH_3CN for 7 days. Anal. Calcd (found) of $C_{27}H_{25}Cl_2CuN_3O_9$: %C = 48.40 (48.09), %H = 3.76 (3.74), %N = 6.27 (6.32). MALDI-TOF MS (m/z) of [Cu(**adpa**)+(ClO_4)]$^+$ for calculated: 551.07; found: 551.01. λ_{max}/nm (ε/$M^{-1}cm^{-1}$) in CH_3CN: 590 (117.9).

Cu_2(**addpa**)

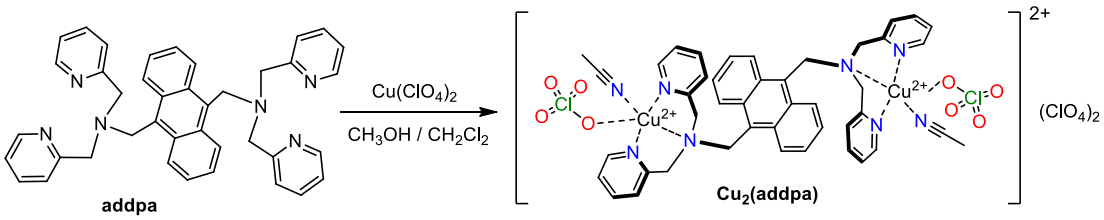

[Cu_2(**addpa**)$(ClO_4)_2$]$(ClO_4)_2$ was prepared from the reaction of **addpa** (0.20 g, 0.33 mmol) and $Cu(ClO_4)_2$ (0.37 g, 1.00 mmol) in CH_2Cl_2/CH_3OH (1:1 v:v). Yield: 0.32 g (85%). Deep green single crystals were obtained by recrystallization of the complex using mixed solvent CH_2Cl_2/CH_3OH.

Anal. Calcd (found) of $C_{40}H_{36}Cl_4Cu_2N_6O_{16}$: %C = 42.68 (42.41), %H = 3.22 (3.31), %N = 7.47 (7.34). ESI-MS (m/z) of [Cu_2(**addpa**)$(ClO_4)_3$]$^+$ for calculated: 1025.00; found: 1025.39. λ_{max}/nm (ε/$M^{-1}cm^{-1}$) in CH_3CN: 593 (273.7).

Cu(**atpa**)

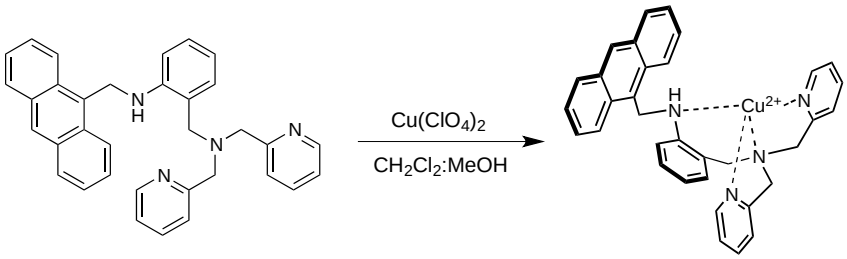

Copper(II) perchlorate (0.30 g, 0.81 mmol) dissolved in MeOH (3.00 mL) was added into the solution of **atpa** (0.2 g, 0.40 mmol) in CH_2Cl_2 (3.00 mL). The mixture was stirred at room temperature until blue precipitates was observed. The reaction mixture was then filtered, and the blue solid was recrystallized by CH_3CN to obtain the [Cu(**atpa**)]$^{2+}$ product (70 % yield). Anal. Calcd (found) of $C_{34}H_{32}Cl_2CuN_4O_9$: %C = 52.69 (52.63), %H = 4.16 (4.12), %N = 7.23 (7.14). ESI-MS (*m/z*) of Cu(**atpa**), [Cu(**atpa**)-H]$^+$ for calculated: 556.18; found: 556.01.

3.2 Studies of reactivity toward O_2 reduction

Unless otherwise noted, all reactions were carried out under inert atmosphere (N_2). All solvents were deoxygenated prior to use by purging N_2 for at least 1 h. The UV-Vis spectral change during the reaction was monitored at ambient temperature using a Varian Cary 50 probe UV-Visible Spectrophotometer with a quartz cuvette (path length = 10 mm).

Generation of copper(I) complexes

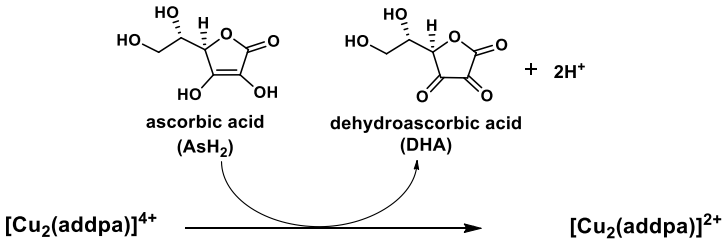

A stock solution of AsH_2 (44 mM) was prepared in a solvent mixture of 5% DMF in CH_3CN or 5% H_2O in CH_3CN. To ensure the absence of O_2 in our reactions, the solution of copper complexes was purged with N_2 gas for 10 min before starting the reaction. In a typical reaction, to a solution of copper(II) complex (1 mM for Cu_2(**addpa**); 2 mM for Cu(**dpa**) and Cu(**adpa**)) in CH_3CN was added an amount of AsH_2 stock solution (0-2 equiv). A color change of the solution to yellow was observed. Monitoring of this reaction by UV-vis spectroscopy showed a reduction of copper(II) complex (λ_{max} around 600 nm corresponding to a *d-d* transition band of d^9 Cu^{II} species) to copper(I) species (no *d-d* transition band).

NMR and EPR samples were prepared as follows: to a solution of copper(II) complex (10 mM) in CD_3CN (550 μL) was added AsH_2 (20 μL, 0.55 equiv dissolved in 15% D_2O in CD_3CN). For Cu(**adpa**) and Cu_2(**addpa**), a color change to yellow was noted, consistent with formation of copper(I) species. When compared to a broad ^{1}H-NMR spectrum of Cu^{II}, the pale-yellow species exhibited a sharp spectrum, supporting an assignment of diamagnetic d^{10} Cu^{I} species. Analysis of ^{1}H-NMR spectrum also revealed a formation of dehydroascorbic acid (an oxidized form of ascorbic acid) after the reaction.

Oxygen reduction reaction (ORR)

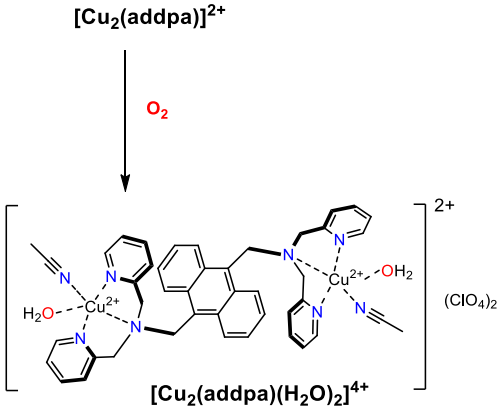

After a complete generation of the copper(I) species (for Cu(**adpa**) and Cu_2(**addpa**)), O_2 was purged into the Cu^{I} solution for 1 h to examine the ORR activity. The reaction can be monitored by spectral change in UV-vis, NMR and EPR.

3.3 H_2O_2 detection by silver nanoprisms (AgNPrs)

To obtain a sufficient amount of O_2^- reduced product after ORR, a catalytic reaction was performed. Into a solution of Cu_2(**addpa**) (10 mM, 0.010 mmol) in CH_3CN was added an excess amount of AsH_2 (10 equiv). Then, the reaction was purged with O_2 for 1 h. The reaction was allowed to stand for 2 h before product determination. Unfortunately, due to the direct reaction of Cu_2(**addpa**) with I^-, we cannot perform iodometric titration for detection and quantification of H_2O_2. However, the H_2O_2 product from ORR was successfully detected by reaction with AgNPrs. Owing to precipitation of AgNPrs in organic solvent, UV-Vis spectral change cannot be investigated. Nevertheless, in the presence of H_2O_2, an obvious color change of the AgNPrs precipitates from magenta to white can be observed by naked eye. After the catalytic ORR, an amount of AgNPrs solution (0.02 mL) was added into the reaction solution

(0.20 mL), and the white precipitates were observed, confirming the production of H_2O_2 after ORR. For a positive control experiment, the same amount of AgNPrs (0.02 mL) was added into H_2O_2 solution (0.1 M) in CH_3CN (0.20 mL), which resulted in the change in color of precipitates from magenta to white. When a negative control reaction was performed (the same condition, but in the absence of Cu_2(**addpa**) or AsH_2), the color of precipitates stayed the same as magenta.

3.4 X-ray crystallography

Crystals of Cu_2(**addpa**) were selected under an optical microscope and glued on glass fiber for single crystal X-ray diffraction experiments. X-ray diffraction data were collected using a Bruker D8 QUEST CMOS using Mo-Kα radiation (λ = 0.7107 Å) and operating at T = 296(2) K. Data were measured using ω and φ scans of 0.5 (d, scan_width)° per frame for 30 (d, scan_rate) seconds using Mo-Kα radiation (50 kV, 30 mA). The total number of runs and images was based on the strategy calculation from the program APEX3. Unit cell indexing was refined using SAINT (Bruker, V8.34A, 2013). Data reduction, scaling and absorption corrections were performed using SAINT (Bruker, V8.34A, 2013) and SADABS-2014/4 (Bruker, 2014/4) was used for absorption correction. The structure was solved in the space group *P*1 with the ShelXT structure solution program using combined Patterson and dual-space recycling methods. The crystal structure was refined by least squares using version 2014/7 of ShelXL. All non-hydrogen atoms were refined anisotropically. Hydrogen atom positions were calculated geometrically and refined using the riding model. The ClO_4^- anions were found to be disordered over two positions. The relative occupation of the disordered ClO_4^- anion was refined as a free variable. All Cl–O bond distances and O···O separations of both (minor and major) fractions of the disordered ClO_4^- anion were restrained to have identical values within 0.02 Å.

3.5 Cyclic voltammetry

Cyclic voltammetric measurements were performed with an Autolab PGSTAT101 potentiostat/galvanostat (Eco Chemie, The Netherlands) using a conventional three-electrode configuration. A glassy carbon electrode with a disk diameter of 3.0 mm was employed as a working electrode. Before use, the electrode was polished with an aqueous suspension of alumina powder and rinsed thoroughly with deionized water. A platinum wire was applied as an auxiliary electrode. All potentials are quoted with respect to a non-aqueous silver/silver ion (Ag/Ag^+) reference electrode; this electrode was externally calibrated with a ferrocene/ferrocenium ion (Fc/Fc^+) redox couple and has a potential of 0.542 V *versus* a standard hydrogen electrode (SHE). Cyclic voltammograms of the copper complexes (1.00 mM) were recorded in a deoxygenated solvent (dimethylformamide, DMF or acetonitrile, CH_3CN) containing 0.10 M tetrabutylammonium hexafluorophosphate ($TBAPF_6$) at scan rates of 50–800 $mV \cdot s^{-1}$. A deaeration procedure was carried out with the aid of ultra-high purity (UHP) nitrogen.

3.6 Computation methods

Geometry optimizations of dinuclear copper catalyst and its related compounds, were carried out using density functional theory (DFT) method. The hybrid density functional B3LYP, the Becke three–parameter hybrid functional combined with the Lee–Yang–Parr correlation functional, using the 6–31G(d,p) basis set have been employed in calculations. The solvent−effect of polarizable continuum model (PCM) using the CPCM (conductor–like PCM,

acetonitrile as a solvent) model with UFF molecular cavity model have been used in the optimization. Therefore, the employed method has been called the CPCM(UFF)/B3LYP/6–31G(d,p) method. All calculations were performed with the Gaussian 09 program.

3.7 Generation of Cu^{I} species in the presence of $Zn(OAc)_2$

Unless otherwise noted, the following experiments were conducted under ambient condition. A stock solution of AsH_2 was prepared. In a typical reaction, a solution of Cu^{II}(**adpa**) was combined with $Zn(OAc)_2$ (8 equiv). To this solution mixture was added AsH_2 stock solution (1.0 equiv). A color change of the solution from blue to pale yellow was observed. The reaction was also monitored by UV-vis spectroscopy, which revealed a complete conversion of the spectrum for Cu^{II}(**adpa**) to the spectrum for a Cu^{I} complex (no *d-d* transition band). The Cu^{I} species seemed to be stable for at least 30 min. When $Zn(OAc)_2$ was changed to $Zn(NO_3)_2$ or $Zn(phen)_2$, however, the reduction was not completed as the *d-d* band of Cu^{II} was present in a significant extent. In fact, they gave the same result as observed in the reaction without $Zn(OAc)_2$. This indicated the presence of OAc^- is necessary to help facilitate the reduction of Cu^{II}(**adpa**) and stabilization of Cu^{I}(**adpa**).

Attempts to characterize this new Cu^{I} complex in the presence of $Zn(OAc)_2$ by mass spectrometry also have been made. Samples for ESI-MS analysis were prepared using the same procedure as for the UV-vis measurements. A prominent peak at mass-to-charge ratio (*m/z*) of 511.1332 was observed, corresponding to $[Cu(\textbf{adpa})\text{-}OAc]^+$. This supported the possibility of OAc^- being coordinated to Cu(**adpa**)..

An NMR sample was prepared as follows: to a solution of Cu^{II}(**adpa**) was combined with $Zn(OAc)_2$. A shift and broadening of a signal corresponding to OAc^- was noted, indicating the coordination of OAc^- to the paramagnetic Cu^{II} center. To this solution was added AsH_2. The solution became pale yellow, consistent with conversion to Cu^{I}**L1**. The yellow product gave a sharp spectrum, corresponding to the Cu^{I} species.

3.8 Reaction in the presence of other divalent metal ions

In a typical reaction for investigation of Cu^{I}(**adpa**) stabilization with divalent metal ions: Zn(OAc)2, $Zn(NO_3)_2$, $Mg(NO_3)_2$, $Ca(NO_3)_2$, $Cd(NO_3)_2$ and $Zn(Phen)_2$, each metal ion or metal complex (8 equiv.) was added into Cu^{II}(**adpa**) solution before the addition of AsH_2 (1 equiv).

3.9 Detection of AsH_2 by fluorescence spectroscopy

Fluorescence analysis were performed in 70% H_2O/CH_3CN buffered at pH 5.6 with acetic acetate (ABS) under ambient condition. The stock solution of 1 mM Cu^{II}(**adpa**) was prepared in 70% H_2O/CH_3CN and then diluted into 10 μM in ABS/CH_3CN buffer solution to analyze the fluorescence, whereas ascorbic acid and other antioxidants (glutathione, citric acid, glucose, lactose, sucrose and fructose) were prepared the stock solution at 0.08 M in H_2O and subsequently preparing at 2 mM in ABS/CH_3CN.

3.10 Studies of selectivity and interferences

For selectivity investigation, the analytes solution (5 equiv., 0.05 mL) was added into ABS/CH_3CN buffer solution of Cu^{II}(**adpa**) (2.00 mL) upon the addition of $Zn(OAc)_2$ (40 equiv, 0.10 mL). The reaction was stirred for 2 min prior to analyze by fluorescence.

3.11 Determination of AsH_2 in vitamin C tablets

Vitamin C tablets were purchased from PT Bayer Indonesia, Depok, Indonesia. The stock sample was prepared by dissolving three vitamin C tablets in milli-Q water (500 mL). After that, insoluble components were removed by filtered with 0.45 μM Millipore filter and diluted for suitable analysis by fluorescence as well as HPLC.

4. Results and Discussion

4.1 Synthesis of copper (II) complexes

All ligands were prepared according to modified published procedures, and were obtained in moderate yields. The Cu(II) complexes were synthesized from reaction of dipicolyl amine-based ligand (**dpa**, **adpa**, **atpa** and **addpa**) and $Cu(ClO_4)_2$. After stirred for a few minutes, the Cu(II) products were spontaneously precipitated. Our choice of Cu over other metals was especially inspired by Nature's choice of Cu over Fe in heme-copper oxidases. An intriguing study indicated that the high redox potential and the rich electron density in the d orbitals of Cu are key to its high reactivity towards oxygen reduction. All copper complexes were also characterized by standard analytical methods including elemental analysis, mass spectrometry, UV-vis and EPR spectroscopy. The structural information was obtained from X-ray crystallography (Figure 1). The UV-vis spectra of all Cu(II) complexes exhibit Cu(II) d-d transition with absorption maxima in range of 580 to 610 nm.

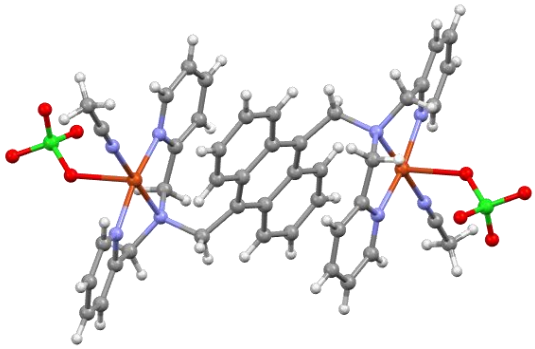

Figure 1. X-ray crystal structure of $[Cu_2$**(adpa)**$(CH_3CN)_2(ClO_4)_2]^{2+}$

The X-ray crystal structure of $[Cu_2$**(adpa)**$(CH_3CN)_2(ClO_4)_2]^{2+}$ (*in collaboration with Assist. Prof. Dr.Kittipong Chainok*) revealed that each Cu center in the complex is five-coordinate square pyramidal with an axially ligated perchlorate at 2.435 Å and a tightly bound CH_3CN at 1.980 Å. The relatively long Cu–O bond was attributed to the Jahn-Teller distortion of d^9 configuration (Cu^{II}) in octahedral field via axial elongation. In addition, our result was similar to those of reported Cu complexes, which exhibited the bond distance between the axial ligand and Cu^{II} in range of 2.3-2.6 Å. It was also speculated that the weakly bound perchlorate would dissociate upon reduction of Cu^{II} to Cu^{I}, resulting in a vacant site for substrate binding during the catalytic reaction.

4.2 Electrochemical properties of the copper(II) complexes.

Cyclic voltammetry was used to examine the electrochemical properties of copper complexes (Cu(**dpa**), Cu(**adpa**) and Cu_2(**addpa**). The cyclic voltammogram in Figure 2(b)-(d) exhibited single redox couple of Cu(II)/Cu(I).

The electrochemical data indicated characteristic metal-based electron transfer corresponding with earlier studies of the reduction of [Cu(**dpa**)]$^{2+}$ and its derivatives.

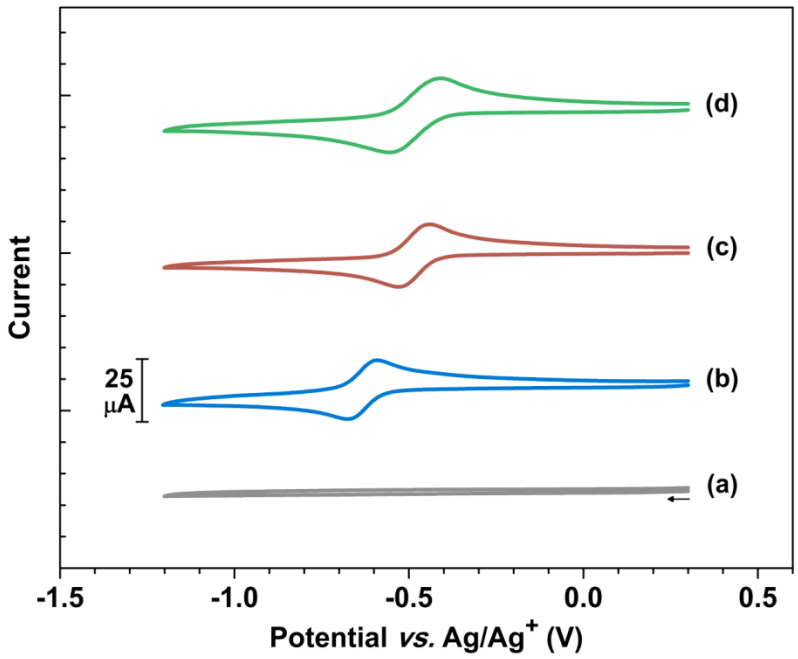

Figure 2. Cyclic voltammograms recorded with a glassy carbon electrode (area = 0.071 cm^2) at 100 mV·s^{-1} from +0.30 to –1.20 to +0.30 V for (a) DMF containing only 0.10 M $TBAPF_6$; and DMF containing 0.10 M $TBAPF_6$ in the presence of 1.00 mM (b) Cu(**dpa**), (c) Cu(**adpa**), and (d) Cu_2(**addpa**).

For comparison of the cathodic electrochemical behavior, copper(II) complexes containing anthracenyl scaffold (Cu(**adpa**) and Cu_2(**addpa**)) were reduced at less negative potential (~100-150 mV) than Cu(**dpa**). This suggested that conjugated-π systems of anthracene help to facilitate in Cu(II) complex reduction. In addition, as compared at same condition copper complexes containing anthracenyl scaffold (Cu(**adpa**) and Cu_2(**addpa**)) tended to be more stable than Cu(**dpa**) in terms of decomposition of Cu(I) to metallic Cu(0).

4.3 Reaction of copper complexes with ascorbic acid

Prior to examine the oxygen reduction reaction (ORR), Cu(I) active species had to be generated by chemical reaction. AsH_2 was introduced in our system to serve as a reducing agent as well as a proton source to participate in ORR. Under N_2 atmosphere, a color of Cu(II) complexes in CH_3CN (blue for [Cu(**dpa**)]$^{2+}$, [Cu(**adpa**)]$^{2+}$, or green for [Cu_2(**addpa**)]$^{4+}$), was changed to yellow upon addition of excess AsH_2 (dissolved in DMF/CH_3CN). This indicated the formation of new species. Monitoring these reactions by UV-vis titration, *d-d* band of Cu(II) decreased upon addition of AsH_2 and completely disappeared when 0.5 equiv or 1.0 equiv of AsH_2 with regards to Cu(**adpa**) and Cu_2(**addpa**) respectively was reached.

The yellow species generated from the reaction between Cu^{II}(**adpa**) and AsH_2 was found to be stable at room temperature for at least 4 h under inert atmosphere. Monitoring this reaction by UV-vis spectroscopy revealed that the *d-d* band of Cu^{II} at 593 nm decreased upon addition of AsH_2 and completely disappeared when 1 equiv of

AsH$_2$ was reached (Figure 3). This result suggested that Cu^{II}(**adpa**) was reduced to Cu^{I}(**adpa**) by 2-electron reducing agent, AsH$_2$ (Scheme 1). Furthermore, the reduction of Cu^{II}(**adpa**) to Cu^{I}(**adpa**) was confirmed by ^{1}H-NMR and EPR spectroscopy (*vide infra*).

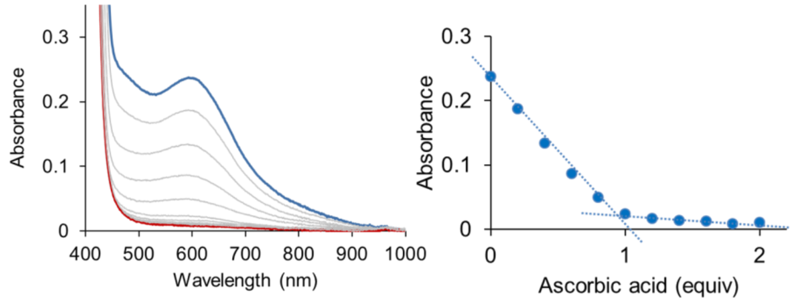

Figure 3. (left) UV-Vis spectral changes upon addition of ascorbic acid (0 – 2.0 equiv) to Cu^{II}(**adpa**) solution (1 mM) in DMF/CH$_3$CN. (right) Plot of Absorbance at 593 nm vs equiv. of AsH$_2$ added

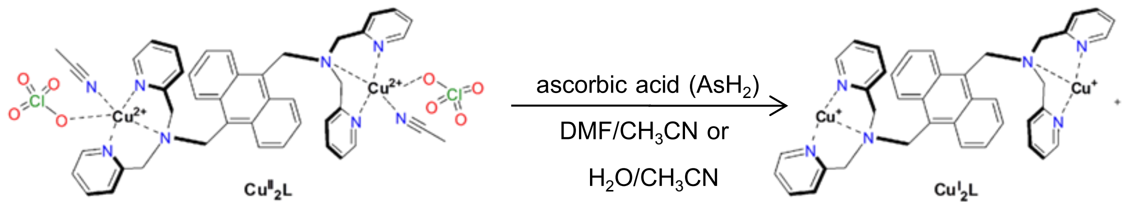

Scheme 1. Formation of Cu^{I}(**adpa**)

In should be noted that [Cu(**dpa**)]$^+$ could not be completely generated even after 9 hours (Figure 4). Whereas in the case of copper complexes bearing anthracenyl moiety (Cu(**adpa**) and Cu$_2$(**addpa**)), *d*-*d* band of Cu(II) was entirely disappeared within 20 min after addition of AsH$_2$ (0.5 or 1.0 equiv). Such difference could be derived from the attribute of ligand structure. This data is in agreement with the result obtained from an electrochemical reduction that the presence of anthracene moiety help to facilitate in Cu(II) reduction process.

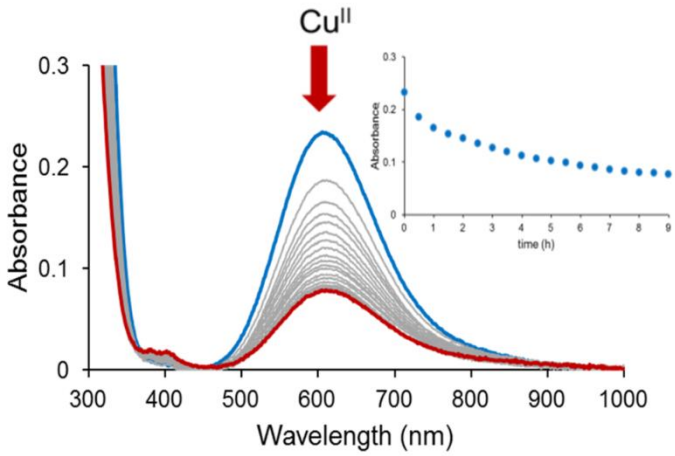

Figure 4. UV-Vis spectral changes upon addition of ascorbic acid (0.5 equiv) to Cu(**dpa**) solution (2 mM) in DMF/CH_3CN. The inset shows plot of absorbance at 606 nm vs times.

4.4 Preparation of Cu^{I}(**adpa**) and its reactivity with O_2

Cu^{I}(**adpa**) can be prepared by reacting Cu^{II}(**adpa**) with AsH_2 in high concentration (up to 10 mM) for EPR and ^{1}H-NMR studies. It was also observed that the yellow solution of Cu^{I}(**adpa**) slowly turned green when exposed to air,, indicating the regeneration of Cu^{II}(**adpa**). Preliminary results from UV-vis, EPR and ^{1}H-NMR spectroscopy showed that the same reaction could be performed in H_2O/CH_3CN instead of DMF/CH_3CN. In fact, Cu^{I}(**adpa**) in H_2O/CH_3CN seemed to be more reactive to O_2 as Cu^{II}(**adpa**) regeneration step was much faster when compared to the same reaction in DMF/CH_3CN. This may be due to DMF serving as a strongly coordinating solvent in place of ClO_4^- which could inhibit the substrate (O_2) binding. Hence, reactivity studies of Cu^{II}(**adpa**) were carried out in H_2O/CH_3CN. ^{1}H-NMR spectroscopy of Cu^{II}(**adpa**):AsH_2 (1:1.5) in D_2O/CD_3CN revealed a diamagnetic spectrum (Figure 5) with sharp peaks at aromatic region for **adpa**, in stark contrast to the paramagnetic spectrum seen for the starting d^9 Cu^{II} complex. The diamagnetic NMR spectrum is consistent with the assignment of d^{10} Cu^{I} product, Cu^{I}(**adpa**). When passing air or O_2 gas into the yellow solution of Cu^{I}(**adpa**), a paramagnetic spectrum of Cu^{II}(**adpa**) was regenerated, corresponding to the color change from yellow to green solution. The new signals around 4 – 5 ppm were assigned to the oxidized form of AsH_2.

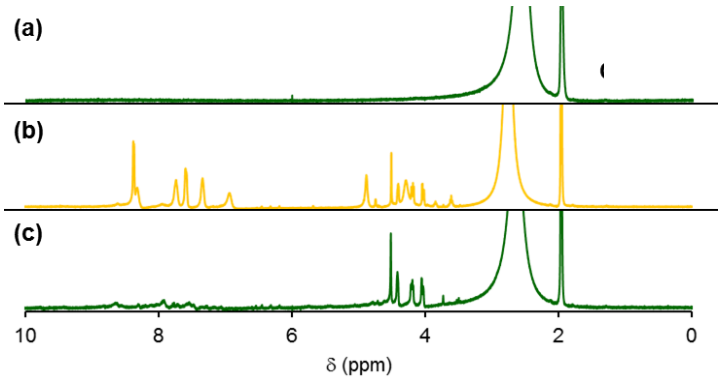

Figure 5. ^{1}H-NMR spectra of (a) Cu^{II}(**adpa**) (10mM), (b) Cu^{II}(**adpa**) + AsH_2 (1:1.5) in D_2O/CD_3CN and (c) after (b) exposed to air for 2 h.

Next, the generation of Cu^{I}(**adpa**) and its O_2 reactivity were confirmed by EPR spectroscopy. The EPR signal due to paramagnetic Cu^{II}(**adpa**) disappeared upon addition of AsH_2 (1.5 equiv), corresponding to the formation of diamagnetic Cu^{I}(**adpa**). The signal then reappeared after the reaction was exposed to air or O_2 (Figure 6).

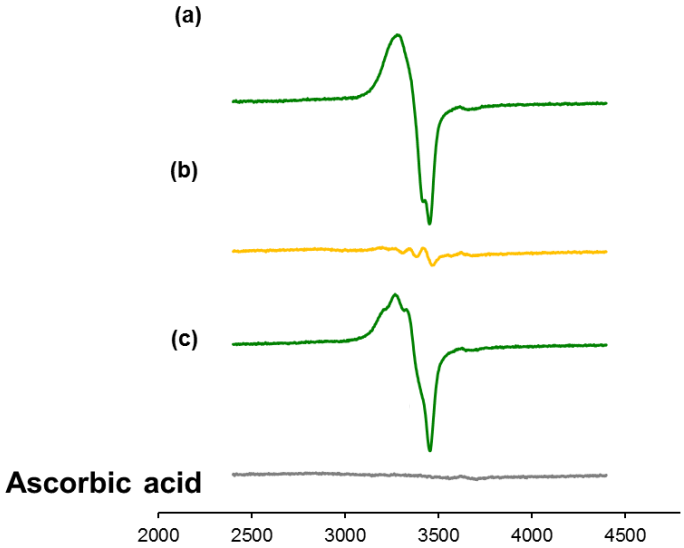

Figure 6. EPR spectra of (a) Cu^{II}(**adpa**) (10 mM in H_2O/CH_3CN), (b) Cu^{II}(**adpa**) + AsH_2 (1:1.5) and (c) Cu^{II}(**adpa**) after reaction with O_2. The experimental parameters: microwave frequency= 9.838 GHz, microwave power= 0.620 mW, modulation amplitude= 5.00 G, modulation frequency= 100 kHz.

4.5 Structural characterization of Cu^{II} species after O_2 reduction.

Efforts were made to obtain single crystals for structural characterization of the Cu^{II} product following reaction of Cu^{II}(**adpa**) with O_2. After the reaction was completed, Et_2O was added to obtain the green precipitates. This solid was then recrystallized by vapor diffusion in CH_2Cl_2/CH_3CN, the same condition to get single crystals of $[\mathbf{Cu_2(adpa)}(CH_3CN)_2(ClO_4)_2]^{2+}$. The mixture was allowed to stand for four weeks to afford dark green crystals, suitable for X-ray diffraction. As shown in Figure 7, the structure of the Cu^{II} product after O_2 reduction resembled that of the Cu^{II} starting material except the Cu^{II} product, $[\mathbf{Cu_2(adpa)}(CH_3CN)_2(H_2O)_2]^{4+}$ having H_2O as an axial ligand instead of ClO_4^-. This may imply that the axially ligated ClO_4^- dissociated from the Cu center to generate a vacant site for O_2 binding during the reaction.

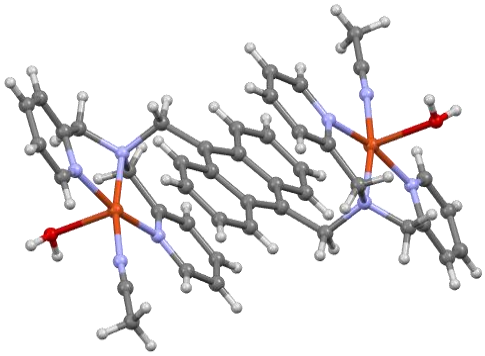

Figure 7. X-ray crystal structure of $[Cu_2(\mathbf{adpa})(CH_3CN)_2(H_2O)_2]^{4+}$.

Interestingly, reactivity of our copper complexes toward O_2 was significantly different. In case of Cu(**adpa**), a yellow solution of $[Cu(\mathbf{adpa})]^+$ species were relatively stable at room temperature under aerobic systems (air or O_2). Monitoring this reaction up to 1 day, the diamagnetic spectrum of Cu(I) species was still observed. In contradict to $[Cu_2(\mathbf{addpa})]^{2+}$, a paramagnetic spectrum was regenerated within an hour corresponding to the color change from yellow to green solution. To clarify the higher ORR activity of Cu_2(**addpa**) over Cu(**adpa**), our initial assumption would be simply derived from its more number of active sites. Reactivity comparison of the two copper complexes with the same equivalents of copper centers i.e., Cu(**adpa**) (2 mM) vs Cu_2(**addpa**) (1 mM) was investigated by UV-vis (Figure 8). Interestingly, ORR activity of $[Cu(\mathbf{adpa})]^+$ was significantly lower than that of $[Cu_2(\mathbf{addpa})]^{2+}$, indicating that the number of active sites could not use to explain for this case. Given the crystal structure and intramolecular $\pi-\pi$ stacking between the pyridyl and aryl rings in $[Cu_2(\mathbf{addpa})]^{4+}$, the synergistic cooperation for O_2 binding between two Cu centers is also not likely to operate. Therefore, the lower reactivity of $[Cu(\mathbf{adpa})]^+$ towards O_2 may be due to the stronger influence from anthracene to stabilize the mononuclear than the dinuclear complex. Overall, Cu_2(**addpa**) showed the best performance for ORR activity.

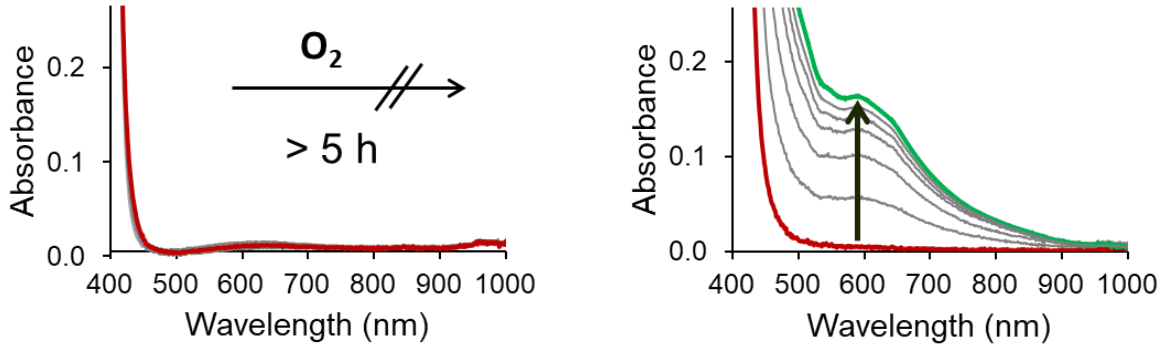

Figure 8. (left) UV-Vis spectra of reaction between $[Cu(\mathbf{adpa})]^{2+}$ (2.0 mM) and ascorbic acid (0.55 equiv) in H_2O/CH_3CN after purging O_2 (0-5 h) and (right) UV-Vis spectral change of reaction between $[Cu_2(\mathbf{addpa})]^{4+}$ (1.0 mM) and ascorbic acid (1.10 equiv) in H_2O/CH_3CN after purging O_2 (0-1 h)

4.6 Catalytic O_2 reduction and proposed intermediate

In the reaction mediated by Cu_2(**addpa**), the amount of AsH_2 was increased to 10 equiv to develop in ORR catalytic cycles. The finding demonstrated that AsH_2 could be completely employed in ORR mediated by Cu_2(**addpa**). The production of dehydroascorbic acid (AsH_2-oxidized product in hydrated bicyclic form) was detected, while the signal of AsH_2 was completely absent. Also, UV-vis data showed 70% recovery of $[Cu_2(\mathbf{addpa})]^{4+}$ after catalytic cycles, suggesting a complete reaction of $[Cu_2(\mathbf{addpa})]^{4+}$ and AsH_2 to generate Cu(I) active species for catalytic ORR. In our system, AsH_2 not only can serve as a reductant but also a proton source for O_2 reduction. This reducing agent offers a unique and efficient system because, unlike other previous reports, an external source of proton is not required in our reaction.

Next, the product obtained from catalytic O_2 reduction was determined. We attempt to detect H_2O_2 production after catalytic ORR by reaction with silver nanoprisms (AgNPrs). A color change of AgNPrs from magenta to white in solution from ORR was observed, implicating that H_2O_2 was produced from ORR. Also, in case of Cu complex or AsH_2 alone, the magenta of AgNPrs was still observed, indicating that white precipitate was obtained from reaction of H_2O_2.

To gain further insights into mechanism for $[Cu_2(\mathbf{addpa})]^{4+}$ mediated catalytic O_2 reduction, computational calculations were next performed. From literature, possible Cu_2O_2 adduct in dioxygen activation reaction could be end-on or side-on peroxo species. In the most cases, end-on Cu_2O_2 species with nucleophilic and basic properties tends to produce H_2O_2 as a product.According to H_2O_2 production in our ORR, possible copper-dioxygen intermediate was proposed to be an end-on species. The Cu_2O_2 structure was optimized by DFT calculation as shown in Figure 9.

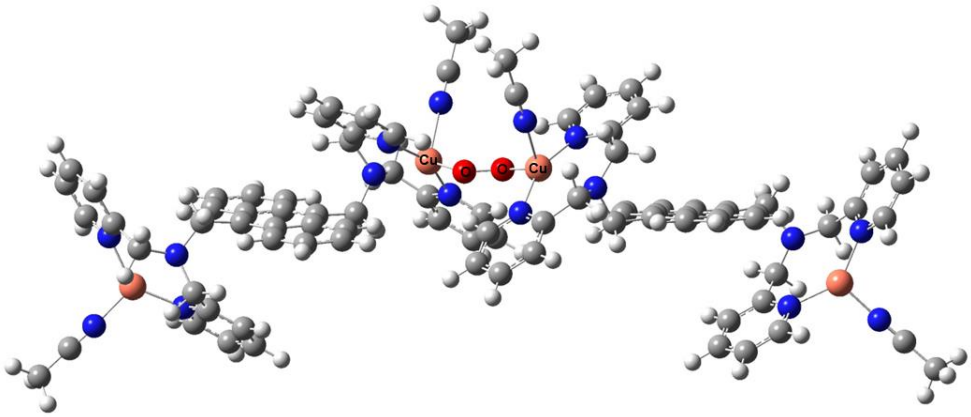

Figure 9. Proposed structure of an end-on Cu_2O_2 intermediate by DFT calculations

At first glance, it might be unusual to propose an end-on peroxo species with tridentate ligands. However, X-ray structure of $[Cu_2(\mathbf{addpa})]^{4+}$ both before and after catalytic O_2 reduction as well as $[Cu_2(\mathbf{addpa})]^{2+}$ from our calculations revealed that CH_3CN served as an additional ligand. As a result, the copper centers possessed insufficient vacant sites to adopt a side-on intermediate. The proposed intermediate was also consistent with our experimental data as its basic and nucleophilic nature would give H_2O_2 product. After protonation of the peroxo intermediate, the other remaining Cu(I) center in each complex could reduce another O_2 molecule to complete the catalytic cycle.

4.7 Reaction of $[Cu(adpa)]^{2+}$ with ascorbic acid under ambient condition

As mentioned earlier, reduction of $[Cu(\mathbf{adpa})]^{2+}$ with AsH_2 in CH_3CN was successfully investigated by UV-vis and ^{1}H-NMR. Both spectroscopic data indicated a complete generation of $[Cu(\mathbf{adpa})]^{+}$ species, and it was found to be relatively stable in the air or O_2 for at least 5 h. This result prompted us to think that this copper complex might find an application in ascorbic acid sensing. However, detection of natural reducing agents should be carried out in aqueous solution for practical use. Thus, the CH_3CN solvent was change to the mixed solvent of H_2O/CH_3CN

(7:3 v/v). It was found that [Cu(**adpa**)]$^{+}$ could not be completely formed and also gradually reoxidized to Cu(II), suggesting its higher reactivity with O_2 in aqueous solution (Figure 10).

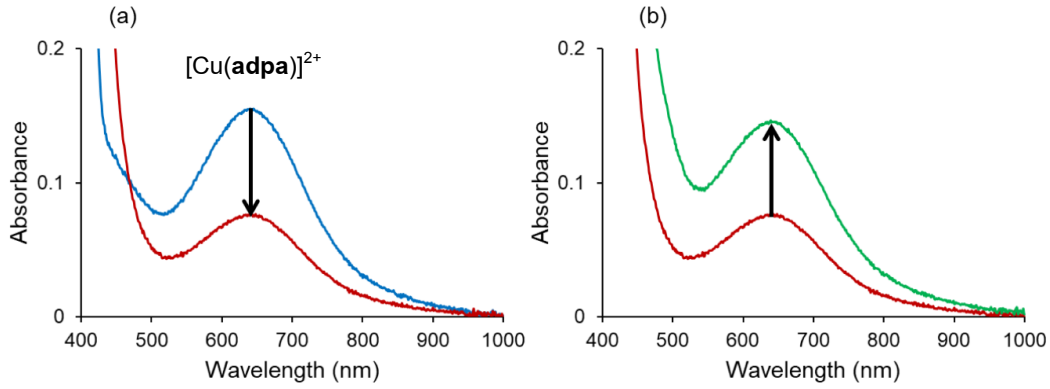

Figure 10. Monitoring *d-d* band of Cu**(adpa)** in H_2O/CH_3CN (7:3 v/v) at (a) 2 min; and (b) 2 h after addition of AsH_2 (1.0 equiv) in aerobic atmosphere

From the previous works, several researchers reported that modulation of secondary coordination sphere such as non-covalent interaction, especially, metal-□ and the addition of electron withdrawing groups (e.g. Lewis acid cations) influences redox potentials of copper center, leading to change in reactivity and stability. In our work, we modulated the secondary coordination sphere of the Cu center by addition of Zn(II) in combination with acetate anions (bridging ligand) to fine-tune the reactivity of copper complexes toward ORR in aqueous solution.

To test our hypothesis, reduction of [Cu(**adpa**)]$^{2+}$ by AsH_2 (1 equiv) in H_2O/CH_3CN (7:3 v/v) was performed under aerobic atmosphere in the presence of 8 equiv of $Zn(OAc)_2$, $Zn(NO_3)_2$ or Zn(phen)$_2$. It was found that *d-d* transition band of Cu(II) (λ_{max} = 632 nm) completely disappeared upon the addition of AsH_2 only in the presence of $Zn(OAc)_2$, and the spectrum was stable for at least 60 min before the *d-d* band started to increase, implying the regeneration of Cu(II) (Figure 11). This could suggest that $Zn(OAc)_2$ can help facilitating reduction of [Cu(**adpa**)]$^{2+}$ and stabilizing the Cu(I) species as well. The results also demonstrated to the important role of acetate anions for Cu(I) stabilization. It was proposed that Zn(II) may help to stabilize Cu(I) species via acetate bridging.

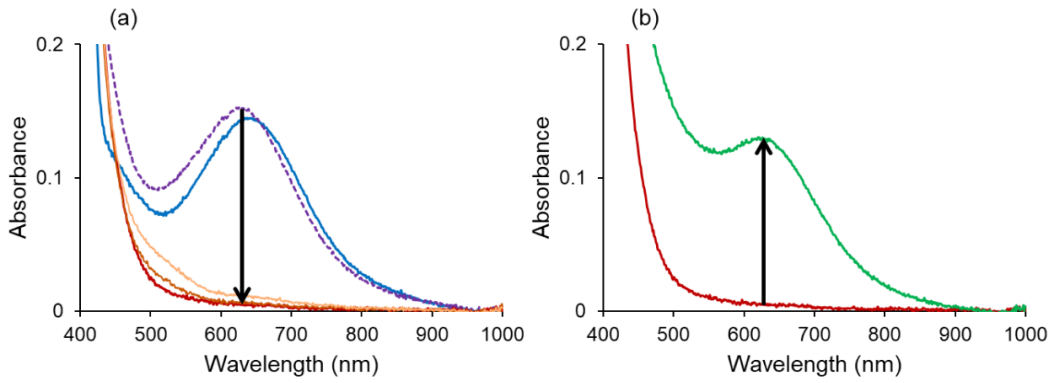

Figure 11. (a) Stability test for Cu(I) species generated from reaction of $[Cu(\mathbf{adpa})]^{2+}$ and AsH_2 in the presence of $Zn(OAc)_2$ in aqueous solution: 2 min (—), 30 min (—) and 60 min (—) after AsH_2 addition (b) Regeneration of $[Cu(\mathbf{adpa})]^{2+}$ after exposed to air for 4 h

Moreover, it should be noted that $[Cu(\mathbf{adpa})]^{+}$ was stable for at least 2 h in H_2O/CH_3CN (1: 4 v/v) buffered with acetic-acetate buffer solution (ABS) at pH 5.6. To confirm that no transmetalation between Zn(II) and Cu(**adpa**), H_2O_2 was employed to reoxidize Cu(I) species from reaction of $[Cu(\mathbf{adpa})]^{2+}$ and AsH_2. The results showed that the $[Cu(\mathbf{adpa})]^{2+}$ was immediately regenerated upon addition of H_2O_2 (Figure 12). This data confirmed that the redox reaction of Cu(**adpa**) in the presence of $Zn(OAc)_2$ was reversible, and transmetalation did not proceed.

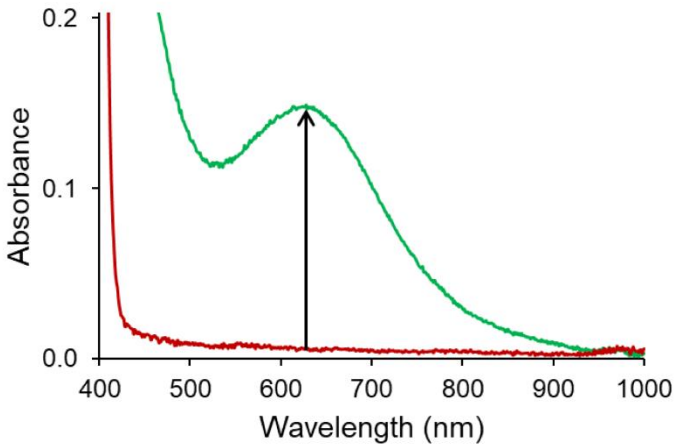

Figure 12. Regeneration of $[Cu(\mathbf{adpa})]^{2+}$ after addition of H_2O_2 (10 equiv) to the solution containing Cu(I) species in aqueous solution

To point out the essential role of Zn(II) for Cu(I) stabilization, the Zn(II) ions was changed to other divalent cations (e.g. Mg(II), Ca(II) and Cd(II)) in Cu(II) reduction reactions. It was found that the $[Cu(\mathbf{adpa})]^{+}$ was stabilized by Zn(II) more than Cd(II), Mg(II) and Ca(II), respectively. The stronger Lewis acidity of Zn(II) was accounted for better stabilizing Cu(I) by delocalization of electrons through OAc^- bridge, analogous to an imidazolate-bridged Cu-Zn model for CuZnSOD. All evidence pointed out that both Zn(II) and OAc^- are required to facilitate reduction of the Cu(II) complex and stabilization of the Cu(I) redox state in aqueous solution.

4.8 Fluorescence measurements for Cu(adpa) and Cu(atpa) in the presence of ascorbic acid

The approach for Cu(I) stabilization by Zn(II) combination of OAc^- was applied in ascorbic acid sensing. Fluorescence spectroscopy was selected due to its high sensitivity, simple and rapid technique. As a molecular sensor, Cu(**adpa**) contains a dipicolylamine Cu active site and anthracene as a sensory unit. Redox state change of the Cu center provides different fluorescent signals. When AsH_2 reacted with copper(II) complex, the Cu(II) was reduced to Cu(I) leading to magnetic properties conversion. $[Cu(\mathbf{adpa})]^{2+}$ did not give the fluorescence signal owing to the presence of Cu(II) paramagnetic ion. Upon addition of AsH_2 to $[Cu(\mathbf{adpa})]^{2+}$, the fluorescent signal was emitted at 421 nm which is consistent with the conversion of Cu(II) to a diamagnetic Cu(I) complex as illustrated in Figure 13. This indicated that the AsH_2 can be detected by our fluorescence sensor, $[Cu(\mathbf{adpa})]^{2+}$.

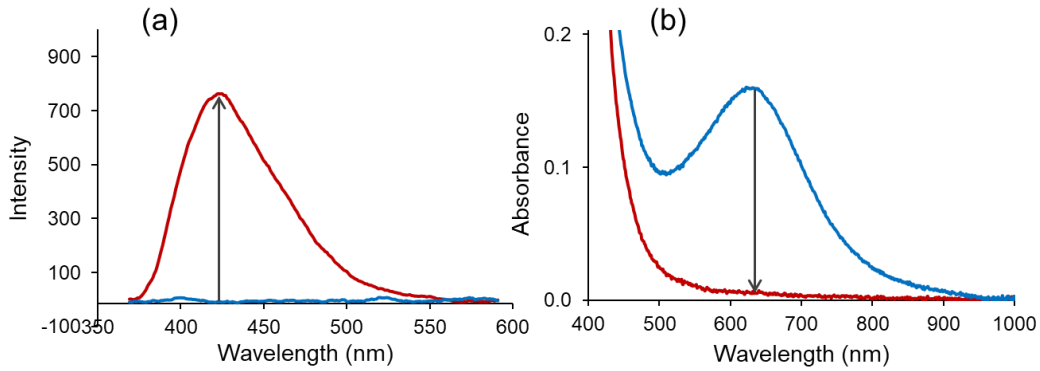

Figure 13. Change in (a) Fluorescence signal (Excitation wavelength = 340 nm, slit setting on instrument = 10 and PMT = 500); and (b) UV-vis spectrum upon addition of AsH_2 (1 equiv) into $[Cu(\mathbf{adpa})]^{2+}$ solution in the presence of Zn(II) in H_2O/CH_3CN (7: 3 v/v) buffered with ABS at pH 5.6

To expand the pH range of our detection, $[Cu(\mathbf{atpa})]^{2+}$ containing a tetradentate ligand was prepared to reduce chelation effect by glutathione. The tetradentate ligand was expected to more tightly bind to the Cu center than the tridentate ligand in **adpa**. The results revealed that Cu(**atpa**) showed highly selective detection for AsH_2 among various natural reducing agents (sugar group, citric acid and glutathione) as compared to Cu(**adpa**). In addition, the molecular probe, Cu(**atpa**) also demonstrated no interference (Figure 14) which was suitable for AsH_2 sensing in the next step.

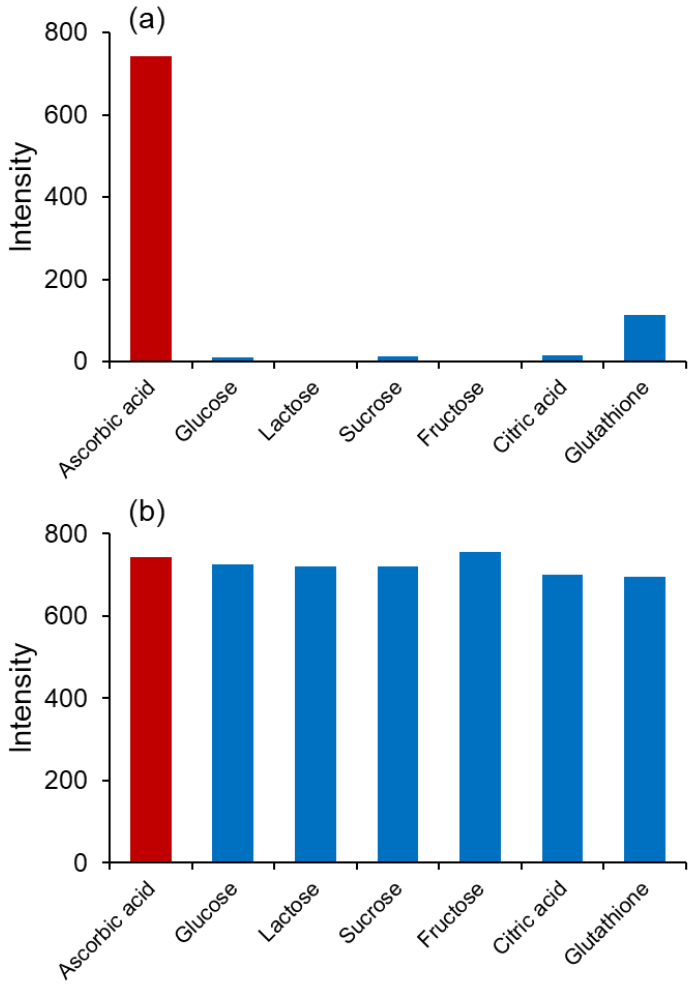

Figure 14. a) Selectivity and (b) interference study for AsH_2 detection using our sensor. The concentration of Cu(**atpa**) = 10 μM, $Zn(OAc)_2$ = 40 equiv and λ_{ex} = 340 nm.

4.9 Limit of detection and determination of AsH_2 in vitamin C tablets

Limit of detection (LOD) for AsH_2 was 163 nM which could be determined by $3\sigma/S$; σ is the standard deviation for the blank solution, n = 10, and S is the slope of the calibration curve. Moreover, our sensor was subsequently employed to measure the AsH_2 amount in vitamin C tablets to verify our accurate detection in real samples. The determination of AsH_2 by our system with standard addition method was consistent with acceptable quantitative analysis by HPLC, and was closed to the amount specified on the vitamin C tablets (1.00 g). Also, recovery was in between 101 and 104, and relative standard deviation was 1.5 - 4.0. This demonstrated the high accuracy of our method.

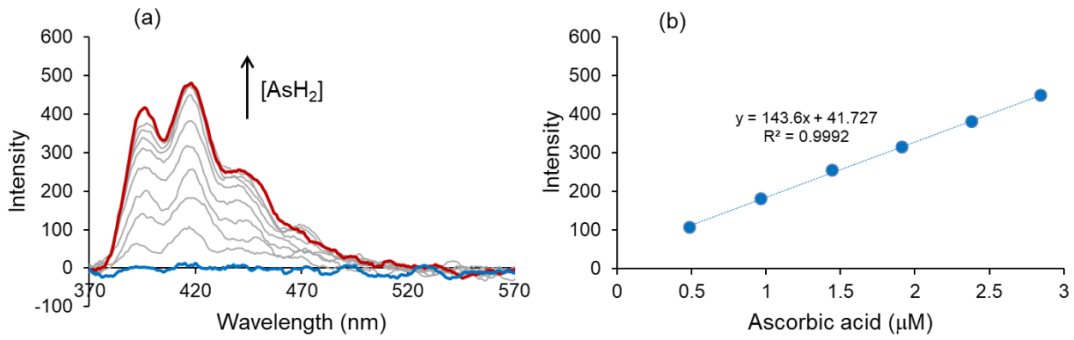

Figure 15. (a) Fluorescence titration curves of Cu(**atpa**) (10 μM) in the presence of $Zn(OAc)_2$ (40 equiv) with AsH_2 and (b) plot between fluorescence intensity and concentration of ascorbic acid (μM) (Fluorescence parameters: excitation wavelength = 340 nm, slit setting on instrument = 10 and PMT = 530)

5. Conclusions

In this research, we pointed out an importance of ligand design to fine-tune reactivity of the metal mediators toward O_2. In the first project, copper complexes with a series of dipicolylamine ligands were developed to activate O_2 and to study the structure-reactivity correlation. Variation of ligand attributes in the copper complexes by introducing conjugated-π systems of anthracenyl scaffold as well as different nuclearity were found to have an effect on ORR activity. For chemical reduction of Cu(II) complexes, ascorbic acid which is an environmentally benign reducing agent was employed to provide both electrons and protons to participate in ORR. The presence of anthracene moiety helps to facilitate the reduction of Cu(II) complex and to stabilize the Cu(I) redox state. Also, it was demonstrated that the dinuclear complex exhibited higher ORR activity than the mononuclear analogue. Overall, Cu_2(**addpa**) showed the best activity for ORR. Our studies indicated that ORR could be mediated by Cu_2(**addpa**) *via* intermolecular two-electron transfer process and subsequently produced H_2O_2 as a product.

As an example of applications from study of structure-reactivity relationship in the first project, a stable complex $[Cu(\textbf{adpa})]^+$ in CH_3CN under aerobic system found a potential use in ascorbic acid sensing. The copper complex rapidly reacted with AsH_2 to generate a stable Cu(I) species which resulted in fluorescence enhancement. Although $[Cu(\textbf{adpa})]^+$ in CH_3CN was ORR inactive, it seemed to be more active in aqueous solution. The problem was solved by modulation of secondary coordination sphere around the copper center. It was found that Zn(II) in combination with OAc^- helped to stabilize the Cu(I) species in aqueous solution. In addition, changing the tridentate ligand in Cu(**adpa**) to a tetradentate ligand of Cu(**atpa**) helped to improve the selectivity for AsH_2 sensing. Furthermore, our sensor was successfully used for AsH_2 detection in vitamin C tablets with a simple, rapid and accurate method.

6. Appendix

6.1 A research article: “Tuning reactivity of copper complexes supported by tridentate ligands leading to two-electron reduction of dioxygen” published in Dalton Transactions (IF = 4.099).

Suktanarak,P.; Watchasit, S.; Chitchak, K.; Plainpan, N.; Chainok, K.; Vanalabhpatana, P.; Pienpinijtham, P.; Suksai, C.; Tuntulani, T.; Ruangpornvisuti, V.; Leeladee, P. *Dalton Transactions*, **2018**, *47*, 16337 – 16349.

Dalton Transactions

PAPER

View Article Online
View Journal | View Issue

Check for updates

Cite this: *Dalton Trans.*, 2018, **47**, 16337

Tuning the reactivity of copper complexes supported by tridentate ligands leading to two-electron reduction of dioxygen†

Pattira Suktanarak,[a] Sarayut Watchasit,[b] Kantima Chitchak,[c] Nukorn Plainpan,[a] Kittipong Chainok,[d] Parichatr Vanalabhpatana,[a,e] Prompong Pienpinijtham,[a] Chomchai Suksai,[f] Thawatchai Tuntulani,[a] Vithaya Ruangpornvisuti[a] and Pannee Leeladee *[a,g]

A series of copper complexes bearing polypyridyl tridentate ligands have been prepared to fine tune their reactivity toward the oxygen reduction reaction (ORR). During the process of preparation of our copper complexes, we successfully obtained two new crystal structures which are $[Cu_2(\mu\text{-}Cl)_2(\mathbf{adpa})_2](ClO_4)_2$ (**2b**) and $[Cu_2(\mathbf{addpa})(CH_3CN)_2(ClO_4)_2](ClO_4)_2$ (**3a**) and a new structure $[Cu_2(\mathbf{addpa})(CH_3CN)_2(H_2O)_2](ClO_4)_4$ (**3b**) captured after the catalytic ORR. Electrochemical studies and stoichiometric chemical reduction of copper(II) complexes by ascorbic acid indicated that the presence of an anthracene unit helps to facilitate the reduction of Cu(II) as well as the stabilisation of Cu(I) species. Regarding oxygen activation, the dinuclear Cu(I) complex **3a** showed significantly higher ORR activity than its analogous mononuclear complex **2a**. Complex **3a** was also found to be relatively robust and competent in catalytic O_2 reduction. The observed H_2O_2 product after this catalysis, together with the data obtained from DFT calculations supported that **3a** exhibited a $2H^+$, $2e^-$ catalytic activity towards the ORR as opposed to the expected $4H^+$, $4e^-$ process usually found in copper complexes with tridentate ligands. The proton (H^+) source for this process was expected from ascorbic acid which also serves as a reducing agent in this reaction. This work highlighted an approach for tuning the ORR activity of the copper complexes by the introduction of a conjugated-π moiety to the supporting ligand.

Received 4th August 2018,
Accepted 17th October 2018

DOI: 10.1039/c8dt03183e

rsc.li/dalton

Introduction

The catalytic reduction of dioxygen molecules (O_2) is one of the most fundamental reactions which plays a crucial role in both biological and industrial processes. In particular, a number of copper proteins are involved in proton-assisted catalytic reduction of O_2 to water (H_2O) and oxygenation of organic substrates accompanied by a two- or four-electron reduction of O_2 depending on the types of enzymes.[1] Thus, the four-electron reduction of O_2 mediated by synthetic copper complexes has gained considerable attention because of its mechanistic implication in multicopper oxidases (MCOs) such as laccases[2] as well as the development of a fuel cell technology using this Earth-abundant metal.[3,4] Recently, the catalytic two-electron reduction of O_2 to H_2O_2 has also attracted great interest since H_2O_2 is a promising candidate as a clean energy carrier and can be used in simple one-compartment fuel cells.[3,4] H_2O_2 is also regarded as a versatile and environmentally benign oxidising agent.[3–5] Compared to a large number of published reports on the catalytic four-electron O_2 reduction

[a]Department of Chemistry, Faculty of Science, Chulalongkorn University, Bangkok 10330, Thailand. E-mail: pannee.l@chula.ac.th
[b]Nuclear Magnetic Resonance Spectroscopic Laboratory, Science Innovation Facility, Faculty of Science, Burapha University, Chonburi 20131, Thailand
[c]Program of Petrochemistry and Polymer Science, Faculty of Science, Chulalongkorn University, Bangkok 10330, Thailand
[d]Materials and Textile Technology, Faculty of Science and Technology, Thammasat University, Pathum Thani 12121, Thailand
[e]Electrochemistry and Optical Spectroscopy Center of Excellence, Department of Chemistry, Faculty of Science, Chulalongkorn University, Bangkok 10330, Thailand
[f]Department of Chemistry and Center for Innovation in Chemistry, Faculty of Science, Burapha University, Chonburi 20131, Thailand
[g]Research Group on Materials for Clean Energy Production STAR, Department of Chemistry, Faculty of Science, Chulalongkorn University, Bangkok 10330, Thailand

†Electronic supplementary information (ESI) available. CCDC 1543792–1543794. For ESI and crystallographic data in CIF or other electronic format see DOI: 10.1039/c8dt03183e

reaction (ORR) with copper-based systems,[6–9] only a few examples have been reported for the two-electron reduction of O_2 catalysed by copper complexes.[10–12] There are a variety of factors that can control the catalytic two- *versus* four-electron reduction of O_2, including the ligand type and nature of the resulting copper–oxygen (Cu_nO_2) intermediates.[11] In this regard, studies of homogeneous metal complexes in solution are particularly useful to gain insight into the mechanistic details of the O_2 activation process.

In the literature, one of the most important strategies to fine tune the reactivity and stability of metal complexes is the ligand design. In particular, several research groups have developed polypyridyl scaffolds, especially pyridyl-based tripodal ligands such as tris(2-pyridylmethyl)amine (**tpa**) and its derivatives to allow spectroscopic characterisation of putative copper–dioxygen species (Cu_nO_2),[8,9,13,14] which have been postulated as key intermediates in several copper-containing proteins.[1,15–17] These synthetic copper complexes have been examined to mediate the oxygen reduction reaction (ORR)[2,6–9] with an ultimate goal to obtain efficient biomimetic catalysts for fuel cell technologies and water treatment.[3,18–20] For example, $[Cu(\mathbf{tpa})(H_2O)]^{2+}$ was shown to have the lowest ORR overpotential at pH 1 when compared to other synthetic copper catalysts. However, modification on the Cu(**tpa**) platform did not show a significant improvement in ORR catalysis. Therefore, more variation in the design of Cu(**tpa**) catalysts is required for further development.[21–23] Recently, a copper complex bearing a **tpa** derivative *i.e.*, 2,2′-dipicolylamine (**dpa**) was studied to mimic the T3-site of laccase and was shown to be an active electrocatalyst for the ORR.[2] Hence, modification of Cu(**dpa**) could be a potential approach for the development of ORR catalysis.

In addition to the types of coordinated ligands, delocalised-π electron moieties could also influence the reactivity and stability of the biomimetic copper complexes. The conjugated-π systems in the ligand tend to participate in non-covalent interactions such as metal–π, anion–π, π–π and H-bonding,[24–33] and these interactions affect the electronic structures of the complex which, in turn, control its reactivity. It has been previously reported that the Cu(I) centre with a pyridyl-based dipicolylamine tridentate ligand can be stabilised by Cu(I)–arene interactions. Itoh and co-workers noted a small change in the supporting ligands *i.e.*, the substituents on the phenyl group of the ligand sidearm and alkyl linker chain, has a huge impact on the Cu(I)–arene interactions and the reactivity towards O_2.[34–38] Moreover, it was demonstrated that a number of copper-based electrocatalysts suffered from their poor long-term stability, partly due to inefficient electron transfer from the support to the catalyst. Therefore, introduction of an anthracene unit to the copper complexes is expected to help in this regard since anthracene and other aromatic groups have been shown to facilitate such an electron transfer process, leading to the observed higher ORR activity.[39–41] In addition, the number of nuclearities in the complexes can result in synergistic cooperation in O_2 binding. In fact, cooperative catalysis has been proposed as a mode of action found in many metalloenzymes.[42] This bimetallic cooperative strategy is particularly useful when the system exhibits higher reactivity than that obtained from the mononuclear analogue. Examples of these metalloenzymes are copper-based oxidases and oxygenases.[43] Inspired by these enzymes, the design of the dinucleating ligand could be useful to control the metal-based catalytic reactivity. In particular, studies on the influence of the linkage on the promotion of electron transfer between two copper sites serve as models for non-coupled binuclear copper enzymes such as dopamine β-monooxygenase (DβM) and peptidylglycine α-hydroxylating monooxygenase (PHM).[44–46] Recently, it was shown that intramolecular π–π stacking interactions were observed when the anthracenyl spacer was employed in a synthetic dinuclear copper complex. These interactions influenced the geometry and electronic properties of the complex, which would have an effect on its reactivity towards O_2 reduction.[14]

Although a number of bioinspired copper complexes based on **tpa** and **dpa** derivatives with aromatic moieties have been reported, new reactivity of copper species is still emerging and remains unexplored.[47,48] Particularly, only a few researchers studied the effect of delocalised π-electron moieties on the ORR activity of the biomimetic copper complexes.[34–37] To the best of our knowledge, the oxidase reactivity of copper complexes bearing dipicolylamine and anthracene scaffolds has not been reported yet.

Herein, a series of bioinspired-copper complexes based on dipicolylamine (**dpa**) and anthracene (Chart 1) for O_2 activation was investigated. The influence of delocalised π-electron moieties (anthracene) and nuclearities (mononuclear *vs.* dinuclear) on the reactivity of the complexes was examined. It was demonstrated that the presence of the anthracene moiety facilitates the Cu(II) reduction process and the reactivity of Cu(I) species. Moreover, ascorbic acid known as a natural reducing agent was introduced in our study as a source of both

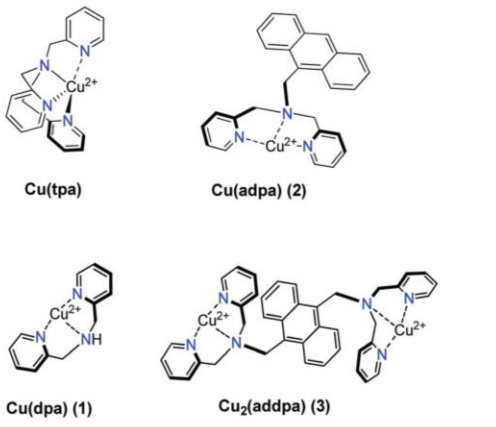

Chart 1

electrons and protons. Our dinuclear copper complex (**3a**) was shown to be competent in the catalytic two-electron reduction of O_2 to H_2O_2. X-ray crystal structures and DFT calculations also helped in gaining further insight into the molecular understanding of the structure–reactivity correlation of the copper complex catalysts.

Results and discussion

Synthesis of the ligands and copper(II) complexes

All ligands were synthesised according to modified published procedures with moderate yields.[49,50] The corresponding Cu(II) complexes were prepared by adding a solution of $Cu(ClO_4)_2$ in CH_3OH to the ligand dissolved in CH_2Cl_2. The Cu(II) products were then precipitated spontaneously. Our choice of copper over other metals was especially inspired by Nature's choice of Cu over Fe in heme-copper oxidases. An intriguing study indicated that the high redox potential and the rich electron density in the d orbitals of Cu are key to its high reactivity towards oxygen reduction.[51] Furthermore, our attempts to crystallise the Cu(II) product after the reaction of Cu^{I}_2(**addpa**) with O_2 resulted in dark green crystals suitable for X-ray structural characterisation (*vide intra*). As a result, we have successfully obtained three new crystal structures which are $[Cu_2(\mu\text{-}Cl)_2(\mathbf{adpa})_2](ClO_4)_2$ (**2b**), $[Cu_2(\mathbf{addpa})(CH_3CN)_2(ClO_4)_2](ClO_4)_2$ (**3a**) and $[Cu_2(\mathbf{addpa})(CH_3CN)_2(H_2O)_2](ClO_4)_4$ (**3b**) by X-ray crystallography (Table 1). All copper complexes were also characterised by other standard analytical methods including elemental analysis, mass spectrometry, and UV-vis and EPR spectroscopy. The UV-vis spectra of all Cu(II) complexes exhibit Cu(II) d–d transitions with absorption maxima in the range of 580 to 610 nm.

X-ray crystal structures

To gain insights into the correlation between the complex structures and their reactivity, all copper complexes were examined crystallographically. The crystal structure of $[Cu(\mathbf{dpa})(CH_3CN)(ClO_4)][ClO_4)]$ (**1**) was previously reported.[52] The geometry around the Cu(II) centre was best described as a distorted square pyramid with the basal plane formed by three nitrogen atoms of the ligand and one nitrogen atom of the acetonitrile molecule. The apical position was found to be occupied by an oxygen atom from the ClO_4^- anion.

Our initial attempt to synthesise $[Cu(\mathbf{adpa})(H_2O)(ClO_4)_2]\cdot 0.5H_2O$ (**2a**) from the reaction of $Cu(ClO_4)_2$ with **adpa** in mixed CH_2Cl_2/CH_3CN solution yielded a dinuclear doubly chloro-bridged copper(II) complex $[Cu_2(\mu\text{-}Cl)_2(\mathbf{adpa})_2](ClO_4)_2$ (**2b**), in which the chloro ligands can only come from CH_2Cl_2. This complex crystallises in the centrosymmetric monoclinic space group $P21/n$ and the asymmetric unit contains a Cu(II) atom, one **adpa** ligand, one Cl^- ligand, one disordered ClO_4^- anion, and unmodeled highly disordered solvent molecules (Fig. S1†). As shown in Fig. 1a, the **adpa** and chloride ions act as a tridentate chelating ligand and as bridging ligands, respectively, by linking the **2a** fragments to form a Cu_2Cl_2 rectangular core with a Cu···Cu separation of 3.5572(9) Å. Each Cu(II) centre displays a five-coordinate distorted square pyramidal geometry, belonging to the SP-I type,[53] with the trigonality parameter τ of 0.18 (τ is defined as $(\beta-\alpha)/60$, where β and α are the two *trans*-basal angles, (ideally, τ = 0 and 1 for square pyramidal and trigonal bipyramidal environments, respectively).[54] The small bite angles of the tridentate **adpa** ligand (*viz.* Cl1–Cu1–N2 = 176.30(7)° and N1–Cu1–N3 = 165.38(10)°, Table S2†) is the most likely cause for the distortion of the ideal square pyramidal environment of the Cu(II) atoms. The Cu–N bond lengths (1.980(2)–2.031(2) Å) and the Cu–Cl bond

Table 1 Crystal data and structural refinement for complexes **2b**, **3a**, and **3b**

Compound	**2b**	**3a**	**3b**
Empirical formula	$C_{54}H_{46}Cl_4Cu_2N_6O_8$	$C_{44}H_{42}Cl_4Cu_2N_8O_{16}$	$C_{44}H_{46}Cl_4Cu_2N_8O_{18}$
Formula weight	1175.85	1207.73	1243.77
Temperature (K)	296	296	296
Wavelength (Å)	0.71073	0.71073	0.71073
Crystal system	Monoclinic	Triclinic	Triclinic
Space group	$P2_1/n$	$P\bar{1}$	$P\bar{1}$
a (Å)	11.5432(11)	8.4013(6)	10.0380(3)
b (Å)	12.0648(12)	9.4328(6)	10.6269(3)
c (Å)	20.0110(18)	16.0385(11)	12.7725(4)
α (°)	90	84.045(2)	109.7640(10)
β (°)	94.684(3)	84.266(2)	95.8450(10)
γ (°)	90	78.661(2)	97.6530(10)
V (Å^3)	2777.6(5)	1235.36(15)	1254.94(7)
Z	2	1	1
D_{calcd} (g cm^{-3})	1.406	1.623	1.646
μ (mm^{-1})	1.015	1.156	1.143
Reflns collected/unique	51 374/5692	29 505/4537	42 084/5996
GOF on F^2	1.023	1.031	1.024
R_{int}, R_{sigma}	0.093, 0.0460	0.1042, 0.0610	0.0401, 0.0260
R_1, wR_2 [$I > 2\sigma(I)$]	0.0448, 0.1120	0.0596, 0.1361	0.0430, 0.1074
R_1, wR_2 (all data)	0.0693, 0.1240	0.1027, 0.1562	0.0618, 0.1175
Max./min. residual (e Å^{-3})	0.47/−0.71	0.59/−0.59	0.60/−0.48

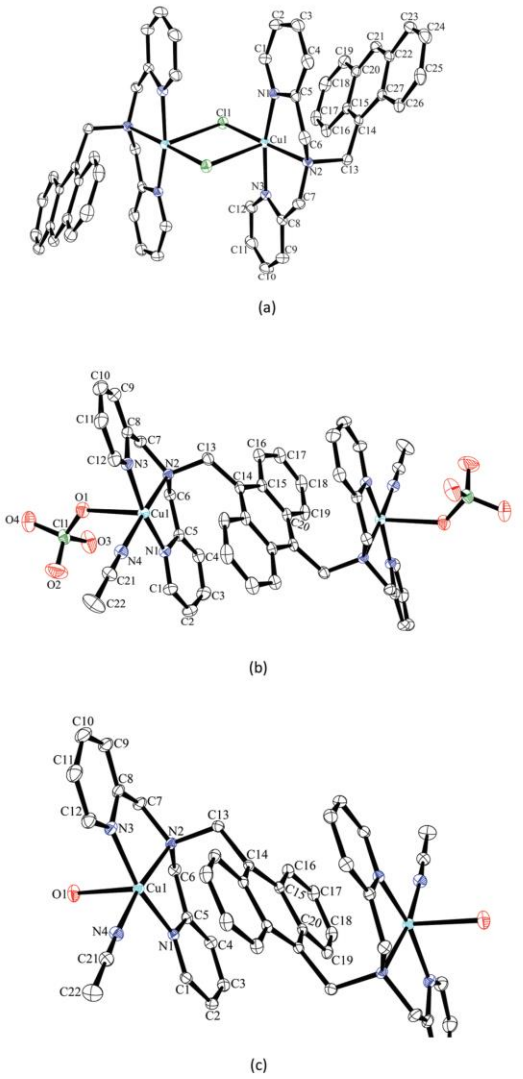

Fig. 1 Coordination environment of the Cu(II) ion in the complexes (a) $[Cu_2(\mu\text{-}Cl)_2(\mathbf{adpa})_2](ClO_4)_2$ (**2b**), (b) $[Cu_2(\mathbf{addpa})(CH_3CN)_2(ClO_4)_2](ClO_4)_2$ (**3a**), and (c) $[Cu_2(\mathbf{addpa})(CH_3CN)_2(H_2O)_2](ClO_4)_4$ (**3b**). Displacement ellipsoids are drawn at 30% probability.

lengths (1.980(2) and 2.031(2) Å, Table S2†) in this complex are comparable to those observed in the dinuclear doubly chloro-bridged Cu(II) complexes with the $[CuN_3Cl_2]$ chromophore.[53,55–57]

In the crystal of the discrete 0D dimers, there exists intramolecular π–π stacking between the pyridyl and aryl rings of the **adpa** ligand (centroid to centroid distance = 3.546(3) Å). Moreover, intermolecular C–H···π interactions are perceived between the adjacent dimers, which assists the formation of 2D supramolecular sheets in the *bc* plane (Fig. S2 and Table S3†). These sheets are further connected *via* C–H···O hydrogen bonds involving the ClO_4^- anion and the **adpa** ligands, completing the 3D supramolecular network (Fig. S3†). Since no chloride source was added during the reaction and crystallisation, the origin of the chloro bridging ligand is likely from the CH_2Cl_2 solvent. In addition, similar reactivities of metal complexes toward a halogenated solvent have been observed previously.[58–61]

To eliminate the effects of Cl^- which is a strong binding anionic ligand and to examine **2a** as a mononuclear complex, **2a** was prepared in the absence of a halogenated solvent following a reported synthetic procedure.[25] The crystal structure of the complex prepared by this method was also reported.[25] The Cu(II) centre adopted a distorted octahedral geometry with three nitrogen atoms from the ligand and one oxygen from water at the equatorial sites and two oxygen atoms from ClO_4^- anions in the axial positions. There was also intermolecular anion–π interaction between the bound ClO_4^- anions and the aromatic rings of the adjacent anthracenyl groups.

Moreover, our structural analysis revealed that **3a** and **3b** crystallise in the triclinic space group $P\bar{1}$, and are dinuclear cationic species as shown in Fig. 1b and c. The asymmetric unit of both compounds contains a half of the centrosymmetric dinuclear complex cation and counter ClO_4^- anions, in which the inversion centres are at the middle of the anthracene ring of the ligands (Fig. S4†). The Cu(II) centre is five-coordinated with the basal plane formed by three nitrogen atoms of the ligand (Cu–N = 1.963(4)–2.032(4) Å for **3a**, and 1.981(2)–2.035(2) Å for **3b**, Table S2†) and one nitrogen atom of the acetonitrile molecule (Cu–N = 1.982(5) Å for **3a** and 1.994(2) Å for **3b**), while the apical position was occupied by a coordinated oxygen of a ClO_4^- anion (Cu–O = 2.442(4) Å) for **3a** or an oxygen atom from a coordinated water molecule (Cu–O = 2.295(2) Å) for **3b**. The geometries around the copper(II) atom in both complexes are best described as distorted square pyramidal CuN_4O_1 environments with the value of the trigonality parameter τ being 0.13 and 0.04 for **3a** and **3b**, respectively. The Cu···Cu separation along the length of the ligands in **3a** (8.9151(14) Å) is slightly longer than that in **3b** (7.7310(6) Å), possibly due to the steric effects as well as the intermolecular interactions involving the coordinated water molecules and ClO_4^- anions at the apical positions. The large Cu···Cu distance found in both complexes resulted in no paramagnetic coupling between the two copper centres as confirmed by EPR analysis (see Fig. 5).

Similar observations were found in the dinuclear Cu(II) complex above, and there exist intermolecular π–π (3.655(3) Å) stacking interactions in the crystal of **3a**. Each dimer in **3a** is linked together by intermolecular π–π stacking between the pyridyl rings of the **adpa** ligands (3.812(4) Å), forming a 1D supramolecular chain parallel to the *c* axis (Fig. S5†). A combination of C–H···O hydrogen bonds (Table S2†) involving the ClO_4^- anions and the **adpa** ligands together with anion···π interactions between the ClO_4^- anion and the pyridyl ring of the **adpa** ligand (O8A···centroid (N3/C8–12) = 3.085(12) Å)

links the 1D chains into the 3D supramolecular structure (Fig. S6†). Significantly, the replacement of ClO_4^- in the apical position by water substituents makes a difference to the solid-state structure of complexes **3a** and **3b**. In the absence of intermolecular π–π stacking and with no anion···π interactions, the overall 3D packing in **3b** is stabilised by O/C–H···O hydrogen bonds (Table S2†) and intramolecular π–π (3.5339(15) Å) stacking interactions (Fig. S7†).

Notably, the structure of the Cu(II) product after O_2 reduction (**3b**) resembled that of the Cu(II) starting material except that complex **3b** has H_2O as an axial ligand instead of ClO_4^-. This may imply that the axially ligated ClO_4^- dissociated from the Cu(II) centre to generate a vacant site for O_2 binding during the reaction.

Electrochemical properties of the copper(II) complexes

To investigate the electrochemical behaviours especially the reduction characteristic of **1**, **2a**, and **3a**, their cyclic voltammograms in deaerated dimethylformamide (DMF) solutions containing 0.10 M tetrabutylammonium hexafluorophosphate ($TBAPF_6$) were acquired in the cathodic domain. Fig. 2 depicts the cyclic voltammograms collected from +0.30 to −1.20 to +0.30 V at a scan rate of 100 mV s^{-1} for the solutions of 1.00 mM Cu(II) complexes. Voltammogram (a) recorded as a background cyclic voltammogram exhibits no significant peaks of DMF–$TBAPF_6$ electrolyte solution. As displayed in voltammograms (b)–(d), the reduction of all three complexes reveals a single Cu(II)–Cu(I) redox couple, and the electrochemical data are summarized in Table 2. These characteristics of metal-centred electron transfer have been seen in earlier studies of the reduction of Cu^{II}(**dpa**) and its derivatives.[14,62–64]

A direct comparison between the cyclic voltammograms of mononuclear **1** and **2a** suggests that the presence of an anthracene moiety in the complex structure helps to facilitate the reduction process since **2a** can be electrochemically reduced at a less negative potential (~150 mV) than **1**. The differences of the cathodic peak potential (E_{pc}) and the anodic peak potential (E_{pa}), symbolised by ΔE_p, of the Cu(II)–Cu(I) redox couple for the **1** and **2a** reduction are 81 and 88 mV, respectively. It is worthwhile to mention that an electron transfer in high-resistance organic media always gives a ΔE_p value larger than the theoretical value of $59/n$ mV[66] and the ΔE_p for a reversible one-electron ferrocene/ferrocenium ion (Fc/Fc^+) redox couple in DMF–0.10 M $TBAPF_6$ has a value of 81 mV (data not shown). In addition, the ratios of anodic and cathodic peak currents (i_{pa}/i_{pc}) for the Cu(II)–Cu(I) redox couple are 0.96–0.99 (approximately 1). All these results confirm that the reduction of **1** and **2a** appears reversible and involves one electron, indicating the stability of the reduced forms of both complexes under these experimental conditions.

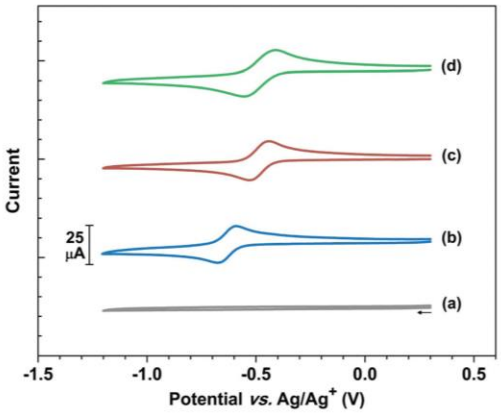

Fig. 2 Cyclic voltammograms recorded with a glassy carbon electrode (area = 0.071 cm^2) at 100 mV s^{-1} from +0.30 to −1.20 to +0.30 V for (a) DMF containing only 0.10 M $TBAPF_6$; and DMF containing 0.10 M $TBAPF_6$ in the presence of 1.00 mM (b) **1**, (c) **2a**, and (d) **3a**.

Table 2 Electrochemical data for the reduction of complexes **1**, **2a**, and **3a** in DMF–0.10 M $TBAPF_6$

Complex	E_{pc} [a] (V)	E_{pa} (V)	$E_{1/2}$ [b] (V)	ΔE_p [c] (mV)	i_{pa}/i_{pc} [d]
1	−0.67	−0.59	−0.63	81	0.96
2a	−0.53	−0.44	−0.48	88	0.99
3a	−0.56	−0.41	−0.48	146	0.95

[a] The potential is quoted with respect to the Ag/Ag^+ reference electrode and externally calibrated with the Fc/Fc^+ redox couple having a potential of 0.542 V *vs.* the standard hydrogen electrode (SHE).[65] [b] $E_{1/2} = (E_{pc} + E_{pa})/2$, when E_{pc} = cathodic peak potential and E_{pa} = anodic peak potential. [c] $\Delta E_p = |E_{pa} - E_{pc}|$. [d] i_{pa}/i_{pc} = (anodic peak current)/(cathodic peak current).

In the case of **3a**, which is a dinuclear complex containing two Cu(II) centres, its reduction takes place at a potential more positive than that during the reduction of **1**, and the larger ΔE_p (146 mV) possibly arises from the overlapping of the peaks for two successive Cu(II)-to-Cu(I) reduction processes. As previously described in the publication dealing with dinuclear copper complexes,[14] the reduction of the second Cu(II) centre occurs at a slightly more negative potential. To check our hypothesis, we evaluated the integrated areas under the background-subtracted cyclic voltammetric curves of **1**, **2a**, and **3a** (Table S4†). Dividing the area (equal to $\int i\,dE$) by the scan rate results in the charge associated with the electron transfer reaction occurring in the experiment, *i.e.*,

$$\left(\int i\,dE\right) \times \upsilon^{-1} = Q \qquad (1)$$

where υ and Q represent the scan rate and charge, respectively. Regardless of the signs, the absolute areas corresponding to Cu(II)-to-Cu(I) reduction in the forward scan (above the *x*-axis) and Cu(I)-to-Cu(II) re-oxidation in the backward scan (below the *x*-axis) were combined. The area and also the charge obtained from the cyclic voltammogram of **3a** are approximately 1.7 times higher than the values from **1** and **2a**, implying the existence of a pair of one-electron Cu(II)-to-Cu(I) reductions at the two Cu(II) centres of **3a**.

Furthermore, the electrochemical behaviour of 1.00 mM **3a** in acetonitrile (CH_3CN)–0.10 M $TBAPF_6$ solution was explored by means of cyclic voltammetry (Fig. S8†). Owing to the solvent effect, more quasireversible feature and two close anodic peaks in the reverse scan are noticeable, confirming the overlap of two separate redox processes. Compared to the cyclic voltammogram of **3a** in DMF–$TBAPF_6$ (Fig. 2), a large positive (~350 mV) shift of the Cu(II)–Cu(I) redox couple peaks, which implies more favourable reduction, was found in CH_3CN medium. Hence, CH_3CN was chosen as one of the solvents used for reactivity studies of the complexes with O_2 in this work.

Cyclic voltammograms for the Cu complexes in DMF containing 0.10 M $TBAPF_6$ were further examined in the potential range extended to −1.80 V (Fig. S9†), allowing the metal-centred reduction of Cu(I) to Cu(0).[67,68] The appearance of a new and sharp anodic peak at −0.32 V along with a small pre-peak around −0.48 V in the voltammogram of **1** reflects the surface-confined process of the reoxidation of the electrode-attached Cu(0).[67–70] For **2a** and **3a**, no obvious peak for the metallic Cu(0) oxidation was detected. However, the formation of a tiny anodic peak/shoulder at about −0.60 V and the current enhancement of the Cu(I)-to-Cu(II) reoxidation peak suggest that the electrogenerated Cu(I) complexes might be fully reduced at a more negative potential. Due to the limited potential window of this voltammetric system, we cannot actually inspect this phenomenon. Under the same conditions, copper complexes containing anthracenyl scaffolds **2a** and **3a** tended to be more stable than Cu(**dpa**) (**1**) in terms of decomposition of Cu(I) to metallic Cu(0). Hence, **2a** and **3a** are expected to be more robust catalysts for the ORR.

Reduction of the copper(II) complex with ascorbic acid

From the UV-vis spectra, all Cu(II) complexes in this study exhibited broad and weak absorption bands around 600 nm, attributed to the forbidden d–d transitions of d^9-copper(II) ions. This UV-vis feature also indicated that all complexes in solution possessed a square-based pyramidal geometry (SBP) around the Cu centres in agreement with the result obtained in solid state by X-ray crystallography for **1** and **3a**.[14,71] **2a** is also expected to adopt a SBP geometry when dissolved in CH_3CN, a similar structure found in the case **3a** as well as other Cu complexes with **dpa** and a benzyl sidearm.[71] In addition, the UV-vis data may imply that intramolecular π–π stacking between the pyridyl and aryl rings of the ligands in **2a** and **3a** still remained in solution.

To investigate the ORR mediated by our copper complexes *via* chemical reduction, ascorbic acid (AsH_2) was introduced in our system as a reducing agent as well as a proton source. Under a N_2 atmosphere, addition of excess AsH_2 (dissolved in DMF/CH_3CN) to the solution of Cu(II) complexes in CH_3CN resulted in a colour change from blue (**1**, **2a**) or green (**3a**) to yellow, indicating the formation of new species. Monitoring these reactions by UV-vis titration revealed that the d–d band of Cu(II) decreased upon the addition of AsH_2 and completely disappeared when 0.5 equiv. or 1.0 equiv. of AsH_2 with respect

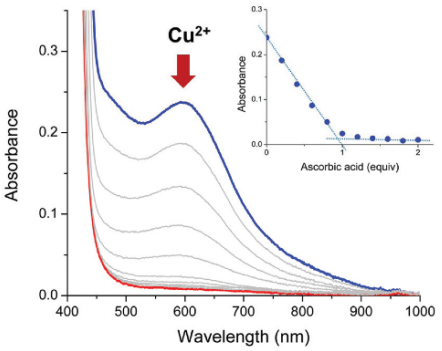

Fig. 3 UV-vis spectral changes upon the addition of AsH_2 (0–2.0 equiv.) to **3a** solution (1 mM) in DMF/CH_3CN. The inset shows the plot of absorbance at 593 nm *vs.* equiv. of AsH_2 added.

to **2a** and **3a** respectively was reached (Fig. 3 and Fig. S10†). This result suggested that AsH_2 served as a 2-electron reductant in our systems. Furthermore, the reduction of Cu(II) to Cu(I) was confirmed by ^{1}H-NMR and EPR spectroscopy (*vide infra*).

Interestingly, reduction of Cu(II) in these complexes was quite different. Upon addition of AsH_2 (0.5 equiv.) to **1**, even after 9 hours the reduction was not complete (Fig. S11†). In contrast, the d–d band of **2a** and **2b** entirely disappeared within 20 min after the addition of AsH_2 (0.5 or 1.0 equiv.). Such a difference could be derived from the attribute of the ligand structure. This is in good agreement with the electrochemical data that Cu complexes bearing an anthracene moiety illustrated a less negative shift of the reduction potential when compared to that of **1**, thus suggesting that the presence of the anthracene moiety helps in facilitating the Cu(II) reduction process.

Preparation of copper(I) complexes and their reactivity with O_2

As suggested by the UV-vis data, reduction of **1** to the Cu(I) species was more difficult than that of the Cu(II) complexes bearing an anthracene moiety. Results from ^{1}H-NMR also led to similar conclusions. Monitoring the reaction of **1** and AsH_2 by ^{1}H-NMR demonstrated that the signals of AsH_2 slowly disappeared, concomitant with the growth of new peaks around 4–5 ppm assigned to the oxidised form of AsH_2 (Fig. S12†). When a stoichiometric amount of AsH_2 was consumed, the diamagnetic spectrum of d^{10} Cu^I(**dpa**) was not observed, which could indicate the instability of the Cu(I) species. In other words, the Cu(I) species bearing the ligand **adpa** and **addpa** are significantly more stable than Cu^I(**dpa**), possibly due to the anthracene moiety which could help to delocalise the charge from nitrogen donors.[72,73] This finding highlighted the effect of delocalised π-electron moieties on the stability of the Cu(I) complexes.

Next, Cu(I) species bearing **adpa** and **addpa** were prepared from the reaction of Cu(II) complexes and AsH_2 at a high con-

centration (up to 10 mM) for ^{1}H-NMR and EPR studies. Preliminary results from UV-vis, EPR and ^{1}H-NMR spectroscopy showed that the same reaction could be performed in H_2O/CH_3CN instead of DMF/CH_3CN. In fact, the Cu(I) species in H_2O/CH_3CN seemed to be more reactive to O_2 since the regeneration step of Cu(II) complexes was much faster when compared to the same reaction in DMF/CH_3CN. This may be due to DMF serving as a strongly coordinating solvent in place of ClO_4^- which could inhibit the substrate (O_2) binding. Hence, reactivity studies of the copper complexes were carried out in H_2O/CH_3CN.

The ^{1}H-NMR spectroscopy of **2a** : AsH_2 (1 : 0.55) and **3a** : AsH_2 (1 : 1.5) in D_2O/CD_3CN revealed diamagnetic spectra with sharp peaks in the aromatic region for the ligands, in stark contrast to the paramagnetic spectra seen for the starting d^9 Cu(II) complexes (Fig. S16† and Fig. 4). The diamagnetic NMR spectra were consistent with those of the d^{10} Cu(I) products. Interestingly, the yellow solution of Cu^I(**adpa**) was found to be stable for at least 1 day at room temperature when exposed to air or O_2 (Fig. S16†). In contrast, when purging air or O_2 gas into the yellow solution of Cu^I_2(**addpa**), a paramagnetic spectrum of **3a** was regenerated within an hour corresponding to the colour change from yellow to green solution. The new signals around 4–5 ppm were assigned to the oxidised form of AsH_2 (Fig. 4).

Our initial assumption was that higher ORR activity of **3a** over **2a** would be simply derived from its more number of active sites. This was tested by comparison of the ORR activity between the two complexes with the same equivalents of copper centres *i.e.*, **2a** (2 mM) *vs.* **3a** (1 mM) (Fig. S17 and S18†). Interestingly, the reaction of Cu^I(**adpa**) + O_2 was much slower than that of **3a**, suggesting that the number of active sites cannot be the only factor responsible for the higher reactivity observed in **3a**. Given the crystal structure and intramolecular π–π stacking between the pyridyl and aryl rings in **3a**, the synergistic cooperation for O_2 binding between two Cu centres is also not likely to operate (*vide infra*). Therefore, the lower reactivity of Cu^I(**adpa**) towards O_2 may be due to the stronger influence of anthracene on the stabilisation of the mononuclear than the dinuclear complex. Since **3a** showed the best performance for ORR activity, we concentrated our further study only on this dinuclear complex.

Next, generation of Cu^I_2(**addpa**) and its O_2 reactivity were confirmed by EPR spectroscopy. The EPR signal due to paramagnetic Cu^{II}_2(**addpa**) disappeared upon addition of AsH_2, corresponding to the formation of diamagnetic Cu^I_2(**addpa**). The signal then reappeared after the reaction was exposed to air or O_2 (Fig. 5). EPR data also suggested that there is no magnetic coupling between the two copper centres. Additionally, the X-ray structure of **3a** revealed the long distance between Cu and Cu (8.915 Å), supporting a noncoupled dinuclear copper complex assignment. These results pointed out that intramolecular cooperative activation of O_2 by the two copper centres could not be operative in our system.

Structural characterisation of copper(II) species after O_2 reduction and its implication in the mechanism for 3a catalysed-O_2 reduction

Efforts were made to obtain single crystals for structural characterisation of the Cu(II) product following the reaction of Cu^I_2(**addpa**) with O_2. After the reaction was complete, Et_2O was added to obtain green precipitates. This solid was then recrystallised by vapour diffusion in CH_2Cl_2/CH_3CN, the same conditions as the crystallisation of **3a**. The mixture was allowed to stand for four weeks to afford dark green crystals, suitable for X-ray diffraction. As shown in Fig. 1(c), the structure of the Cu(II) product after O_2 reduction (complex **3b**) resembled that of the Cu(II) starting material except that **3b** has H_2O as an axial ligand instead of ClO_4^-. This may imply that the axially ligated ClO_4^- dissociated from the Cu centre to generate a vacant site for O_2 binding during the reaction. The coordinated H_2O

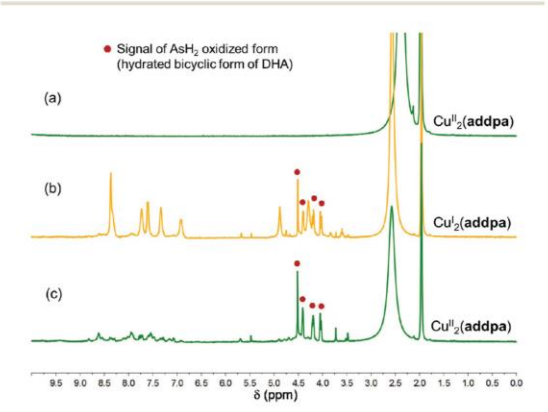

Fig. 4 ^{1}H-NMR spectra of (a) **3a** (10 mM) and (b) **3a** + AsH_2 (1 : 1.5 equiv.) in D_2O/CD_3CN and (c) after (b) was exposed to air for 2 h.

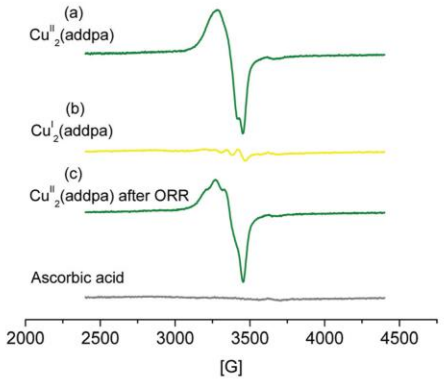

Fig. 5 EPR spectra of (a) **3a** (10 mM in CH_3CN), (b) **3a** + AsH_2 (1 : 1.5) and (c) (b) +O_2. The experimental parameters: microwave frequency = 9.838 GHz, microwave power = 0.620 mW, modulation amplitude = 5.00 G, modulation frequency = 100 kHz.

could be derived from residual water in the solvent or the product from the disproportionation of H_2O_2.

Catalytic O_2 reduction and the proposed mechanism

After performing the ORR mediated by **3a** + AsH_2 (1.5 equiv.), quantitative analysis by UV-vis and EPR signals showed that 85% of Cu_2^{II}(**addpa**) could be regenerated. This suggests that our Cu complex is quite robust and could be applicable for catalysis. Following the catalytic O_2 reduction of **3a** + AsH_2 (10 equiv.), ^{1}H-NMR data revealed the production of dehydroascorbic acid (AsH_2-oxidised product in hydrated bicyclic form),[74] whereas the signal of AsH_2 was completely absent. Also, 70% recovery of Cu_2^{II}(**addpa**) was obtained after catalytic cycles (Fig. S21†). This indicated that AsH_2 fully reacted with Cu_2^{II}(**addpa**) to generate the Cu(I) active species for the catalytic ORR. In our system, AsH_2 can not only serve as a reductant but also a H^+ source for O_2 reduction *via* the 2-e$^-$ process. This reducing agent offers a unique and efficient system because, unlike other previous reports, an external source of proton is not required in our reaction. With the readily available protons in the reaction, it was not surprising that the Cu–peroxo intermediate (usually observed by UV-vis) could not be detected in our case.

Next, the product obtained from catalytic O_2 reduction was determined. Typically, catalytic O_2 reduction in the presence of a proton source (AsH_2) can result in the production of H_2O_2 (2e$^-$, 2H$^+$ process) or H_2O (4e$^-$, 4H$^+$ process).[23] In our case, generation of H_2O_2 after the catalytic ORR was confirmed by reaction with silver nanoprisms (AgNPrs) according to a previous research study.[75] Unfortunately, quantitative analysis of H_2O_2 by UV-vis could not be achieved in our reaction solutions owing to the precipitation of starch-coated AgNPrs in CH_3CN. Nevertheless, a colour change of AgNPr precipitates could be observed by the naked eye, indicating the production of H_2O_2 (Fig. S22†). For a positive control reaction, in the presence of H_2O_2 (0.1 M), the magenta colour of AgNPr precipitates was changed to white colour due to the oxidation of AgNPrs to Ag(I) by H_2O_2. The white precipitates were analysed by scanning electron microscopy (SEM) and energy dispersive X-ray analysis (EDX) to determine the elemental composition. The data from the EDX technique showed the presence of carbon (C) and oxygen (O), which are the elemental components in starch, and silver (Ag) in the white precipitates. This suggested that the Ag(I) species probably precipitated along with starch in the systems leading to the observation of white precipitates. From our ORR catalysed by the dinuclear copper complex, the same colour change of the AgNPr precipitates from magenta to white was observed, indicative of H_2O_2 production from the ORR. Also, if the reaction contains only Cu complex or AsH_2 alone, the magenta AgNPr precipitates were still observed. It should also be noted that our attempt to detect and quantify H_2O_2 produced from O_2 reduction by iodometric titration was not successful due to the direct reaction between Cu_2(**addpa**) and iodide.

To further support our proposed mechanism of two-electron reduction of oxygen to H_2O_2 mediated by our copper complex, the number of electrons consumed per oxygen molecule was evaluated. This method has been used in both electro- and chemical catalyses.[6,76,77] Determined by ^{1}H-NMR with O_2 as a limiting agent, the relative stoichiometry of O_2 to DHA (an oxidised product from AsH_2) was obtained. It was found that 1 equiv. of DHA was produced for each equivalent of O_2 used in the reaction. This can translate to approximately 2 electrons consumed per oxygen molecule in the ORR. This result pointed out that Cu_2(**addpa**) mainly catalysed the ORR *via* the 2e$^-$, 2H$^+$ process to give the H_2O_2 product (eqn (2)) although a possibility that a small amount of H_2O produced *via* the 4e$^-$, 4H$^+$ process (eqn (3)) proceeding concomitantly cannot be absolutely ruled out.

$$O_2 + AsH_2 \rightarrow H_2O_2 + DHA \quad (2)$$

$$O_2 + 2\ AsH_2 \rightarrow 2\ H_2O + 2\ DHA \quad (3)$$

To gain further insights into the mechanism of Cu_2^{II}(**addpa**)-mediated catalytic O_2 reduction, computational calculations were next performed. From the literature, possible Cu_2O_2 adducts in the dioxygen activation reaction might be end-on or side-on peroxo species. Generally, end-on Cu_2O_2 exhibiting nucleophilic and basic properties tends to produce H_2O_2 *via* protonation. According to H_2O_2 production in our ORR, a possible copper–dioxygen intermediate would be an end-on species which is in agreement with the most stable structure of Cu_2O_2 optimized by DFT calculations as shown in Fig. 6.

At first glance, it might be unusual to propose an end-on peroxo species with tridentate ligands. However, the X-ray structure of Cu_2^{II}(**addpa**) both before and after catalytic O_2 reduction as well as Cu_2^{I}(**addpa**) from our calculations (Fig. S25†) revealed that CH_3CN served as an additional ligand. As a result, the copper centres might possess insufficient vacant sites to adopt a side-on intermediate. The proposed intermediate was also consistent with our experimental data in that its basic and nucleophilic nature would give the H_2O_2 product. It should be mentioned that dioxygen activation by intermolecular coupling between two dinuclear copper(I) complexes has already been presented in the literature.[78] After the protonation of the peroxo intermediate, the other remaining Cu(I) centre in each complex can reduce another O_2 molecule to complete the catalytic cycle (Fig. S27†).

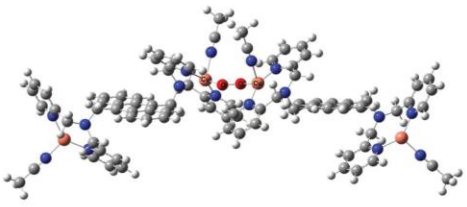

Fig. 6 Proposed end-on Cu_2O_2 intermediate in this work from DFT calculations.

Conclusions

Copper complexes bearing dipicolylamine-based tridentate ligands were prepared to examine for their reactivity toward dioxygen activation. All complexes were structurally characterised by X-ray crystallography as well as their properties using electrochemical and spectroscopic techniques. The Cu(I) active species were generated by reaction of the copper(II) complex with ascorbic acid, which could serve as a reducing agent and a proton source. The influence of conjugated-π systems and nuclearity of the complex on ORR activity was highlighted. Both electrochemical analysis and chemical reaction studies revealed that the anthracene moiety can facilitate in the reduction of the Cu(II) complex as well as the stability of the Cu(I) species. Although cooperative O_2 binding was not expected in **3a** due to the long distance between the two copper centres, our results showed that the dinuclear complex **3a** exhibited significantly higher ORR activity than its mononuclear analogue **2a**. **3a** was also found to be relatively robust and competent in the catalytic two-electron reduction of O_2 leading to the production of H_2O_2. This experimental result is in good agreement with the data obtained from DFT calculations. The basic findings here may serve as useful information for future design of catalysts for use in substrate oxidation as well as application in sustainable and clean energy conversion.

Experimental section

Materials

For ligand and copper complex syntheses, commercially available reagents and solvents were purchased with high purity grade and used without further purification or dried over molecular sieves (3 or 4 Å) prior to use unless otherwise noted. For reactivity studies, all solvents of the highest purity grade were purchased from Merck and dried with molecular sieves 3 or 4 Å prior to use. Ascorbic acid was obtained from Aldrich and was purified according to published purification methods.[79] Deuterated-solvents for NMR analysis were purchased from Cambridge Isotope Laboratories, Inc. 2,2′-Dipicolylamine (**dpa**),[49] 9-[(2,2′-dipicolylamino)methyl]anthracene (**adpa**)[50] and 9,10-bis[(2,2′-dipicolylamino)methyl]anthracene (**addpa**)[50] were prepared according to literature procedures.

Instrumentation

Nuclear Magnetic Resonance (NMR) spectra were recorded on a 400 MHz Varian Mercury spectrometer at 298 K. Mass spectra were recorded by Electrospray Ionization Mass Spectrometry (ESI-MS) on a Bruker Daltonics microOTOF and by matrix-assisted laser desorption/ionization (MALDI) time-of-flight (TOF) mass spectrometry (MS) on a Bruker Daltonics MALDI-TOF. UV-vis spectra were recorded on a Varian Cary 50 probe UV-visible spectrophotometer. Electron paramagnetic resonance (EPR) spectra were recorded at 298 K using a Bruker EMX-Micro spectrometer. Scanning electron microscopy (SEM) and energy dispersive X-ray analysis (EDX) was carried out using a scanning electron microscope JSM-IT100.

Synthesis and characterisation of copper(II) complexes

General procedure. All complexes were synthesised under a N_2 atmosphere at room temperature. To a stirred solution of the ligand was added dropwise a solution of $Cu(ClO_4)_2{\cdot}(H_2O)_6$ dissolved in CH_3OH. The reaction was stirred for 2 h, after which the solid product was precipitated and filtered.

Caution! Perchlorate is a potentially explosive substance. Experiments should be handled carefully.

Cu^{II}(**dpa**) (**1**) was prepared from the reaction of **dpa** (0.20 g, 1.00 mmol) and $Cu(ClO_4)_2$ (0.56 g, 1.51 mmol) in CH_2Cl_2/CH_3OH (1 : 1 v : v). Yield: 0.28 g (60%). Blue single crystals suitable for X-ray structure determination were obtained by recrystallisation of the complex by layer diffusion in CH_2Cl_2/CH_3CN for 7 days. Anal. calcd (found) of $C_{12}H_{15}Cl_2CuN_3O_9$: %C = 30.04 (30.34), %H = 3.15 (3.05), %N = 8.76 (8.72). MALDI-TOF MS (m/z) of $[\mathbf{1} - H]^+$ for calculated: 261.03; found: 261.23. λ_{max}/nm (ε/M^{-1} cm^{-1}) in CH_3CN: 606 (117.2).

Cu^{II}(**adpa**) (**2a**) was prepared according to a modified published method.[25] Reaction of **adpa** (0.15 g, 0.39 mmol) and $Cu(ClO_4)_2$ (0.16 g, 0.43 mmol) in CH_3OH resulted in dark green products. Yield: 0.15 g (61%). The single crystals suitable for X-ray crytallography were recrystallised by vapour diffusion of Et_2O into the solution of **2a** in CH_3CN for 7 days. Anal. calcd (found) of $C_{27}H_{25}Cl_2CuN_3O_9$: %C = 48.40 (48.09), %H = 3.76 (3.74), %N = 6.27 (6.32). MALDI-TOF MS (m/z) of $[\mathbf{2a} + (ClO_4)]^+$ for calculated: 551.07; found: 551.01. λ_{max}/nm (ε/M^{-1} cm^{-1}) in CH_3CN: 590 (117.9).

$[Cu_2(\mu\text{-}Cl)_2(\mathbf{adpa})_2](ClO_4)_2$ (**2b**) was prepared from the reaction of **adpa** (0.20 g, 0.51 mmol) and $Cu(ClO_4)_2$ (0.29 g, 0.77 mmol) in CH_2Cl_2/CH_3OH (1 : 1 v : v). The crystalline product was obtained by the layer diffusion method with CH_3CN/Et_2O for 1 day. ESI-MS (m/z) of $[\mathbf{2b} + (Cl)]^+$ for calculated: 487.09; found: 487.09, and $[\mathbf{2b} + (ClO_4)]^+$ for calculated: 551.07; found: 551.07.

Cu^{II}(**addpa**) (**3a**) was prepared from the reaction of **addpa** (0.20 g, 0.33 mmol) and $Cu(ClO_4)_2$ (0.37 g, 1.00 mmol) in CH_2Cl_2/CH_3OH (1 : 1 v : v). Yield: 0.32 g (85%). Deep green single crystals were obtained by recrystallisation of the complex using a mixed solvent CH_2Cl_2/CH_3OH. Anal. calcd (found) of $C_{40}H_{36}Cl_4Cu_2N_6O_{16}$: %C = 42.68 (42.41), %H = 3.22 (3.31), %N = 7.47 (7.34). ESI-MS (m/z) of $[\mathbf{3a} + (ClO_4)_3]^+$ for calculated: 1025.00; found: 1025.39. λ_{max}/nm (ε/M^{-1} cm^{-1}) in CH_3CN: 593 (273.7).

$[Cu_2(\mathbf{addpa})(CH_3CN)_2(H_2O)_2](ClO_4)_4$ (**3b**). Complex **3b** was prepared from catalytic O_2 reduction by **3a** with AsH_2. To a stirred solution of **3a** in CH_3CN under N_2 at room temperature, AsH_2 (1.5 equiv.) in 5% DMF/CH_3CN was added. The mixture was stirred for 1 h, resulting in a yellow solution of Cu^{I}_2(**addpa**). After that, the solution was exposed to air and stirred for another 4 h to give a green solution of Cu(II) species. The solid product was precipitated upon addition of Et_2O to the

mixture. This solid was recrystallised in CH_2Cl_2/CH_3CN to give dark green crystals of **3b**.

Studies of reactivity toward O_2 reduction

Unless otherwise noted, all reactions were carried out under an inert atmosphere (N_2). All solvents were deoxygenated prior to use by purging N_2 for at least 1 h. The UV-vis spectral change during the reaction was monitored at ambient temperature using a Varian Cary 50 probe UV-visible spectrophotometer with a quartz cuvette (path length = 10 mm).

Generation of copper(I) complexes. A stock solution of AsH_2 (44 mM) was prepared in a solvent mixture of 5% DMF in CH_3CN or 5% H_2O in CH_3CN. To ensure the absence of O_2 in our reactions, the solution of copper complexes was purged with N_2 gas for 10 min before starting the reaction. In a typical reaction, to a solution of copper(II) complex (1 mM for **3a**; 2 mM for **1** and **2a**) in CH_3CN was added an amount of AsH_2 stock solution (0 − 2 equiv.). A colour change of the solution to yellow was observed. Monitoring of this reaction by UV-vis spectroscopy showed a reduction of the copper(II) complex (λ_{max} around 600 nm corresponding to a d–d transition band of d^9 Cu(II) species) to copper(I) species (no d–d transition band).

NMR and EPR samples were prepared as follows: to a solution of copper(II) complex (10 mM) in CD_3CN (550 μL) was added AsH_2 (20 μL, 0.55 equiv. for **2a**, whereas 1.5 equiv. for **3a** dissolved in 15% D_2O in CD_3CN). For **2a** and **3a**, a colour change to yellow was noted, consistent with the formation of copper(I) species. When compared to a broad ^{1}H-NMR spectrum of Cu(II), the pale-yellow species exhibited a sharp spectrum, supporting an assignment of diamagnetic d^{10} Cu(I) species. Analysis of the ^{1}H-NMR spectrum also revealed the formation of dehydroascorbic acid (an oxidised form of ascorbic acid) after the reaction.

Oxygen reduction reaction (ORR). After a complete generation of the copper(I) species (for **2a** and **3a**), O_2 was purged into the Cu(I) solution for 1 h to examine the ORR activity. The reaction can be monitored by the spectral change in UV-vis, NMR and EPR.

H_2O_2 detection by silver nanoprisms (AgNPrs)

To obtain a sufficient amount of O_2-reduced product after the ORR, a catalytic reaction was performed. To a solution of **3a** (10 mM, 0.010 mmol) in CH_3CN was added an excess amount of AsH_2 (10 equiv.). Then, the reaction was purged with O_2 for 1 h. The reaction was allowed to stand for 2 h before product determination. Unfortunately, due to the direct reaction of **3a** with I^-, we cannot perform iodometric titration for detection and quantification of H_2O_2. However, the H_2O_2 product from the ORR was successfully detected by reaction with AgNPrs. Owing to the precipitation of AgNPrs in an organic solvent, the UV-vis spectral change cannot be investigated. Nevertheless, in the presence of H_2O_2, an obvious colour change of the AgNPr precipitates from magenta to white can be observed by the naked eye. After the catalytic ORR, a certain amount of AgNPr solution (0.02 mL) was added to the reaction solution (0.20 mL), and the white precipitates were observed, confirming the production of H_2O_2 after the ORR. For a positive control experiment, the same amount of AgNPrs (0.02 mL) was added to the H_2O_2 solution (0.1 M) in CH_3CN (0.20 mL), which resulted in the change in the colour of precipitates from magenta to white. When a negative control reaction was performed (the same conditions, but in the absence of **3a** or AsH_2), the colour of the precipitates remained the same as magenta.

Determination of the number of electrons consumed per oxygen molecule in the ORR

Deuterated solvents for NMR analysis were saturated with O_2 prior to use in the reaction. In a typical experiment, a stock solution of Cu_2(**addpa**) in the O_2-saturated CD_3CN (6.0 mM) was prepared. This solution (550 μL) was then transferred to an NMR tube fitted with a septum. To this solution was added an excess amount of AsH_2 (0.0264 mmol) in D_2O to obtain the final mixed solvent of 5% D_2O/CD_3CN (600 μL). After that, the reaction was stirred for 1 h and then analysed by ^{1}H-NMR. The reaction was carried out in triplicate. It should be noted that allowing the solution to react longer than 1 h also gave the same result. However, if this complete reaction was exposed to O_2 afterward, the excess AsH_2 would react with O_2 and more dehydroascorbic acid (DHA) yield was observed. This indicated that the reaction was complete within an hour and O_2 as the limiting agent could be used up. The relative yield of DHA which is an oxidised form of AsH_2 was calculated based on 3 runs to determine the relative stoichiometry of O_2 to DHA. It was found that about 1 equiv. of DHA was produced for each equivalent of O_2 consumed. In other words, a total of around 2 electrons (1.9–2.4 e^-) per oxygen molecule were consumed in the oxygen reduction.

X-ray crystallography

Crystals of complexes **2b**, **3a**, and **3b** were selected under an optical microscope and glued on glass fiber for single crystal X-ray diffraction experiments. X-ray diffraction data were collected using a Bruker D8 QUEST CMOS using Mo-Kα radiation (λ = 0.7107 Å) and operating at T = 296(2) K. Data were obtained using ω and ϕ scans of 0.5 (d, scan_width)° per frame for 30 (d, scan_rate) seconds using Mo-Kα radiation (50 kV, 30 mA). The total number of runs and images was based on the strategy calculation from the program APEX3. Unit cell indexing was refined using SAINT (Bruker, V8.34A, 2013). Data reduction, scaling and absorption corrections were performed using SAINT (Bruker, V8.34A, 2013) and SADABS-2014/4 (Bruker, 2014/4) was used for absorption correction.[80] The structure was solved in the space group *P*1 with the ShelXT structure solution program using combined Patterson and dual-space recycling methods.[81] The crystal structure was refined by least squares using version 2014/7 of ShelXL.[82] All non-hydrogen atoms were refined anisotropically. Hydrogen atom positions were calculated geometrically and refined using the riding model. For **2b**, the solvent masking procedure as implemented in OLEX2[83] was used to remove the

electronic contribution of disordered and partially occupied solvent molecules from the refinement. A comment relating to the use of these routines appears in the "Refinement special details" section of the cif file. For **3a** and **3b**, the ClO_4^- anions were found to be disordered over two positions. The relative occupation of the disordered ClO_4^- anion was refined as a free variable. All Cl–O bond distances and O···O separations of both (minor and major) fractions of the disordered ClO_4^- anion were restrained to have identical values within 0.02 Å. A summary of crystal data and relevant refinement parameters for **2b**, **3a**, and **3b** is given in Table S1 in the ESI.† Selected bond lengths and bond angles are provided in Table S2.† Hydrogen bond geometry is also given in Table S3.† The CCDC numbers of **2b**, **3a**, and **3b** are 1543792, 1543793, and 1543794,† respectively.

Cyclic voltammetry

Cyclic voltammetric measurements were performed with an Autolab PGSTAT101 potentiostat/galvanostat (Eco Chemie, The Netherlands) using a conventional three-electrode configuration. A glassy carbon electrode with a disk diameter of 3.0 mm was employed as a working electrode. Before use, the electrode was polished with an aqueous suspension of alumina powder and rinsed thoroughly with deionized water. A platinum wire was applied as an auxiliary electrode. All potentials are quoted with respect to a non-aqueous silver/silver ion (Ag/Ag^+) reference electrode; this electrode was externally calibrated with a ferrocene/ferrocenium ion (Fc/Fc^+) redox couple and has a potential of 0.542 V *versus* a standard hydrogen electrode (SHE).[65] Cyclic voltammograms of the copper complexes (1.00 mM) were recorded in a deoxygenated solvent (dimethylformamide, DMF or acetonitrile, CH_3CN) containing 0.10 M tetrabutylammonium hexafluorophosphate ($TBAPF_6$) at scan rates of 50–800 mV s^{-1}. A deaeration procedure was carried out with the aid of ultra-high purity (UHP) nitrogen.

Computation methods

Geometry optimizations of the dinuclear copper complex and its related species, were carried out using the density functional theory (DFT) method. The hybrid density functional B3LYP, the Becke three-parameter hybrid functional[84] combined with the Lee–Yang–Parr correlation functional,[84] using the 6-31G(d,p) basis set[85,86] were employed in calculations. The solvent-effect of the polarizable continuum model (PCM)[87–93] using the CPCM (conductor-like PCM, acetonitrile as a solvent) model[94–96] with the UFF molecular cavity model were used in the optimization. Therefore, the employed method was called the CPCM(UFF)/B3LYP/6-31G(d,p) method. All calculations were performed with the Gaussian 09 program.[97]

Conflicts of interest

There are no conflicts of interest to declare.

Acknowledgements

This work was supported by the Thailand Research Fund (P. L., TRG 5880235) and Grants for the Development of New Faculty Staff, Ratchadaphiseksomphot Endowment Fund. P. S. is grateful for the scholarship from the Science Achievement Scholarship of Thailand (SAST) and acknowledges financial support from The 90th Anniversary of Chulalongkorn University Fund. K. C. and P. V. would like to express their sincere gratitude to the Grant for Join Funding, Ratchadaphiseksomphot Endowment Fund.

Notes and references

1 E. I. Solomon, P. Chen, M. Metz, S.-K. Lee and A. E. Palmer, *Angew. Chem., Int. Ed.*, 2001, **40**, 4570–4590.
2 E. C. Tse, D. Schilter, D. L. Gray, T. B. Rauchfuss and A. A. Gewirth, *Inorg. Chem.*, 2014, **53**, 8505–8516.
3 S. Fukuzumi, Y. Yamada and K. D. Karlin, *Electrochim. Acta*, 2012, **82**, 493–511.
4 Y. Yamada, S. Yoshida, T. Honda and S. Fukuzumi, *Energy Environ. Sci.*, 2011, **4**, 2822–2825.
5 S. Fukuzumi, *Biochim. Biophys. Acta*, 2016, **1857**, 604–611.
6 M. Asahi, S. Yamazaki, S. Itoh and T. Ioroi, *Dalton Trans.*, 2014, **43**, 10705–10709.
7 D. Das, Y. M. Lee, K. Ohkubo, W. Nam, K. D. Karlin and S. Fukuzumi, *J. Am. Chem. Soc.*, 2013, **135**, 4018–4026.
8 S. Fukuzumi, H. Kotani, H. R. Lucas, K. Doi, T. Suenobu, R. L. Peterson and K. D. Karlin, *J. Am. Chem. Soc.*, 2010, **132**, 6874–6875.
9 S. Kakuda, R. L. Peterson, K. Ohkubo, K. D. Karlin and S. Fukuzumi, *J. Am. Chem. Soc.*, 2013, **135**, 6513–6522.
10 D. Das, Y. M. Lee, K. Ohkubo, W. Nam, K. D. Karlin and S. Fukuzumi, *J. Am. Chem. Soc.*, 2013, **135**, 2825–2834.
11 S. Fukuzumi, L. Tahsini, Y. M. Lee, K. Ohkubo, W. Nam and K. D. Karlin, *J. Am. Chem. Soc.*, 2012, **134**, 7025–7035.
12 S. Kakuda, C. J. Rolle, K. Ohkubo, M. A. Siegler, K. D. Karlin and S. Fukuzumi, *J. Am. Chem. Soc.*, 2015, **137**, 3330–3337.
13 D. Maiti, J. S. Woertink, A. A. Narducci Sarjeant, E. I. Solomon and K. D. Karlin, *Inorg. Chem.*, 2008, **47**, 3787–3800.
14 A. Gomila, N. Le Poul, J. M. Kerbaol, N. Cosquer, S. Triki, B. Douziech, F. Conan and Y. Le Mest, *Dalton Trans.*, 2013, **42**, 2238–2253.
15 E. I. Solomon, J. W. Ginsbach, D. E. Heppner, M. T. Kieber-Emmons, C. H. Kjaergaard, P. J. Smeets, L. Tian and J. S. Woertink, *Faraday Discuss.*, 2011, **148**, 11–39.
16 L. M. Mirica, X. Ottenwaelder and T. D. P. Stack, *Chem. Rev.*, 2004, **104**, 1013–1046.
17 E. A. Lewis and W. B. Tolman, *Chem. Rev.*, 2004, **104**, 1047–1076.
18 A. Faur Ghenciu, *Curr. Opin. Solid State Mater. Sci.*, 2002, **6**, 389–399.
19 D. K. Ross, *Vacuum*, 2006, **80**, 1084–1089.

20 Z. Chen, S. Chen, S. Siahrostami, P. Chakthranont, C. Hahn, D. Nordlund, S. Dimosthenis, J. K. Norskov, Z. Bao and T. F. Jaramillo, *React. Chem. Eng.*, 2017, **2**, 239–245.
21 K. D. Karlin, N. Wei, B. Jung, S. Kaderli, P. Niklaus and A. D. Zuberbuehler, *J. Am. Chem. Soc.*, 1993, **115**, 9506–9514.
22 M. P. Jensen, E. L. Que, X. Shan, E. Rybak-Akimova and L. Que Jr., *Dalton Trans.*, 2006, 3523–3527.
23 M. A. Thorseth, C. E. Tornow, E. C. M. Tse and A. A. Gewirth, *Coord. Chem. Rev.*, 2013, **257**, 130–139.
24 K. Kubo and A. Mori, *J. Mater. Chem.*, 2005, **15**, 2902.
25 B. Antonioli, B. Buchner, J. K. Clegg, K. Gloe, K. Gloe, L. Gotzke, A. Heine, A. Jager, K. A. Jolliffe, O. Kataeva, V. Kataev, R. Klingeler, T. Krause, L. F. Lindoy, A. Popa, W. Seichter and M. Wenzel, *Dalton Trans.*, 2009, 4795–4805.
26 C. L. Davies, E. L. Dux and A. K. Duhme-Klair, *Dalton Trans.*, 2009, 10141–10154.
27 S. Burattini, B. W. Greenland, D. H. Merino, W. Weng, J. Seppala, H. M. Colquhoun, W. Hayes, M. E. Mackay, I. W. Hamley and S. J. Rowan, *J. Am. Chem. Soc.*, 2010, **132**, 12051–12058.
28 Y. Hitomi, T. Nagai and M. Kodera, *Chem. Commun.*, 2012, **48**, 10392–10394.
29 J. W. Nugent, H. Lee, H. S. Lee, J. H. Reibenspies and R. D. Hancock, *Chem. Commun.*, 2013, **49**, 9749–9751.
30 F. Huang and G. Feng, *RSC Adv.*, 2014, **4**, 484–487.
31 J. W. Nugent, H. Lee, H. S. Lee, J. H. Reibenspies and R. D. Hancock, *Inorg. Chem.*, 2014, **53**, 9014–9026.
32 J. W. Nugent, J. H. Reibenspies and R. D. Hancock, *Inorg. Chem.*, 2015, **54**, 9976–9988.
33 E. E. Karslyan, A. O. Borissova and D. S. Perekalin, *Angew. Chem., Int. Ed.*, 2017, **56**, 5584–5587.
34 T. Osako, Y. Tachi, M. Taki, S. Fukuzumi and S. Itoh, *Inorg. Chem.*, 2001, **40**, 6604–6609.
35 T. Osako, Y. Ueno, Y. Tachi and S. Itoh, *Inorg. Chem.*, 2003, **42**, 8087–8097.
36 T. Osako, Y. Tachi, M. Doe, M. Shiro, K. Ohkubo, S. Fukuzumi and S. Itoh, *Chemistry*, 2004, **10**, 237–246.
37 T. Osako, S. Terada, T. Tosha, S. Nagatomo, H. Furutachi, S. Fujinami, T. Kitagawa, M. Suzuki and S. Itoh, *Dalton Trans.*, 2005, 3514–3521.
38 S. Itoh and Y. Tachi, *Dalton Trans.*, 2006, 4531–4538.
39 M. T. Meredith, M. Minson, D. Hickey, K. Artyushkova, D. T. Glatzhofer and S. D. Minteer, *ACS Catal.*, 2011, **1**, 1683–1690.
40 F. Giroud and S. D. Minteer, *Electrochem. Commun.*, 2013, **34**, 157–160.
41 R.-C. Wang, T.-L. Yin, P.-J. Wei and J.-G. Liu, *RSC Adv.*, 2015, **5**, 66487–66493.
42 J. I. van der Vlugt, *Eur. J. Inorg. Chem.*, 2012, **2012**, 363–375.
43 I. A. Koval, P. Gamez, C. Belle, K. Selmeczi and J. Reedijk, *Chem. Soc. Rev.*, 2006, **35**, 814–840.
44 S. T. Prigge, A. S. Kolhekar, B. A. Eipper, R. E. Mains and L. M. Amzel, *Nat. Struct. Mol. Biol.*, 1999, **6**, 976–983.
45 A. de la Lande, S. Martí, O. Parisel and V. Moliner, *J. Am. Chem. Soc.*, 2007, **129**, 11700–11707.
46 D. J. Cardenas, J. M. Cuerva, M. Alias, E. Bunuel and A. G. Campana, *Chemistry*, 2011, **17**, 8318–8323.
47 S. Kim, J. W. Ginsbach, A. I. Billah, M. A. Siegler, C. D. Moore, E. I. Solomon and K. D. Karlin, *J. Am. Chem. Soc.*, 2014, **136**, 8063–8071.
48 I. Garcia-Bosch, R. E. Cowley, D. E. Diaz, M. A. Siegler, W. Nam, E. I. Solomon and K. D. Karlin, *Chemistry*, 2016, **22**, 5133–5137.
49 C. Incarvito, M. Lam, B. Rhatigan, A. L. Rheingold, C. J. Qin, A. L. Gavrilova and B. Bosnich, *J. Chem. Soc., Dalton Trans.*, 2001, 3478–3488.
50 A. Ojida, Y. Mito-oka, M.-A. Inoue and I. Hamachi, *J. Am. Chem. Soc.*, 2002, **124**, 6256–6258.
51 A. Bhagi-Damodaran, M. A. Michael, Q. Zhu, J. Reed, B. A. Sandoval, E. N. Mirts, S. Chakraborty, P. Moënne-Loccoz, Y. Zhang and Y. Lu, *Nat. Chem.*, 2016, 1–7.
52 Y. Yang, C. Lu, H. Wang and X. Liu, *Dalton Trans.*, 2016, **45**, 10289–10296.
53 I. Banerjee, P. N. Samanta, K. K. Das, R. Ababei, M. Kalisz, A. Girard, C. Mathoniere, M. Nethaji, R. Clerac and M. Ali, *Dalton Trans.*, 2013, **42**, 1879–1892.
54 A. W. Addison, T. N. Rao, J. Reedijk, J. van Rijn and G. C. Verschoor, *J. Chem. Soc., Dalton Trans.*, 1984, 1349–1356.
55 S. Mandal, F. Lloret and R. Mukherjee, *Inorg. Chim. Acta*, 2009, **362**, 27–37.
56 N. R. Sangeetha and S. Pal, *Polyhedron*, 2000, **19**, 1593–1600.
57 Y. Sikdar, R. Modak, D. Bose, S. Banerjee, D. Bienko, W. Zierkiewicz, A. Bienko, K. Das Saha and S. Goswami, *Dalton Trans.*, 2015, **44**, 8876–8888.
58 R. Angamuthu, P. Byers, M. Lutz, A. L. Spek and E. Bouwman, *Science*, 2010, **327**, 313–315.
59 I. M. Angulo, E. Bouwman, S. M. Lok, M. Lutz, W. P. Mul and A. L. Spek, *Eur. J. Inorg. Chem.*, 2001, **2001**, 1465–1473.
60 D. A. Safin, M. G. Babashkina, M. Bolte, D. B. Krivolapov, M. L. Verizhnikov, A. R. Bashirov and A. Klein, *Inorg. Chim. Acta*, 2011, **366**, 19–26.
61 D. A. Safin, M. G. Babashkina, A. Klein, M. Bolte, D. B. Krivolapov and I. A. Litvinov, *Inorg. Chem. Commun.*, 2009, **12**, 913–915.
62 Y. Sugai, S. Fujii, T. Fujimoto, S. Yano and Y. Mikata, *Dalton Trans.*, 2007, 3705–3709.
63 V. Y. Tyurin, A. A. Moiseeva, D. B. Shpakovsky and E. R. Milaeva, *Electroanal. Chem.*, 2015, **756**, 212–221.
64 K. A. Bussey, A. R. Cavalier, M. E. Mraz, K. D. Oshin, A. Sarjeant and T. Pintauer, *Polyhedron*, 2016, **114**, 256–267.
65 V. V. Pavlishchuk and A. W. Addison, *Inorg. Chim. Acta*, 2000, **298**, 97–102.
66 A. J. Bard and L. R. Faulkner, *Electrochemical Methods: Fundamentals and Applications*, Wiley, New York, 2nd edn, 2000.

67 Z. Ma, L. Wei, E. C. Alegria, L. M. Martins, M. F. Guedes da Silva and A. J. Pombeiro, *Dalton Trans.*, 2014, **43**, 4048–4058.
68 S. M. d. M. Romanowski, F. Tormena, V. A. d. Santos, M. d. F. Hermann and A. S. Mangrich, *J. Braz. Chem. Soc.*, 2004, **15**, 897–903.
69 C. W. Anderson, K. R. Lung and T. A. Nile, *Inorg. Chim. Acta*, 1984, **85**, 33–36.
70 H. Khoshro, H. R. Zare and R. Vafazadeh, *J. CO_2 Util.*, 2015, **12**, 77–81.
71 A. Kunishita, J. D. Scanlon, H. Ishimaru, K. Honda, T. Ogura, M. Suzuki, C. J. Cramer and S. Itoh, *Inorg. Chem.*, 2008, **47**, 8222–8232.
72 G. Zhang, G. Yang and J. S. Ma, *J. Chem. Crystallogr.*, 2006, **36**, 631–636.
73 J. Wang, S. Liu, S. Xu, F. Zhao, H. Xia and Y. Wang, *J. Organomet. Chem.*, 2017, **846**, 351–359.
74 Q. Wang, W. L. Man, W. W. Lam and T. C. Lau, *Chem. Commun.*, 2014, **50**, 15799–15802.
75 K. Nitinaivinij, T. Parnklang, C. Thammacharoen, S. Ekgasit and K. Wongravee, *Anal. Methods*, 2014, **6**, 9816–9824.
76 R. L. Shook, S. M. Peterson, J. Greaves, C. Moore, A. L. Rheingold and A. S. Borovik, *J. Am. Chem. Soc.*, 2011, **133**, 5810–5817.
77 T. Wada, H. Maki, T. Imamoto, H. Yuki and Y. Miyazato, *Chem. Commun.*, 2013, **49**, 4394–4396.
78 J. Serrano-Plana, I. Garcia-Bosch, A. Company and M. Costas, *Acc. Chem. Res.*, 2015, **48**, 2397–2406.
79 W. L. F. Armarego and D. D. Perrin, *Purification of Laboratory Chemicals*, 1996.
80 Bruker, *Saint 8.34 software*, Madison, WI, USA, 2013.
81 G. M. Sheldrick, *Acta Crystallogr., Sect. A: Found. Adv.*, 2015, **71**, 3–8.
82 G. M. Sheldrick, *Acta Crystallogr., Sect. C: Struct. Chem.*, 2015, **71**, 3–8.
83 O. V. Dolomanov, L. J. Bourhis, R. J. Gildea, J. A. K. Howard and H. Puschmann, *J. Appl. Crystallogr.*, 2009, **42**, 339–341.
84 A. D. Becke, *J. Chem. Phys.*, 1993, **98**, 5648–5652.
85 M. S. Gordon, *Chem. Phys. Lett.*, 1980, **76**, 163–168.
86 W. J. Hehre, R. Ditchfield and J. A. Pople, *J. Chem. Phys.*, 1972, **56**, 2257–2261.
87 V. Barone, M. Cossi and J. Tomasi, *J. Chem. Phys.*, 1997, **107**, 3210–3221.
88 V. Barone, M. Cossi and J. Tomasi, *J. Comput. Chem.*, 1998, **19**, 404–417.
89 E. Cancès, B. Mennucci and J. Tomasi, *J. Chem. Phys.*, 1997, **107**, 3032–3041.
90 M. Cossi, V. Barone, R. Cammi and J. Tomasi, *Chem. Phys. Lett.*, 1996, **255**, 327–335.
91 M. Cossi, V. Barone, B. Mennucci and J. Tomasi, *Chem. Phys. Lett.*, 1998, **286**, 253–260.
92 B. Mennucci and J. Tomasi, *J. Chem. Phys.*, 1997, **106**, 5151–5158.
93 S. Miertuš and J. Tomasi, *Chem. Phys.*, 1982, **65**, 239–245.
94 V. Barone and M. Cossi, *J. Phys. Chem. A*, 1998, **102**, 1995–2001.
95 M. Cossi and V. Barone, *J. Chem. Phys.*, 1998, **109**, 6246–6254.
96 M. Cossi, N. Rega, G. Scalmani and V. Barone, *J. Comput. Chem.*, 2003, **24**, 669–681.
97 M. J. Frisch, G. W. Trucks, H. B. Schlegel, G. E. Scuseria, M. A. Robb, J. R. Cheeseman, *et al.*, *Gaussian 09, Revision D.01*, Wallingford CT, 2014.

6.2 A research article: “Stabilisation of copper(I) polypyridyl complexes toward aerobic oxidation by zinc(II) in combination with acetate anions: a facile approach and application in ascorbic acid sensing in aqueous solution” published in Dalton Transactions (IF = 4.099).

Suktanarak,P.; Ruangpornvisuti, V.; Suksai, C.; Tuntulani, T.; Leeladee, P. *Dalton Transactions*, **2019**, *48*, 997 – 1005.

Dalton Transactions

PAPER

View Article Online
View Journal | View Issue

Check for updates

Cite this: *Dalton Trans.*, 2019, **48**, 997

Stabilisation of copper(I) polypyridyl complexes toward aerobic oxidation by zinc(II) in combination with acetate anions: a facile approach and its application in ascorbic acid sensing in aqueous solution†

Pattira Suktanarak,[a] Vithaya Ruangpornvisuti,[a] Chomchai Suksai,[b] Thawatchai Tuntulani[a] and Pannee Leeladee *[a,c]

Received 3rd September 2018,
Accepted 12th December 2018

DOI: 10.1039/c8dt03580f

rsc.li/dalton

A new and facile approach to stabilise copper(I) complexes in aqueous solution by the addition of zinc(II) ions in combination with acetate ions (OAc^-) was demonstrated. This stability enhancement toward the aerobic oxidation of copper(I) species was investigated by various techniques including UV-vis spectroscopy, ^{1}H-NMR, FT-IR, and ESI-MS. Our experimental results together with DFT calculations led to a proposed structure of $[(\mathbf{adpa})Cu\text{-}OAc\text{-}Zn(OAc)(H_2O)_2]^{+/2+}$. It was also postulated that zinc(II) with its Lewis acidity may attract electrons from the Cu centre through the bridging ligands (OAc^-), resulting in the lower reactivity of Cu(I) with O_2. In addition, this strategy was shown to be applicable to ascorbic acid detection by monitoring a change in the redox states of copper complexes using fluorescence spectroscopy. Moreover, it was demonstrated that the method was sensitive and accurate for the quantitative analysis of ascorbic acid in vitamin C tablets.

Introduction

Copper is an abundant and redox-active metal. It is frequently employed as a redox catalyst in a wide range of both synthetic and biological reactions.[1–4] In nature, copper containing enzymes serve as mediators for substrate conversion. Typically, Cu(II) centres in the enzymes will be reduced to Cu(I) reactive species for further catalytic processes. Interestingly, there are several enzymes which can generate Cu(I) active intermediates using ascorbic acid (vitamin C, AsH_2) as a reducing agent such as dopamine β-hydroxylase (DβH), peptidylglycine α-hydroxylating monooxygenase (PHM) and ascorbate oxidase (AO).[5,6] Likewise, synthetic metal complexes show high potential in AsH_2 oxidation.[7–12] Hence, redox active metals including copper are potentially applicable as a sensor probe for AsH_2 by monitoring the changes in the redox state of the metal.

Ascorbic acid (vitamin C, AsH_2) is an essential antioxidant playing a vital role in biological processes. In addition, the AsH_2 level positively correlates with several diseases including cardiovascular disease, viral infection and Alzheimer's disease as well as anticancer therapy.[13–16] On the other hand, the lower level of AsH_2 can lead to the development of diabetes or cognitive impairment.[17–19] Also, AsH_2 has been used as an additive substance in food, beverages and pharmaceutical formulations for oxidative protection. Because of its advantages in food quality control and healthcare, the development of a simple method for AsH_2 detection has gained considerable attention. Recently, a number of research studies reported sensors for AsH_2 based on materials such as quantum dots, Au nanoparticles and C-dots/Fe(III).[20–26] However, these materials could be suffering from reproducibility and characterisation. On the other hand, molecular probes (*e.g.*, metal complexes) can be characterised in terms of molecular structures, chemical properties and mechanistic studies with routine spectroscopic techniques. In addition, these methods are quite repeatable.

Unfortunately, the utilisation of Cu complexes in the field of molecular sensors *via* a redox reaction (Cu(II) → Cu(I)) is usually hampered by the instability of the Cu(I) species in aqueous solution under aerobic conditions.[27,28] Therefore, new strategies for the stabilisation of the active species (Cu(I))

[a]*Department of Chemistry, Faculty of Science, Chulalongkorn University, Bangkok 10330, Thailand. E-mail: pannee.l@chula.ac.th*
[b]*Department of Chemistry and Centre for Innovation in Chemistry, Faculty of Science, Burapha University, Chonburi 20131, Thailand*
[c]*Research Group on Materials for Clean Energy Production STAR, Department of Chemistry, Faculty of Science, Chulalongkorn University, Bangkok 10330, Thailand*
†Electronic supplementary information (ESI) available. See DOI: 10.1039/c8dt03580f

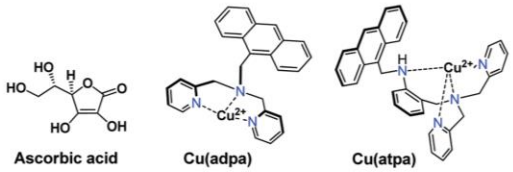

Chart 1 Ascorbic acid (AsH_2) and copper complexes used in this study.

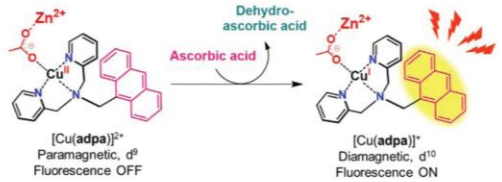

Fig. 1 Proposed acetate-bridged Zn(II)–Cu(I/II)**adpa** complex and the mechanism for AsH_2 detection.

are of particular importance for developing a simple, rapid and accurate sensor for the detection of antioxidants. It has been demonstrated that copper(I) can be stabilised by metal–π interactions relying on the ligand attributes with conjugated π systems or by coordinating solvents (*i.e.* acetonitrile).[29–32] We initially tried to stabilise Cu(I) using acetonitrile as the solvent due to its facile procedure. Unfortunately, our Cu(I) complex, Cu^{I}(**adpa**) (Chart 1) was not stable in aqueous solution despite the presence of acetonitrile.

Herein, we report a new approach to stabilise Cu(I) polypyridyl complexes toward aerobic oxidation by Zn(II) ions in combination with acetate anions (OAc^-) as shown in Fig. 1. We proposed that the positively-charged Zn^{2+} may stabilise Cu(I) by attracting electrons through acetate bridging ligands. This secondary coordination sphere modulation was inspired by an imidazolate-bridged Cu–Zn model for superoxide dismutase (CuZnSOD) enzymes.[33–37] Our simple and easy approach was then applied for the accurate detection of AsH_2 in vitamin C tablets with good sensitivity. To the best of our knowledge, this is the first example of copper complexes as fluorescent probes *via* a reversible redox reaction for AsH_2 detection.

Results and discussion

Reaction of the Cu(II) complex and ascorbic acid

To establish distinct spectroscopic patterns between Cu(I) and Cu(II) species and confirm the successful reaction of our copper complexes and AsH_2, the reaction of Cu^{II}(**adpa**) and AsH_2 was initially performed under a N_2 atmosphere in CH_3CN. Upon the addition of AsH_2 to the solution of Cu^{II}(**adpa**), a color change from blue to pale yellow was observed. Monitoring of this reaction by UV-vis spectroscopy and ^{1}H-NMR confirmed that Cu^{II}(**adpa**) was reduced to Cu(I) species in concomitance with the oxidation of AsH_2 as evidenced by the observed production of dehydroascorbic acid (Fig. S1 and S2†). It should be noted that the same result was obtained when the reaction was carried out in the presence of O_2, and the Cu(I) species seemed to be stable for at least 5 h. In contrast, when the solvent was changed to H_2O/CH_3CN (7 : 3 v/v) under ambient conditions, Cu^{I}(**adpa**) could not be completely formed and gradually reoxidised by air to Cu(II), suggesting its instability in aqueous solution. However, performing the reactions in aqueous solution is essential for the detection of biological substances including natural reducing agents owing to their solubility in water.

Cu(I) stability enhancement toward aerobic oxidation by the modulation of the secondary coordination sphere

From the heteronuclear metalloenzymes in nature, we learn that Zn^{2+} not only serves as a mediator for catalytic substrate conversion, but also plays a crucial role in the stabilisation of enzymes and proteins.[38] A synthetic model for CuZnSOD demonstrated the vital role of Zn^{2+} in controlling the redox potentials of Cu(II) ions through the imidazole (Im) bridge for the desired catalytic reaction.[36] From this inspiration, we came up with the idea that Zn^{2+} in combination with bridging ligands may help to facilitate Cu(II) reduction and stabilise our Cu(I) species in aqueous solution under aerobic conditions. Thus, we first proved our assumption by the addition of Zn^{2+} and Im in the reaction of Cu^{II}(**adpa**) + AsH_2 in H_2O/CH_3CN (7 : 3 v/v). As a result, it seemed that the reduction of Cu(II) to Cu(I) was facilitated as the Cu(II) d–d band was dramatically decreased when monitored by UV-vis spectroscopy. However, the reaction started to be cloudy after 15 min which hampered a prolonged monitoring of this reaction. Then, we also tried to add histidine (His) instead of Im, and found that Cu(II) was fully reduced to Cu(I). However, His was not well-dissolved in our solvent system. It should be noted that His contains not only the Im side chain, but also a carboxyl group which can serve as a bridging ligand. Therefore, we sought for other alternatives, and thought that acetate anions (OAc^-) might be a good candidate since they have been demonstrated as a bridge between two metal centres in dinuclear complexes.[39–43] To test our hypothesis, the reduction of Cu^{II}(**adpa**) by AsH_2 (1 mol equiv.) in H_2O/CH_3CN (7 : 3 v/v) was performed under aerobic conditions in the presence of 8 mol equiv. of $Zn(OAc)_2$, $Zn(NO_3)_2$ or Zn(phen)$_2$. Fig. 2 indicates that the d–d transition band of Cu(II) (λ_{max} = 632 nm) completely disappeared upon the addition of AsH_2 only in the presence of $Zn(OAc)_2$, and the spectrum was stable for at least 60 min before the d–d band started to come back, implying the regeneration of Cu(II). This could suggest that $Zn(OAc)_2$ can help facilitating the reduction of Cu^{II}(**adpa**) and stabilising the Cu(I) species as well. Moreover, the reversible d–d band of Cu(II) (Fig. S4†) confirmed that no transmetalation occurred between Zn^{2+} and Cu(**adpa**) during the redox reaction of Cu(**adpa**) in the presence of $Zn(OAc)_2$.

Furthermore, the importance of Zn^{2+} in stabilising Cu^{I}(**adpa**) was highlighted by comparative reactions using

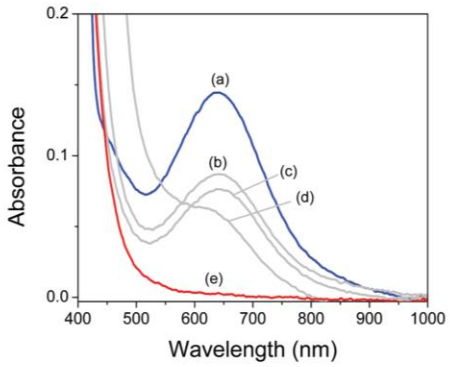

Fig. 2 UV-vis spectra of (a) 2 mM Cu^{II}(**adpa**); (b) Cu^{II}(**adpa**) + AsH_2 (1 mol equiv.); Cu^{II}(**adpa**) + AsH_2 (1 mol equiv.) in the presence of 8 mol equiv. (c) $Zn(NO_3)_2$, (d) $Zn(phen)_2$, and (e) $Zn(OAc)_2$ in H_2O/CH_3CN (7 : 3 v/v) at room temperature.

other redox inactive cations with OAc^- *i.e.*, Na^+, Mg^{2+} and Ca^{2+} instead of Zn^{2+} (Fig. 3 and S7†). It was found that in the presence of such metal ions, the Cu(II) d–d band was suddenly decreased upon the addition of AsH_2, suggesting that all metal ions with OAc^- are likely to facilitate the Cu(II) reduction by AsH_2. However, all Cu(II) spectra gradually returned after 5 min, except the one with $Zn(OAc)_2$ of which the Cu(I) species could be stabilised for at least 60 min. Therefore, it is conclusive that both Zn^{2+} and OAc^- are required to facilitate the reduction of the Cu(II) complex and stabilise the Cu(I) redox state. We also proposed that Zn^{2+} as a good Lewis acid may help to stabilise Cu(I) by the delocalisation of electrons through the OAc^- bridge, analogous to an imidazolate-bridged Cu–Zn model for CuZnSOD.[36]

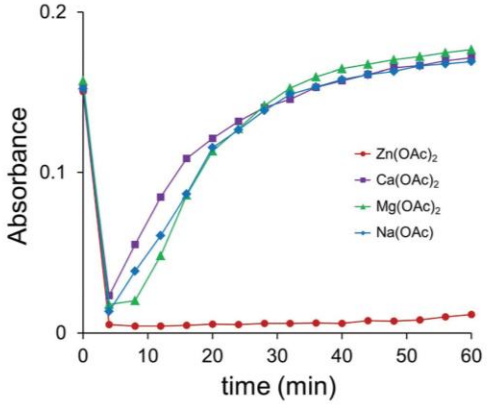

Fig. 3 Change in the absorbance of Cu(II) for the reactions of 2 mM Cu^{II}(**adpa**) with AsH_2 (1 mol equiv.) in the presence of various redox inactive cations as a function of time. Each reaction was performed in H_2O/CH_3CN (7 : 3 v/v) at room temperature.

It is worth mentioning that the influence of a Lewis acid on the redox potential of the metal centre has been previously demonstrated.[44–46] Therefore, the electrochemical behaviours of our Cu(I)/(II)(**adpa**) redox couple in the absence and presence of $Zn(OAc)_2$ were studied by cyclic voltammetry. It was found that the reduction potential of Cu^{II}(**adpa**) did not change significantly after adding $Zn(OAc)_2$, but Cu(I) seemed to be reoxidized less than that in the absence of $Zn(OAc)_2$. In addition, when the supporting electrolyte was changed from an acetic–acetate buffer to a non-coordinated electrolyte (potassium hexafluorophosphate, KPF_6), a similar result was obtained. These electrochemical results might suggest that the reoxidation of Cu(I) to Cu(II) is more difficult in the presence of $Zn(OAc)_2$.

To rule out the possibility that the pH change caused by Lewis acid Zn(II) ions may be responsible for the stability of Cu(I), a comparative study in the buffered solvent (acetic–acetate buffer solution, pH 5.6) was carried out (Fig. S18†). In the reaction of Cu^{II}(**adpa**) + AsH_2 in the absence of Zn(II), Cu(I) was not fully formed and gradually reoxidised to Cu(II) within 20 min. On the other hand, in the presence of Zn(II) under the same conditions, the Cu(I) complex was stabilised up to 40 min.

Proposed structure of $[(adpa)Cu\text{-}OAc\text{-}Zn(OAc)(H_2O)_2]^{+/2+}$

To shed some light on how $Zn(OAc)_2$ helps to stabilise the Cu^I species, we sought to investigate the interaction between Cu^{II}(**adpa**) and $Zn(OAc)_2$ by spectroscopic techniques, ESI-MS, and DFT calculations which led to a proposed structure of $[(adpa)Cu\text{-}OAc\text{-}Zn(OAc)(H_2O)_2]^{+/2+}$. To begin with, our first structural evidence on the proposed structure came from FT-IR analysis. Since the carboxylate group can coordinate to the metal ions in various ways, a number of research studies examined the vibrational frequencies of acetate salts to correlate with their structure and employed this relationship to predict the coordination mode of OAc^- in metal complexes.[41,42,47] Deacon and Phillips[41] reported that the frequency separation between the COO^- antisymmetric and symmetric stretching vibrations or the $\Delta\nu_{a-s}$ values for the species with different binding modes usually fall in the following order:

$$\Delta\nu_{a-s}(\text{unidentate}) > \Delta\nu_{a-s}(\text{ionic}) \sim \Delta\nu_{a-s}(\text{bridging}) > \Delta\nu_{a-s}(\text{bidentate}).$$

It should be noted that OAc^- has been reported as a bridging ligand in both homo- and heterometallic complexes.[39–43] The FT-IR spectrum of our precipitate obtained from the reaction between Cu^{II}(**adpa**) and $Zn(OAc)_2(H_2O)_2$ is shown in Fig. 4e in comparison with those of $Zn(OAc)_2(H_2O)_2$ (bidentate), Cu^{II}(**adpa**), Na(OAc) (ionic), and a solid mixture of $Zn(OAc)_2(H_2O)_2$ + Cu^{II}(**adpa**). It can be seen that our precipitate from the reaction showed two new peaks at 1561 and 1385 cm^{-1} which could be assigned to asymmetric and symmetric COO^- stretching, respectively. Since these new signals did not match with the starting material $Zn(OAc)_2(H_2O)_2$ and free OAc^- (ionic), it suggested that OAc^- might form a new

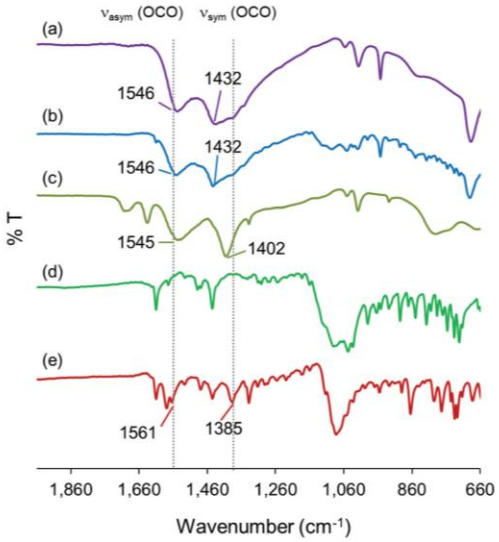

Fig. 4 Comparison of the FT-IR spectra of (a) $Zn(OAc)_2(H_2O)_2$; (b) solid mixture of $Zn(OAc)_2(H_2O)_2$ + Cu^{II}(**adpa**); (c) Na(OAc); (d) Cu^{II}(**adpa**) and (e) precipitate from the reaction of Cu^{II}(**adpa**) + $Zn(OAc)_2(H_2O)_2$.

coordination. Notably, the shifts in these vibrational frequencies are quite similar to those observed for acetate bridging in several carboxylate-bridged copper complexes (*e.g.* Cu–Cu, Cu–Ca).[42,48–50] The $\Delta\nu_{a-s}$ value of 176 cm^{-1} from our sample is quite close to that from the heterometallic carboxylate-bridged Cu–Ca complex (180),[42] but significantly different from that of bidentate OAc^- in $Zn(OAc)_2(H_2O)_2$ ($\Delta\nu$ = 114). These data pointed that OAc^- might serve as a bridging ligand between Zn^{2+} and Cu^{II}(**adpa**). To support this hypothesis, an optimised structure of $[$(**adpa**)Cu-OAc-Zn(OAc)$(H_2O)_2]^{2+}$ was obtained from the DFT calculations with the CPCM(UFF)/B3LYP/6-311+G(d,p) basis set. It was found that the O–C–O angle of the acetate bridge was 121.8° which is relatively close to that of the heterometallic bidentate acetate bridge of the Cu–Ca complex (121.5(3)°),[43] Zn–Ca (122.9, 123.9 and 124.3°) and Zn–Mg (123.9 and 124.9°).[39]

To gain further support for the proposed structure of $[$(**adpa**)Cu-OAc-Zn(OAc)$(H_2O)_2]^{2+}$ in the solution phase, we also monitored the Cu^{II}(**adpa**) + $Zn(OAc)_2(H_2O)_2$ reaction by UV-vis spectroscopy and ^{1}H-NMR. Interestingly, upon the addition of $Zn(OAc)_2(H_2O)_2$ to Cu^{II}(**adpa**), a slight shift in the d–d band of Cu(II) and a significant change in the ^{1}H-NMR signal of OAc^- were observed. The ^{1}H-NMR signal of OAc^- in Cu^{II}(**adpa**) + $Zn(OAc)_2(H_2O)_2$ was broadening and shifted to 2.6 ppm, indicating the coordination of OAc^- to Cu(II). For comparison, when Na(OAc) was added to Cu^{II}(**adpa**), the ^{1}H-NMR signal of CH_3COO^- (OAc^-) could not be observed (Fig. S8†). This suggested the difference in the coordination of OAc^- between these two systems. As a bridging ligand between the Zn(II) and Cu(II) complex, OAc^- may have a weaker paramagnetic influence of Cu(II) than that in the Cu^{II}(**adpa**) + Na(OAc) solution. In addition, the ESI-MS data clearly showed that OAc^- from $Zn(OAc)_2(H_2O)_2$ could bind to Cu(II) (see the ESI†). All of these results support the finding that the formation of $[$(**adpa**)Cu-OAc-Zn(OAc)$(H_2O)_2]^{2+}$ is feasible.

In the case of the Cu(I) species, the reaction of Cu^{II}(**adpa**) + $Zn(OAc)_2(H_2O)_2$ and AsH_2 gave rise to a prominent signal at *m*/*z* 512.1356 in the ESI-MS spectrum, corresponding to $[Cu^{I}$(**adpa**) + (OAc^-) + $H^+]^+$. It might be implied that OAc^- could coordinate to the Cu(I) centre in a similar manner to that found in the Cu(II) compound, Cu^{II}(**adpa**). Unfortunately, the interaction of the Cu(I) complex and $Zn(OAc)_2(H_2O)_2$ could not be investigated by other spectroscopic techniques due to the limitations of our system. Therefore, we turned our attention to studying this interaction and proposing the structure using DFT calculations. As a result, a DFT-optimised structure of $[$(**adpa**)Cu-OAc-Zn(OAc)$(H_2O)_2]^+$, together with its frontier orbitals, was obtained as shown in Fig. 5 and Fig. S13–15.† Markedly, a significant change in the highest occupied molecular orbital (HOMO) delocalisation on the copper(I) centre in the presence and absence of $Zn(OAc)_2(H_2O)_2$ was noted. In $[$(**adpa**)Cu-OAc-Zn(OAc)$(H_2O)_2]^+$, the HOMO orbital is delocalized to the Cu(I) centre substantially less than that of the Cu complex without $Zn(OAc)_2(H_2O)_2$. This result is consistent with our experimental finding that the Cu(I) complex is significantly less reactive toward O_2 in the presence of $Zn(OAc)_2$. However, when there is only OAc^- bound to the Cu(I) centre without Zn^{2+}, the HOMO is delocalised around the Cu(I) ion and its coordination site which is in agreement with our reactivity study that Cu^{I}(**adpa**) + NaOAc seemed to react with O_2 to

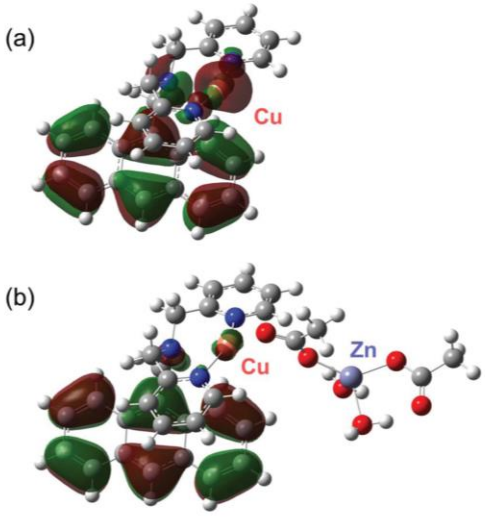

Fig. 5 Plots of the HOMOs of (a) Cu^{I}(**adpa**) and (b) Cu^{I}(**adpa**)/Zn $(OAc)_2{\cdot}(H_2O)_2$, computed at the CPCM(UFF)/B3LYP/6-311+G(d,p) level of theory.

generate the Cu(II) product. We account for the stability of Cu^{I}(**adpa**) in the presence of $Zn(OAc)_2$ by the role of Zn^{2+} as a good Lewis acid. Due to its electron-withdrawing properties, Zn^{2+} may help to attract electrons from the Cu(I) active site *via* the acetate bridge, leading to a less electron density on the Cu centre. This rationale was consistent with the fact that Cu^{I}(**adpa**) + $Zn(OAc)_2$ exhibited less reactivity toward O_2 when compared to Cu^{I}(**adpa**) itself. Given the proposed structure, we also speculate that the bridge through OAc^- and Zn^{2+} may help to provide a steric encumber which inhibits the oxidizing agent (*e.g.* O_2) to react with the Cu(I) centre.

All of these results are in agreement with our proposal that OAc^- coordinated to the copper centre and could serve as a bridging ligand between the Cu(I)/(II) and Zn^{2+} ions resulting in the stabilisation of the Cu(I) species under aerobic conditions. Next, this approach was tested for its applicability to AsH_2 sensing.

Application in ascorbic acid sensing by fluorescence

Our approach was applied to detect AsH_2 by fluorescence spectroscopy because of its high sensitivity. As a molecular sensor, Cu(**adpa**) contains a dipicolylamine Cu active site and anthracene as a sensory unit. A change in the redox states of the Cu centre would give a different fluorescence spectrum. As expected, Cu^{II}(**adpa**) did not show fluorescence signals owing to the disturbance of the paramagnetic species, Cu(II).[51] The addition of AsH_2 resulted in a significant fluorescence enhancement at 421 nm which is consistent with the conversion of Cu(II) to a diamagnetic Cu(I) complex as illustrated in Fig. 6.

Because ascorbic acid is a hexanoic sugar acid with two acidic protons (pK_a 4.04 and 11.34),[21] the effects of pH and interferences from common natural reducing agents (*i.e.*, reducing sugar, citric acid, and glutathione) were investigated next. The results showed that pH had a large influence on our AsH_2 detection in terms of both sensitivity and selectivity (Fig. S19†). At pH 4, a satisfactory fluorescence intensity and high selectivity for AsH_2 detection were achieved. However, the selectivity was significantly lower at a higher pH due to Cu chelation by glutathione.[52–56]

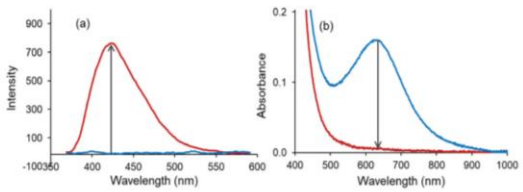

Fig. 6 Change in (a) the fluorescence signal (excitation wavelength = 340 nm, slit setting on the instrument = 10 and PMT = 500); and (b) UV-vis spectrum upon the addition of AsH_2 (1 mol equiv.) to the Cu^{II}(**adpa**) solution in the presence of Zn(II) in H_2O/CH_3CN (7 : 3 v/v) buffered with ABS at pH 5.6.

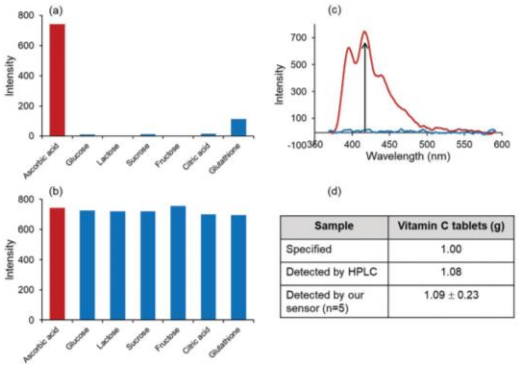

Sample	Vitamin C tablets (g)
Specified	1.00
Detected by HPLC	1.08
Detected by our sensor (n=5)	1.09 ± 0.23

Fig. 7 (a) Selectivity and (b) interference study for AsH_2 detection using our sensor; (c) fluorescence spectral change upon the addition of AsH_2 to Cu(**atpa**) + $Zn(OAc)_2$; and (d) detection of ascorbic acid in vitamin C tablets. The concentration of Cu(**atpa**) = 10 μM, $Zn(OAc)_2$ = 40 mol equiv. and λ_{ex} = 340 nm.

To decrease the influence of the chelation of Cu ions by analytes and to expand the pH range of our detection, we decided to prepare Cu^{II}(**atpa**) (Chart 1) for our further studies. As a tetradentate ligand, **atpa** was expected to bind Cu ions more tightly than a tridentate ligand, **adpa**. Hence, copper sequestration by glutathione will be less pronounced. Our results confirmed this assumption as shown in Fig. 7. In addition, our limit of detection (LOD) for AsH_2 was determined to be 163 nM which is relatively low ($3\sigma/S$; σ is the standard deviation for the blank solution, n = 10, and S is the slope of the calibration curve).

Moreover, our approach was then employed to measure the AsH_2 amount in vitamin C tablets to verify our accurate detection in real samples. The measurements by our sensor, Cu^{II}(**atpa**), in comparison with HPLC were done using the standard addition method. The result from our method was in good agreement with that from standard HPLC and was close to the amount specified on the vitamin C tablets. Our recovery was in between 101 and 104, and the relative standard deviation was 1.5–4.0. This demonstrated the high accuracy of our method.

Conclusions

In conclusion, we presented a new strategy to stabilise Cu(I) complexes. Our experiments demonstrated that a combination of Zn^{2+} ions and OAc^- can stabilise Cu(I) species in aqueous solution under aerobic conditions. This approach was subsequently applied to detect AsH_2 in vitamin C tablets with high accuracy. Our strategy would also attract interest in other areas such as catalysis for the control of stability and reactivity of metal complexes for mechanistic investigation. Undoubtedly, this approach would pave the way for designing copper complexes as molecular sensors for biological applications.

Experimental

Materials and methods

Solvents of HPLC grade were purchased from Merck and used without further purification. Milli-Q was prepared using ultrapure water systems. Deuterated NMR solvents were purchased from Cambridge Isotope Laboratories, Inc. NMR experiments were carried out using a 400 MHz Varian Mercury spectrometer. All UV-vis spectra were recorded by using a Varian Cary 50 probe UV-visible spectrophotometer with a quartz cuvette (path length = 10 mm). Fluorescence spectra were obtained using a Varian spectrofluorometer with Cary Eclipse, a pulsed xenon lamp and a photomultiplier tube detector. Mass spectra were obtained by Electrospray Ionization Mass Spectrometry (ESI-MS) on a Bruker Daltonics microOTOF. IR measurements were carried out on a Thermo, Nicolet 6700 FT-IR in ATR mode. Cyclic voltammetry was performed on an μAutolab Type III potentiostat under an N_2 atmosphere. This system contained a three-electrode cell: glassy carbon as the working electrode, Pt wire as the counter electrode and $Ag/AgNO_3$ (0.01 M) as the reference electrode. For HPLC analysis, the amounts of ascorbic acid in vitamin C tablets were determined using a Varian Prostar with a C-18 column (C18 4.6 × 250 mm, 5 μm, Phenomenex), pumped at a flow rate of 1.5 mL min^{-1}. Vitamin C tablets were purchased from PT Bayer Indonesia, Depok, Indonesia. All copper complexes and ligands were prepared according to modified published procedures.[57–61]

Caution! Perchlorate is a potentially explosive salt. Experiments should be carefully handled.

Computation methods

The density functional theory (DFT) method, the hybrid density functional theory of Becke's three parameter exchange functional[62] with the Lee–Yang–Parr correlation functional[63] (B3LYP), using the 6-311+G(d,p) basis set[64,65] was employed. All structure optimizations in aqueous solution using the B3LYP/6-311+G(d,p) method combination with the solvent effect of the polarizable continuum model (PCM)[66–72] using the CPCM (conductor-like PCM, water as a solvent) model[73–75] with the UFF molecular cavity model,[64] called the CPCM(UFF)/B3LYP/6-311+G(d,p) level of theory, were carried out. All calculations were performed with the Gaussian09 program.[76] The molecular graphics for relevant compounds and their frontier orbitals (HOMOs and LUMOs) were plotted and visualised using the GaussView 5.0.9 program.[77]

Reaction of Cu^{II}(adpa) and ascorbic acid (AsH_2) in CH_3CN

All solvents were deoxygenated prior to use by purging N_2 for at least 1 h. A stock solution of AsH_2 was prepared in a solvent mixture of 5% H_2O in CH_3CN (44 mM). To a solution of Cu^{II}(**adpa**) (2.0 mM) in CH_3CN was added the AsH_2 stock solution (0.55 mol equiv.). A color change of the solution from blue to pale yellow was observed. Monitoring of this reaction by UV-vis spectroscopy showed a complete reduction of Cu^{II}(**adpa**) (λ_{max} = 591 nm corresponding to a d–d transition band of d^9 Cu^{II} species) to Cu^{I}(**adpa**) (no d–d transition band). When exposed to air, this pale-yellow species was found to be stable for at least 5 h. An NMR sample was prepared as follows: to a solution of Cu^{II}(**adpa**) (10 mM) in CD_3CN (550 μL) was added AsH_2 (20 μL, 0.55 mol equiv. dissolved in 15% D_2O in CD_3CN). A color change from blue to pale yellow was noted, consistent with the formation of Cu^{I}(**adpa**). When compared to a broad ^{1}H-NMR spectrum of Cu^{II}(**adpa**), the pale-yellow species exhibited a sharp spectrum, supporting an assignment of diamagnetic d^{10} Cu^{I} species. An analysis of the ^{1}H-NMR spectrum also revealed the formation of dehydroascorbic acid (an oxidized form of ascorbic acid) after the reaction. When the reaction was carried out in the presence of O_2, the same result was obtained.

Generation of Cu^{I} species in the presence of $Zn(OAc)_2$

Unless otherwise noted, the following experiments were conducted under ambient conditions. A stock solution of AsH_2 (80 mM) was prepared in H_2O/CH_3CN (7 : 3 v/v). In a typical reaction, a solution of Cu^{II}(**adpa**) (2.0 mM) was combined with $Zn(OAc)_2$ (8.0 mol equiv.) in H_2O/CH_3CN (7 : 3 v/v). To this solution mixture was added the AsH_2 stock solution (1.0 mol equiv.). A color change of the solution from green to pale yellow was observed. The reaction was also monitored by UV-vis spectroscopy, which revealed a complete conversion of the spectrum for Cu^{II}(**adpa**) (λ_{max} = 632 nm) to the spectrum for a Cu^{I} complex (no d–d transition band). The Cu^{I} species seemed to be stable for at least 60 min. When $Zn(OAc)_2$ was changed to $Zn(NO_3)_2$ or Zn(phen)$_2$; however, the reduction was not completed as the d–d band of Cu^{II} was present to a significant extent. In fact, they gave the same result as observed in the reaction without $Zn(OAc)_2$. This indicated that the presence of OAc^- is necessary to help facilitate the reduction of Cu^{II}(**adpa**) and the stabilisation of Cu^{II}(**adpa**).

Attempts at characterising this new Cu complex in the presence of $Zn(OAc)_2$ by mass spectrometry have also been made. Samples for the ESI-MS analysis were prepared in 7 : 3 (v/v) H_2O/CH_3CN. A prominent peak at a mass-to-charge ratio (*m*/*z*) of 511.1332 (calc. *m*/*z* 511.13) was observed in the reaction of Cu^{II}(**adpa**) + $Zn(OAc)_2(H_2O)_2$ (1 : 8 mol equiv.), corresponding to $[Cu^{II}$(**adpa**) + $OAc]^+$. On the other hand, *m*/*z* at 512.1356 (calc. *m*/*z* 512.14) which corresponded to $[Cu^{I}$(**adpa**) + (OAc^-) + $(H^+)]^+$ was found when the solution mixture of Cu^{II}(**adpa**) + Zn $(OAc)_2(H_2O)_2$ was added to AsH_2 (5 mol equiv.). This supported the possibility of OAc^- being coordinated to Cu(II/I)**adpa**.

In addition to ESI-MS, the coordination of $Zn(OAc)_2(H_2O)_2$ on the Cu^{II} centre was also investigated by IR spectroscopy. The solid sample for IR analysis was prepared from the reaction of Cu^{II}(**adpa**) and $Zn(OAc)_2{\cdot}(H_2O)_2$ (8 mol equiv.) in 7 : 3 (v/v) H_2O/CH_3CN. After being stirred for around 10 min, the solution mixture was precipitated under reduced pressure to remove CH_3CN and obtain a dark green solid. The solid was filtered for subsequent analysis by IR spectroscopy in the ATR mode.

An NMR sample was prepared as follows: a solution of Cu^{II}(**adpa**) (10 mM) in CD_3CN (550 μL) was combined with $Zn(OAc)_2$ (8.0 mol equiv. dissolved in D_2O/CD_3CN 7 : 3 v/v). A

shift and broadening of a signal corresponding to OAc^- was noted, indicating the coordination of OAc^- to the paramagnetic Cu^{II} centre. To this solution was added AsH_2 (50 μL, 5.0 mol equiv. dissolved in D_2O/CD_3CN 7 : 3 v/v). The solution became pale yellow, consistent with the conversion to Cu^{I}(**adpa**). The yellow product gave a sharp spectrum, corresponding to the Cu^{I} species.

Effect of pH

Acetic–acetate buffer solutions (ABS) with pH 4.0–5.6 and phosphate buffer solution (PBS) with pH 6.0–8.0 were prepared in H_2O/CH_3CN (7 : 3 v/v). In a typical reaction, to a solution of Cu^{II}(**adpa**) (10 μM) in a buffer solution with the desired pH (2.00 mL) was added $Zn(OAc)_2$ (100 μL, 40 mol equiv. dissolved in H_2O/CH_3CN 7 : 3 v/v). To this solution mixture was then added a stock solution of AsH_2 (50 μL, 5 mol equiv. dissolved in H_2O/CH_3CN 7 : 3 v/v). It should be mentioned that a color change of the solution could not be observed with the naked eye at this low concentration. After being stirred for 2 min, the reaction was monitored by fluorescence spectroscopy, which revealed an emission band at λ_{max} = 423 nm. (Fluorescence parameters: excitation wavelength = 340 nm, slit setting on the instrument = 10 and PMT = 500).

To demonstrate the effect of pH on AsH_2 detection in the presence of a possible interference, a solution of glutathione (GSH, 5.0 mol equiv.) or a mixture of AsH_2 (5.0 mol equiv.) and GSH (5.0 mol equiv.) was used instead of AsH_2.

Reaction in the presence of other divalent metal ions

A stock solution of AsH_2 (80 mM) and $M(OAc)_n$ (M = Zn^{2+}, Na^+, Ca^{2+} or Mg^{2+}) was prepared in H_2O/CH_3CN (7 : 3 v/v). In a typical reaction, Cu^{II}(**adpa**) (2 mM) in 2.00 mL of H_2O/CH_3CN (7 : 3 v/v) was combined with $M(OAc)_n$ (8 mol equiv., 100 μL). After being stirred for 2 min, the solution was monitored by UV-vis spectroscopy. To this solution mixture was added the AsH_2 stock solution (1.0 mol equiv., 50 μL). An immediate color change of the solution from green to pale yellow was observed. The reaction was also monitored by UV-vis spectroscopy, showing a complete conversion of the spectrum for Cu^{II}(**adpa**) (λ_{mzx} = 635 nm) to the spectrum for a Cu^{I} complex.

Reaction in the presence of other bridging ligands

A solution mixture of Cu^{II}(**adpa**) (2 mM) and a bridging ligand (16 mol equiv. of imidazole, or histidine) was prepared in 2.00 mL of H_2O/CH_3CN (7 : 3 v/v). A solution of $Zn(NO_3)_2$ (8 mol equiv., 100 μL) was then added. To this reaction mixture was added the AsH_2 stock solution (1.0 mol equiv., 50 μL). The reaction was stirred for 2 min before being monitored by UV-vis spectroscopy.

Studies of selectivity and interferences by fluorescence spectroscopy

Acetic–acetate buffer solutions (ABS) with pH 5.6 were prepared in H_2O/CH_3CN (7 : 3 v/v). In a typical reaction, to a solution of Cu^{II}(**adpa**) or Cu^{II}(**atpa**) (10 μM) in the buffer solution (2.00 mL) was added $Zn(OAc)_2$ (100 μL, 40 mol equiv. dissolved in H_2O/CH_3CN 7 : 3 v/v). To this solution mixture was then added a stock solution of AsH_2 (50 μL, 5 mol equiv. dissolved in H_2O/CH_3CN 7 : 3 v/v). After being stirred for 2 min, the reaction was monitored by fluorescence spectroscopy (fluorescence parameters: excitation wavelength = 340 nm, slit setting on the instrument = 10 and PMT = 500 for Cu(**adpa**); PMT = 530 for Cu(**atpa**)).

For the selectivity study, the addition of AsH_2 was changed to glucose, lactose, sucrose, fructose, citric acid or glutathione. For the interference study, the addition of AsH_2 was changed to the mixture of AsH_2 (5.0 mol equiv.) and a possible interfering substance (5.0 mol equiv. of glucose, lactose, sucrose, fructose, citric acid or glutathione).

Sample preparation for the determination of AsH_2 in vitamin C tablets

Three tablets of vitamin C were dissolved in Milli-Q water (500.00 mL). The solution was then filtered with a 0.45 μM Millipore filter to remove insoluble components. An amount of the filtrate (31 μL) was then transferred to a volumetric flask and diluted to 10.00 mL with ABS (pH 5.6) in H_2O/CH_3CN (7 : 3 v/v). The amount of ascorbic acid in vitamin C tablets was determined by the standard addition method.

Conflicts of interest

There are no conflicts of interest to declare.

Acknowledgements

This work was supported by the Thailand Research Fund (P. L., TRG 5880235) and Grants for the Development of New Faculty Staff, Ratchadaphiseksomphot Endowment Fund. P. S. is grateful for the scholarship from the Science Achievement Scholarship of Thailand (SAST). Also, we would like to thank assistant professor Prompong Pienpinijtham for the helpful discussion.

Notes and references

1 J. Serrano-Plana, I. Garcia-Bosch, A. Company and M. Costas, *Acc. Chem. Res.*, 2015, **48**, 2397–2406.
2 C. E. Elwell, N. L. Gagnon, B. D. Neisen, D. Dhar, A. D. Spaeth, G. M. Yee and W. B. Tolman, *Chem. Rev.*, 2017, **117**, 2059–2107.
3 L. M. Mirica, X. Ottenwaelder and T. D. P. Stack, *Chem. Rev.*, 2004, **104**, 1013–1046.
4 J. J. Liu, D. E. Diaz, D. A. Quist and K. D. Karlin, *Isr. J. Chem.*, 2016, **56**, 9–10.
5 E. I. Solomon, P. Chen, M. Metz, S.-K. Lee and A. E. Palmer, *Angew. Chem., Int. Ed.*, 2001, **40**, 4570–4590.
6 E. I. Solomon, J. W. Ginsbach, D. E. Heppner, M. T. Kieber-Emmons, C. H. Kjaergaard, P. J. Smeets, L. Tian and J. S. Woertink, *Faraday Discuss.*, 2011, **148**, 11–39.

7 A. A. Holder, R. F. G. Brown, S. C. Marshall, V. C. R. Payne, M. D. Cozier, W. A. Alleyne and C. O. Bovell, *Transition Met. Chem.*, 2000, **25**, 605–611.
8 M. M. T. Khan and A. E. Martell, *J. Am. Chem. Soc.*, 1967, **89**, 7104–7111.
9 U. R. Pokharel, F. R. Fronczek and A. W. Maverick, *Nat. Commun.*, 2014, **5**, 5883.
10 S. Senapati, S. P. Das and A. K. Patnaik, *Adv. Phys. Chem.*, 2012, **2012**, 1–5.
11 Q. Wang, W. L. Man, W. W. Lam and T. C. Lau, *Chem. Commun.*, 2014, **50**, 15799–15802.
12 Y.-N. Wang, K.-C. Lau, W. W. Y. Lam, W.-L. Man, C.-F. Leung and T.-C. Lau, *Inorg. Chem.*, 2009, **48**, 400–406.
13 S. A. Bsoul and G. T. Terezhalmy, *J. Contemp. Dent. Pract.*, 2004, **5**, 1–14.
14 Q. Chen, M. G. Espey, M. C. Krishna, J. B. Mitchell, C. P. Corpe, G. R. Buettner, E. Shacter and M. Levine, *Proc. Natl. Acad. Sci. U. S. A.*, 2005, **102**, 13604–13609.
15 Q. Chen, M. G. Espey, A. Y. Sun, C. Pooput, K. L. Kirk, M. C. Krishna, D. B. Khosh, J. Drisko and M. Levine, *Proc. Natl. Acad. Sci. U. S. A.*, 2008, **105**, 11105–11109.
16 X. Chen, Y. Xu, H. Li and B. Liu, *Sens. Actuators, B*, 2017, **246**, 344–351.
17 S. Dixit, A. Bernardo, J. M. Walker, J. A. Kennard, G. Y. Kim, E. S. Kessler and F. E. Harrison, *ACS Chem. Neurosci.*, 2015, **6**, 570–581.
18 Y. Matsuoka, K. Ohkubo, T. Yamasaki, M. Yamato, H. Ohtabu, T. Shirouzu, S. Fukuzumi and K.-I. Yamada, *RSC Adv.*, 2016, **6**, 60907–60915.
19 F. Sun, K. Iwaguchi, R. Shudo, Y. Nagaki, K. Tanaka, K. Ikeda, S. Tokumaru and S. Kojo, *Clin. Sci.*, 1999, **96**, 185–190.
20 J. Gong, X. Lu and X. An, *RSC Adv.*, 2015, **5**, 8533–8536.
21 S. Huang, F. Zhu, Q. Xiao, W. Su, J. Sheng, C. Huang and B. Hu, *RSC Adv.*, 2014, **4**, 46751–46761.
22 R. Liu, R. Yang, C. Qu, H. Mao, Y. Hu, J. Li and L. Qu, *Sens. Actuators, B*, 2017, **241**, 644–651.
23 Q. Ma, Y. Li, Z. H. Lin, G. Tang and X. G. Su, *Nanoscale*, 2013, **5**, 9726–9731.
24 C. Mi, T. Wang, P. Zeng, S. Zhao, N. Wang and S. Xu, *Anal. Methods*, 2013, **5**, 1463.
25 H. W. Park, S. M. Alam, S. H. Lee, M. M. Karim, S. M. Wabaidur, M. Kang and J. H. Choi, *Luminescence*, 2009, **24**, 367–371.
26 Y. Zhang, B. Li and C. Xu, *Analyst*, 2010, **135**, 1579–1584.
27 Y. Hitomi, T. Nagai and M. Kodera, *Chem. Commun.*, 2012, **48**, 10392–10394.
28 S. Kim, M. A. Minier, A. Loas, S. Becker, F. Wang and S. J. Lippard, *J. Am. Chem. Soc.*, 2016, **138**, 1804–1807.
29 T. Osako, Y. Tachi, M. Doe, M. Shiro, K. Ohkubo, S. Fukuzumi and S. Itoh, *Chemistry*, 2004, **10**, 237–246.
30 T. Osako, Y. Tachi, M. Taki, S. Fukuzumi and S. Itoh, *Inorg. Chem.*, 2001, **40**, 6604–6609.
31 T. Osako, S. Terada, T. Tosha, S. Nagatomo, H. Furutachi, S. Fujinami, T. Kitagawa, M. Suzuki and S. Itoh, *Dalton Trans.*, 2005, 3514–3521.
32 T. Osako, Y. Ueno, Y. Tachi and S. Itoh, *Inorg. Chem.*, 2003, **42**, 8087–8097.
33 I. A. Abreu and D. E. Cabelli, *Biochim. Biophys. Acta*, 2010, **1804**, 263–274.
34 M. Lintuluoto, C. Yamada and J. M. Lintuluoto, *J. Phys. Chem. B*, 2017, **121**, 7235–7246.
35 Y.-C. Fang, H.-C. Lin, I. J. Hsu, T.-S. Lin and C.-Y. Mou, *J. Phys. Chem. C*, 2011, **115**, 20639–20652.
36 H. Ohtsu, Y. Shimazaki, A. Odani, O. Yamauchi, W. Mori, S. Itoh and S. Fukuzumi, *J. Am. Chem. Soc.*, 2000, **122**, 5733–5741.
37 J. A. Tainer, E. D. Getzoff, J. S. Richardson and D. C. Richardson, *Nature*, 1983, **306**, 284–287.
38 K. A. McCall, C.-C. Huang and C. A. Fierke, *J. Nutr.*, 2000, **130**, 1437S–1446S.
39 C. Escobedo-Martínez, M. C. Lozada, D. Gnecco, R. G. Enriquez, M. Soriano-García and W. F. Reynolds, *J. Chem. Crystallogr.*, 2012, **42**, 794–802.
40 P. Gentschev, M. Lüken, N. Möller, A. Rompel and B. Krebs, *Inorg. Chem. Commun.*, 2001, **4**, 753–756.
41 G. B. Deacon and R. J. Phillips, *Coord. Chem. Rev.*, 1980, **33**, 227–250.
42 N. F. Curtis, *J. Chem. Soc. A*, 1968, 1579–1584.
43 D. A. Langs and C. R. Hare, *Chem. Commun.*, 1967, 890–891.
44 S. Fukuzumi, K. Ohkubo, Y.-M. Lee and W. Nam, *Chemistry*, 2015, **21**, 17548–17559.
45 E. Y. Tsui, R. Tran, J. Yano and T. Agapie, *Nat. Chem.*, 2013, **5**, 293.
46 E. Y. Tsui and T. Agapie, *Proc. Natl. Acad. Sci. U. S. A.*, 2013, **110**, 10084–10088.
47 M. Nara, H. Morii and M. Tanokura, *Biochim. Biophys. Acta*, 2013, **1828**, 2319–2327.
48 S. Youngme, C. Chailuecha, G. A. van Albada, C. Pakawatchai, N. Chaichit and J. Reedijk, *Inorg. Chim. Acta*, 2005, **358**, 1068–1078.
49 S. Youngme, C. Chailuecha, G. A. van Albada, C. Pakawatchai, N. Chaichit and J. Reedijk, *Inorg. Chim. Acta*, 2004, **357**, 2532–2542.
50 W. Huang, D. Hu, S. Gou, H. Qian, H. K. Fun, S. S. S. Raj and Q. Meng, *J. Mol. Struct.*, 2003, **649**, 269–278.
51 D. Maheshwaran, T. Nagendraraj, P. Manimaran, B. Ashokkumar, M. Kumar and R. Mayilmurugan, *Eur. J. Inorg. Chem.*, 2017, **2017**, 1007–1016.
52 J. Liu, H. Liu, Y. Li and H. Wang, *J. Biol. Phys.*, 2014, **40**, 313–323.
53 R. Yang, X. Guo, L. Jia and Y. Zhang, *Microchim. Acta*, 2017, **184**, 1143–1150.
54 G. R. You, H. J. Jang, T. G. Jo and C. Kim, *RSC Adv.*, 2016, **6**, 74400–74408.
55 C. Guo, P. Li, M. Pei and G. Zhang, *Sens. Actuators, B*, 2015, **221**, 1223–1228.
56 M. S. Kim, J. M. Jung, J. H. Kang, H. M. Ahn, P.-G. Kim and C. Kim, *Tetrahedron*, 2017, **73**, 4750–4757.

57 U. Khamjumphol, S. Watchasit, C. Suksai, W. Janrungroatsakul, S. Boonchiangma, T. Tuntulani and W. Ngeontae, *Anal. Chim. Acta*, 2011, **704**, 73–86.
58 B. Antonioli, B. Buchner, J. K. Clegg, K. Gloe, K. Gloe, L. Gotzke, A. Heine, A. Jager, K. A. Jolliffe, O. Kataeva, V. Kataev, R. Klingeler, T. Krause, L. F. Lindoy, A. Popa, W. Seichter and M. Wenzel, *Dalton Trans.*, 2009, 4795–4805.
59 S. C. Burdette, C. J. Frederickson, W. Bu and S. J. Lippard, *J. Am. Chem. Soc.*, 2003, **125**, 1778–1787.
60 A. Ojida, Y. Mito-oka, M.-A. Inoue and I. Hamachi, *J. Am. Chem. Soc.*, 2002, **124**, 6256–6258.
61 C. Incarvito, M. Lam, B. Rhatigan, A. L. Rheingold, C. J. Qin, A. L. Gavrilova and B. Bosnich, *J. Chem. Soc., Dalton Trans.*, 2001, 3478–3488.
62 A. D. Becke, *J. Chem. Phys.*, 1993, **98**, 5648–5652.
63 C. Lee, W. Yang and R. G. Parr, *Phys. Rev. B: Condens. Matter Mater. Phys.*, 1988, **37**, 785–789.
64 R. C. Binning and L. A. Curtiss, *J. Comput. Chem.*, 1990, **11**, 1206–1216.
65 A. D. McLean and G. S. Chandler, *J. Chem. Phys.*, 1980, **72**, 5639–5648.
66 M. Cossi, V. Barone, B. Mennucci and J. Tomasi, *Chem. Phys. Lett.*, 1998, **286**, 253–260.
67 V. Barone, M. Cossi and J. Tomasi, *J. Comput. Chem.*, 1998, **19**, 404–417.
68 B. Mennucci and J. Tomasi, *J. Chem. Phys.*, 1997, **106**, 5151–5158.
69 E. Cancès, B. Mennucci and J. Tomasi, *J. Chem. Phys.*, 1997, **107**, 3032–3041.
70 V. Barone, M. Cossi and J. Tomasi, *J. Chem. Phys.*, 1997, **107**, 3210–3221.
71 M. Cossi, V. Barone, R. Cammi and J. Tomasi, *Chem. Phys. Lett.*, 1996, **255**, 327–335.
72 S. Miertuš and J. Tomasi, *Chem. Phys.*, 1982, **65**, 239–245.
73 M. Cossi, N. Rega, G. Scalmani and V. Barone, *J. Comput. Chem.*, 2003, **24**, 669–681.
74 M. Cossi and V. Barone, *J. Chem. Phys.*, 1998, **109**, 6246–6254.
75 V. Barone and M. Cossi, *J. Phys. Chem. A*, 1998, **102**, 1995–2001.
76 M. J. Frisch, G. W. Trucks, H. B. Schlegel, G. E. Scuseria, M. A. Robb, J. R. Cheeseman and *et al.*, *Gaussian 09, Revision D.01*, Wallingford CT, 2014.
77 R. Dennington, T. Keith and J. Millam, *GaussView, Version 5*, Semichem Inc., Shawnee Mission, KS, 2009.

7. Output

7.1 International Journal Publication

- Two research articles entitled “Tuning reactivity of copper complexes supported by tridentate ligands leading to two-electron reduction of dioxygen” published in Dalton Transaction (IF = 4.099).

  Dalton Transactions, **2018**, *47*, 16337 – 16349.

  “Stabilisation of copper(I) polypyridyl complexes toward aerobic oxidation by zinc(II) in combination with acetate anions: a facile approach and application in ascorbic acid sensing in aqueous solution” submitted to Dalton Transaction (IF = 4.099).

  Dalton Transactions, **2019**, *48*, 997 – 1005.

7.2 Application

-

7.3 Others

- Bio-inspired Transition Metal Complexes: Synthesis, Reactivity and Applications. **Invited oral presentation** at the 41st Congress on Science and Technology of Thailand (STT41), Nakhon Ratchasima, Thailand, November 7, 2015.
- Synthesis and Reactivity of a Dinuclear Copper Complex Toward Oxygen Reduction. **Poster presentation** at Pure and Applied Chemistry International Conference 2016 (PACCON2016), Bangkok, Thailand, February 9, 2016.